INSTITUTO SUPERIOR TÉCNICO
Universidade Técnica de Lisboa

Development of a Guidance and Control Design Tool for Entry Space Vehicles with Different Lift-over-Drag Ratios

Luis André Carraça Guerreiro

Dissertação para a obtenção do Grau de Mestre em

Engenharia Aeroespacial

Júri:

Presidente:	Prof. Doutor João Miranda Lemos (DEEC)
Orientador:	Prof. Doutor Paulo Jorge Soares Gil (DEM)
Vogal:	Prof. Doutor José Raúl Carreira Azinheira (DEM)

20 de Julho de 2011

Acknowledgments

To Professor Paulo Gil, for all the afternoons spent talking, discussing, theorizing, and for all the time dedicated to reviewing my work.

To Emanuele Di Sotto, João Branco and Nuno Paulino, without whom this work would have been impossible.

To my family, for all their support, and to my dear girlfriend, for all her patience and dedication, and her indispensable one word contribution.

To all my friends, for their positive spirit and good humour, and particularly Liron, who actively discussed with me some of the pratical problems I had.

To the GMV group, for providing the conditions for developing my work.

Resumo

Uma ferramenta de simulação de re-entrada - REACTIVE - para análise e projecto de diferentes técnicas de guiamento e controlo, foi desenvolvida. Esta ferramenta integra um simulador com três graus de liberdade e vários algoritmos de re-entrada, em particular o sistema de guiamento da cápsula Apollo, o do Space Shuttle, e o Enhanced E-Guide, um algoritmo para re-entrada de veículos com elevado coeficiente de sustentação que usa a técnica de Inversão Dinâmica Não-linear.

Um procedimento semi-analítico para geração de um perfil longitudinal de re-entrada, para a fase de aproximação de um veículo com elevado coeficiente de sustentação, foi também desenvolvido e integrado na ferramenta REACTIVE. O procedimento, foi validado por uma série de testes Monte-Carlo, gera um perfil de referência recorrendo a aproximações analíticas da altitude e do ângulo de descida que garantem que as condições iniciais e finais sejam satisfeitas, enquanto que os requisitos de alcance são garantidos usando o método dos mínimos quadrados e determinando a lei de ângulo de pranchamento adequada. Este procedimento semi-analítico permite a geração instantânea do perfil de referência e é adequado a uma instalação embarcada.

A ferramenta REACTIVE reune todos estes algoritmos de guiamento e controlo no mesmo ambiente de simulação, e generaliza-os de modo a que sejam aplicáveis a toda a classe de veículos que lhes está associada, desde cápsulas a veículos com a razão entre a sustentação e a resistência moderada e elevada. Tendo sido inicialmente usado para simular a re-entrada no planeta Terra, a ferramenta REACTIVE foi depois estendida ao cenário de re-entrada em Marte.

Palavras-chave: re-entrada, guiamento e controlo, veículos espaciais de re-entrada, razão entre a sustentação e a resistência, ferramenta de simulação, Apollo, Space Shuttle, veículo com coeficiente de sustentação elevado, geração de perfil de referência, aproximação de TAEM.

Abstract

A re-entry simulation tool - REACTIVE - that allows for the analysis and design of different guidance and control tecniques was developed. It integrates a 3-DoF simulator and several guidance algorithms, namely the Apollo Entry Guidance, the Shuttle Entry Guidance and the Enhanced E-Guide, a guidance scheme for a high lift-over-drag vehicle that uses the Non-linear Dynamic Inversion technique.

A semi-analytical procedure for the generation of a longitudinal profile tailored for the targeting phase (triggered at $V \approx 5$ km/s and lasting up to Terminal Area Energy Management conditions) of a high lift-over-drag re-entry vehicle was also developed and integrated into REACTIVE. The procedure, validated through a series of Monte-Carlo tests, generates a reference profile using analytical approximations of the altitude and flight-path angle which ensure that initial and final conditions are met, while the downrange criteria is satisfied by means of Least-Squares and determination of the suitable bank angle law. This semi-analytical approach allows instantaneous generation of the reference profile and is thus suitable for onboard installation.

The REACTIVE tool collects all these guidance and control approaches in the same simulation environment, and successfully generalizes them, so that they are not restricted to the associated baseline vehicles and are suitable to be applied to the respective vehicle classes, which range from capsules to moderate and high lift-over-drag vehicles. Having been used for Earth re-entry, REACTIVE has also been extended to the Mars scenario.

Keywords: re-entry, guidance and control, entry space vehicles, lift-over-drag, simulation tool, Apollo, Space Shuttle, high lift, reference profile generation, TAEM targeting.

Contents

List of Figures

List of Tables

List of Acronyms

3-DoF	Three Degrees of Freedom
6-DoF	Six Degrees of Freedom
CM	Command Module
EIP	Entry Interface Point
GNC	Guidance, Navigation and Control
GC	Guidance and Control
HAC	Heading Alignment Cone
$\mathbf{L/D}$	Lift-over-Drag
LQR	Linear Quadratic Regulator
NDI	Non-linear Dynamic Inversion
PID	Proportional Integrative Derivative
RPG	Reference Profile Generation
RV	Re-entry Vehicle
STS	Space Transportation System
TAEM	Terminal Area Energy Management
TBVP	Two-point Boundary Value Problem

List of Symbols

C_D	Drag coefficient
C_L	Lift coefficient
D	Drag
g	Gravity
g_n	Standard gravity
H_s	Altitude scale height
h	Altitude
I	Inertia matrix
L	Lift
$\vec{M}$	Moments and torques of the applied forces
M	Mach number
m	Mass
$\dot{Q}$	Heat flux
q	Dynamic pressure
R	Planet radius
$\vec{r}$	Position vector
r	Distance to Earth center
S	Surface area
s	Downrange to landing site
V	Velocity norm
$\vec{v}$	Velocity vector
v_s	Sound speed
α	Angle of attack
β	Angle of sideslip
χ	Latitude
γ	Flight path angle
λ	Longitude
μ	Earth gravitational parameter
ψ	Heading angle
ω	Planet angular velocity
ω_0	Natural frequency of second-order system
ρ	Atmospheric air density
ρ_0	Reference atmospheric air density
σ	Bank angle
$\sigma\,[.]$	Standard deviation
ξ	Damping ratio of second-order system

Chapter 1

Introduction

1.1 Context

1.1.1 Objective

Atmospheric entry is one of the most intricate problems in the Aerospace field. It concerns the dynamics and kinematics of a body coming from space that encounters significant planet atmosphere along its trajectory, either descending from a planet orbit, as is the case of satellites or entry space vehicles, or originating from eccentric hyperbolic orbits, as is the case of meteoroids.

This work aims at integrating re-entry Guidance, Navigation and Control (GNC) algorithms into a single simulation tool oriented for the design and testing of entry guidance and control solutions. Several guidance algorithms are consolidated, prototyped and developed, so as to render the tool suitable for simulating different types of re-entry vehicles.

This work was developed in a collaboration between Instituto Superior Técnico (IST) and the aerospace company GMV, deriving from the participation of GMV in ESA's Highlift project.

1.1.2 Background

The goal of atmospheric entry is to put a space vehicle on the ground safely. For this to happen several conditions must be met: the vehicle must not burn, the trajectory must ensure descent, aerodynamic load limits must not be exceeded, the vehicle must have minimal guidance capabilities to guarantee that the correct path is followed, etc. Constraints are different depending on the type of vehicle, initial conditions, and if it is manned.

Once atmospheric contact is established, three outcomes are possible: the body may skip out of the atmosphere and return to space; the body may be destroyed due to the action of atmospheric resistance; the body may traverse through the atmospheric layer and reach the planet surface. Of the three possible entry scenarios, the skip out scenario occurs when the entry body impacts the planet atmosphere with a shallow angle, for which insufficient drag is generated to slow it down. As a consequence, it is not able to follow a path directing to the planet surface and rebounds off the planet atmosphere back into space again.

The scenario which leads to the destruction of the entry body occurs when it impacts the planet atmosphere with a steep angle of entry, which results in an excessive descent rate and drag force acting on the vehicle. This eventually leads to the burning up of the vehicle by the action of heat fluxes (or heat loads)[1] that the body coating cannot cope with, or to the desintegration of the vehicle by the application of extreme loads, as the atmosphere becomes denser.

[1] Heat flux is the heat transferred to the entry body per second, while heat load is the integral of the heat flux, that is, the total heat transferred to the entry body

In practice, the entry body may reach the planet surface if the angle with which it impacts the atmospheric layer is within a tight range of values, or in other words, if the Entry Interface Point (EIP) conditions are within the interval that leads to feasible re-entry trajectories, denominated entry corridor. This is best visualized in figure 1.1 [2], where the three different regions of possible outcomes are identified.

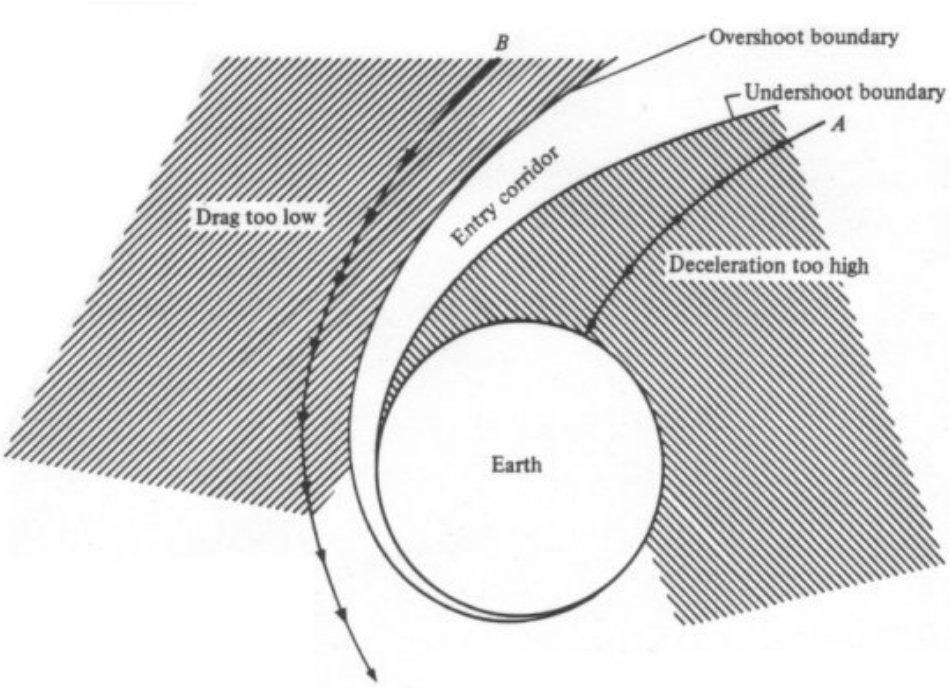

Figure 1.1: Bounded entry corridor [2].

The scenario where planet surface is reached may itself be divided into three different types of entry configurations: ballistic entry, lifting entry, and skip entry. The categorization of an entry configuration is determined by the ability of the vehicle to generate a lift force when entering the planet atmosphere, that is, by its lift-to-drag ratio (L/D) characteristics.

Approximate ballistic entry occurs when the body's L/D is low, tipically when $L/D < 0.5$, which is the case of meteoroids, intercontinental missiles, or capsule-like vehicles, *e.g.* the Apollo Command Module (Apollo CM), the Soyuz, or all the re-entry vehicles (RV)s that have performed Mars entry. In this case, the body's most defining parameter is the ballistic coefficient B_{C} [13]

$$B_{\mathrm{C}} = \frac{m}{C_D S}, \tag{1.1}$$

where m is the body mass, C_D is the drag coefficient and S is the presented area. In a ballistic entry the body follows an almost straight path through atmosphere, sustaining high heat fluxes and significant g-loads. Its point of impact is almost fully determined by its entry angle in the atmosphere, and reduced steering is available (or no steering at all, if $L/D = 0$).

In the case of lifting entry it is considered that $L/D \geq 0.5$. The only example that exists of successful lifting entry is the Space Shuttle Orbiter, that uses its ability of generating a significant lift force to dissipate energy in a controlled fashion during re-entry, being also capable of changing its trajectory to reach the landing site safely. This leads to an important difference between ballistic and lifting entry: in a ballistic setting the entry body becomes invariably wasted due to the excessive damage it takes from the huge heat fluxes/g-loads, while in a lifting entry it is possible to save the re-entry body and reuse in future missions.

The case of the skip-entry was actually never used. For the Apollo mission the skip-entry possibility was

studied, but later discarded. This kind of entry configuration consists on impacting planet atmosphere at an angle such that the entry body rebounds off the atmosphere but is kept in a trajectory that will enable it to enter atmosphere some time later, with reduced entry velocity. However, this is a complex and dangerous process which has been avoided so far.

In any of these entry configurations, the entry body must dissipate significant amounts of energy. Considering that the body reaches zero velocity at ground level, its kinetic energy must be zero at planet surface, which implies that the energy dissipated during atmospheric entry must be equal to the body kinetic energy in orbit. The total energy in orbit per unit mass E is [41]

$$E = \frac{V^2}{2} - \frac{\mu}{r}, \tag{1.2}$$

where V is the body (orbital) velocity, μ is the gravitational parameter, and r is the distance to the planet center. If planet Earth is considered, the kinetic energy of, for example, a Low-Earth Orbit (LEO) is of the order of magnitude of 30 MJ/kg; for a Lunar Transfer Orbit (LTO), the kinetic energy doubles to 60 MJ/kg. To give a more precise idea, the Apollo CM reached a re-entry temperature of more than 3000 K; carbon, which has the highest melting and sublimation point of all elements, sublimates at 3800 K [45].

In order to deal with the complex issue of dissipating these amounts of energy, the banking capabilities of the entry body can be used, in the case where $L/D > 0$. This approach consists in laterally rotating the vehicle from the local vertical (defined as the direction of the gravity force), *i.e.* banking the vehicle, hence re-directing the lift vector, reducing its vertical component and increasing its lateral component, as shown in figure 1.2. With reduced lift in vertical direction, the descent rate and the aerodynamic decelaration increase, which is equivalent to breaking the RV longitudinally. These banking maneuvers thus allow for dissipation of energy in a controlled fashion, but introduce crossrange deviation from target that must be corrected for by bank angle sign reversals.

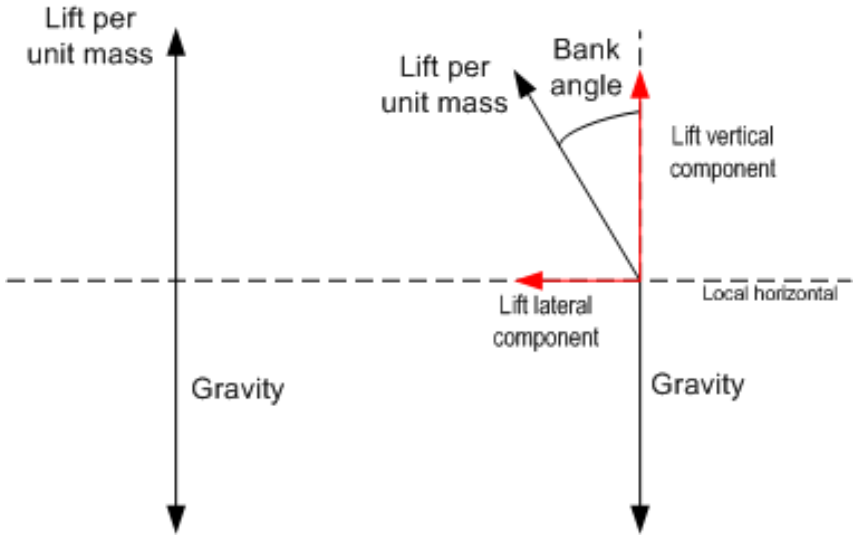

Figure 1.2: Use of the bank angle to control lift, viewing the vehicle from behind: on the left, the case of zero bank angle; on the right, the bank angle is different from zero and the lift vector in the vertical direction is reduced, which increases the descent rate and the aerodynamic drag, and reduces the covered downrange.

In the case of a re-entry vehicle (RV), the banking maneuvers are selected by a GNC system, that is responsible for guiding and controlling the RV through its entry trajectory until the final conditions, in this case Terminal Area Energy Management (TAEM) conditions, are met. Generally, a GNC system is composed of three main functions: the navigation function, the guidance function, and the control function. The navigation

function is responsible for processing the vehicle sensor outputs and produce estimates of the vehicle state[2]. The guidance and control functions work in paralel, in the sense that the first uses the estimates provided by navigation to produce reference commands, that are fed to the control function which is responsible for tracking this reference.

1.2 The re-entry problem

1.2.1 Entry dynamics

The entry vehicle translational and rotational motion can be described using classical Newtonian-Euler mechanics. The full dynamic and kinematic equations, written in the Earth Centered Earth Fixed (ECEF) reference frame[3], are [29, 44]

$$\frac{\mathrm{d}\,\vec{r}}{\mathrm{d}\,t} = \vec{v}, \tag{1.3a}$$

$$\vec{F} = m\frac{\mathrm{d}\,\vec{v}}{\mathrm{d}\,t} + 2m\vec{\omega}\times\bar{v} + m\vec{\omega}\times(\vec{\omega}\times\vec{r}), \tag{1.3b}$$

$$\vec{\omega}_{\mathrm{B}} = I^{-1}\left(\vec{M}_{\mathrm{B}} - \vec{\omega}_{\mathrm{B}}\times I\vec{\omega}_{\mathrm{B}}\right), \tag{1.3c}$$

$$\vec{M}_{\mathrm{B}} = \vec{M}_{\mathrm{A_B}} + \vec{M}_{\mathrm{F_B}} + \vec{M}_{\mathrm{T_B}}, \tag{1.3d}$$

where t is the time independent variable, $\vec{r}$ and $\vec{v}$ are the position and velocity vectors, $\vec{F}$ is the total force applied on the re-entry vehicle, m is the vehicle mass, $\vec{\omega}$ is the Earth's angular velocity, $\vec{\omega}_{\mathrm{B}}$ is the angular velocity of the vehicle, I is its inertia matrix, $\vec{M}_{\mathrm{B}}$ is the total moment applied on the vehicle, and $\vec{M}_{\mathrm{A_B}}$, $\vec{M}_{\mathrm{F_B}}$, $\vec{M}_{\mathrm{T_B}}$ are the moments of forces and torques applied to the vehicle resulting from the actuating surfaces, the aerodynamic forces and the thrusting forces, respectively.

Equation set (1.3) fully characterizes the point-mass vehicle motion and its attitude. However, as discussed in [43], the translational motion, determined by equations 1.3a and 1.3b, is mostly associated to long-period trajectory dynamics, whereas the rotational motion, characterized by equations 1.3c and 1.3d, is associated to short-period oscillations. It is thus possible to decouple these two kinds of dynamics: most guidance approaches consider only the translational point-mass trajectory dynamics, while the short period oscillations are addressed by inner-loop attitude control algorithms. In this work the dynamics decoupling simplification is adopted, and the RV motion is solely determined by 1.3a and 1.3b. Instead of a six-degree of freedom (6-DoF) dynamics, a three-degree of freedom (3-DoF) longitudinal dynamics is thus considered.

[2] In this work the navigation function is not considered, which means that the state-space of the vehicle is assumed to be known at every time-step for the GC system.

[3] Reference frames are thoroughly discussed in chapter 2, section 2.2

Equations 1.3a and 1.3b may be rewritten in the Intrinsic reference frame[4] [29, 34]

$$\frac{\mathrm{d}\,h}{\mathrm{d}\,t} = V\sin\gamma \tag{1.4a}$$

$$\frac{\mathrm{d}\,\chi}{\mathrm{d}\,t} = V\frac{\cos\gamma\sin\psi}{r\cos\lambda} \tag{1.4b}$$

$$\frac{\mathrm{d}\,\lambda}{\mathrm{d}\,t} = V\frac{\cos\gamma\cos\psi}{r} \tag{1.4c}$$

$$\frac{\mathrm{d}\,V}{\mathrm{d}\,t} = -D - g\sin\gamma + \omega^2 r\cos\lambda\left[\sin\gamma\cos\lambda - \sin\lambda\cos\gamma\cos\psi\right] \tag{1.4d}$$

$$\begin{aligned}\frac{\mathrm{d}\,\gamma}{\mathrm{d}\,t} = \frac{1}{V}\Bigg[&\left(\frac{V^2}{r} - g\right)\cos\gamma + L\cos\sigma \\ &+ 2\omega V\cos\lambda\sin\psi + \omega^2 r\cos\lambda\left(\cos\gamma\cos\lambda - \sin\gamma\sin\lambda\cos\psi\right)\Bigg]\end{aligned} \tag{1.4e}$$

$$\begin{aligned}\frac{\mathrm{d}\,\psi}{\mathrm{d}\,t} = \frac{1}{V}\Bigg[&L\frac{\sin\sigma}{\cos\gamma} + \frac{V^2}{r}\cos\gamma\sin\psi\tan\lambda \\ &- 2\omega V\left(\tan\gamma\cos\lambda\cos\psi - \sin\lambda\right) + \frac{\omega^2 r}{\cos\gamma}\sin\lambda\cos\lambda\sin\psi\Bigg],\end{aligned} \tag{1.4f}$$

where r is the RV distance to the Earth center, h is the altitude (in fact $r = R + h$, where R is the Earth radius, which means that r and h only differ by a constant), χ and λ are the RV latitude and longitude, respectively, V is the RV velocity norm, γ is the flight path angle (FPA), defined as the angle between the velocity vector and the vector orthogonal to the position vector in the plane of these two vectors, and ψ is the heading angle, defined as the angle measured from North in the clockwise direction. Moreover, L and D are the aerodynamic lift and drag force norms per unit mass, respectively, g is the norm of the gravity vector, and σ is the bank angle, which is used by the Guidance and Control (GC) system as the main control variable.

This geometry is better visualized in figure 1.3.

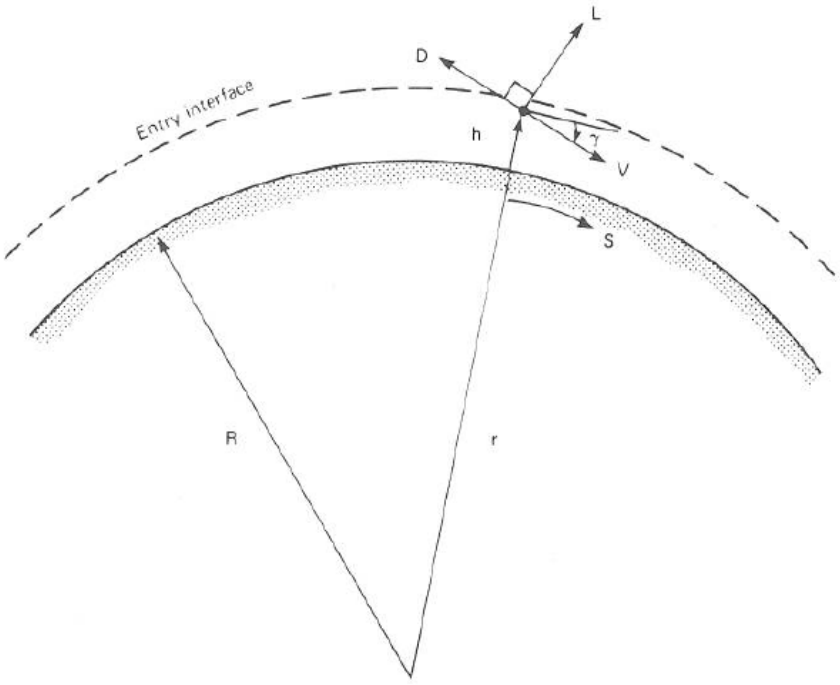

Figure 1.3: Geometry of the entry dynamics in the intrinsic reference frame [13].

Note that besides the bank angle, other two attitude angles are relevant in the 3-DoF setting: the angle of attack α and the angle of sideslip β. The angle of attack is the angle between an entry vehicle's principal

[4] Reference frames are thoroughly discussed in chapter 2, section 2.2

axis and the longitudinal relative velocity vector, and is used to evaluate the lift and drag forces. The angle of sideslip is the angle between the velocities along the vehicle's principal and lateral axis. In this work, a coordinated motion of the vehicle is assumed, which implies a zero-sideslip condition, and the zero side force.

Writing the 3-DoF approximation in this reference frame allows for a more intuitive interpretation of the entry motion, where the position and velocity vectors are characterized by

$$\text{position } \bar{p} = \begin{bmatrix} \chi \\ \lambda \\ h \end{bmatrix} \text{ and velocity } \bar{v} = \begin{bmatrix} V \\ \gamma \\ \psi \end{bmatrix}. \tag{1.5}$$

Apart from the sensitivity to EIP conditions and the huge loads of energy that must be dissipated by the RV during re-entry, the non-linearity and coupling of the (approximate) equations of motion (1.4) add another level of difficulty to the already complex re-entry problem. The re-entry profile is thus affected by EIP conditions that are mission and vehicle dependent, and is subject to stringent constraints with respect to maximum heat fluxes and aerodynamic loads, impacting TAEM conditions and vehicle design. On the other hand, vehicle design is critical for the definition of EIP and TAEM conditions, and for the determination of the re-entry profile and of the associated constraints. The intricacy of the re-entry problem thus leads to iterative approaches for finding appropriate GC solutions, which may be neither definite nor closed.

1.2.2 Bounds and constraints

The precise definition of the entry region is fundamentally conditioned by the planet's atmosphere. In the case of the Earth the atmosphere becomes relevant at altitudes below 120 km [29], at which point the air density is about 2.2×10^{-8} kg/m^3, and for altitudes lower than 20 km the Earth atmosphere is dense enough, about 8.9×10^{-2} kg/m^3 (and the RV has been significantly slowed down), to enable the deployment of parachutes, aerodynamic surface actuation, or any other techniques, to initiate the descent and landing phase. Therefore, in entry analysis, the EIP conditions are characterized by the vehicle state-space vector (1.5) at approximately 120 km of altitude, and the TAEM conditions (the point at which entry is considered to be concluded) are set at approximately 20 km of altitude. Termination of the entry phase is further characterized by the specification of a Heading Alignment Cone (HAC), defined by the maximum heading error $\Delta\psi$ (difference between RV and landing site heading angles) allowed for the RV at TAEM conditions

$$|\Delta\psi| \leq \Delta\psi_{\text{TAEM}}. \tag{1.6}$$

The clear identification of the upper and lower bounds of the entry region allows to look at the entry problem as a Two-point Boundary Value Problem (TBVP), fully characterized by (1.4), and the EIP and TAEM conditions.

Entry corridor constraints also bound this TBVP in terms of the region where entry solutions are feasible. These corridor constraints can be divided into four different classes [28]: the path, stability, performance, and trimmability constrains. The stability constraints are related to the vehicle dynamic equilibrium, which can be analysed only when the moment equations (1.3c) and (1.3d) are taken into account; the performance and trimmability constraints are associated with the aerodynamic characteristics of the vehicle: in this respect it is assumed that there is a reference angle of attack conform with the aerodynamic performance and trimmability requirements (this is further discussed in 1.3). Therefore, only the path constraints are relevant in the 3-DoF re-entry analysis. These are [34] the maximum heat flux, maximum aerodynamic acceleration (both were

already identified earlier in the discussion), maximum dynamic pressure, and the equilibrium glide condition:

$$\dot{Q} \leq \dot{Q}_{\max}, \tag{1.7a}$$

$$\left\| \vec{L} + \vec{D} \right\| / g_n \leq n_{\max}, \tag{1.7b}$$

$$q \leq q_{\max}, \tag{1.7c}$$

$$\left(\frac{V^2}{r} - g \right) \cos\gamma + L \cos\sigma \leq 0, \tag{1.7d}$$

where $\dot{Q}$ is the heat flux, $g_n = 9.80665\ m/s^2$ is the standard gravity, n is the number of acceleration g's (the acceleration of gravity at surface), q is the dynamic pressure. The constraints in (1.7) are mapped in the altitude-velocity plane in figure 1.4, using the requirements for the high lift-over-drag vehicle Phoebus [9].

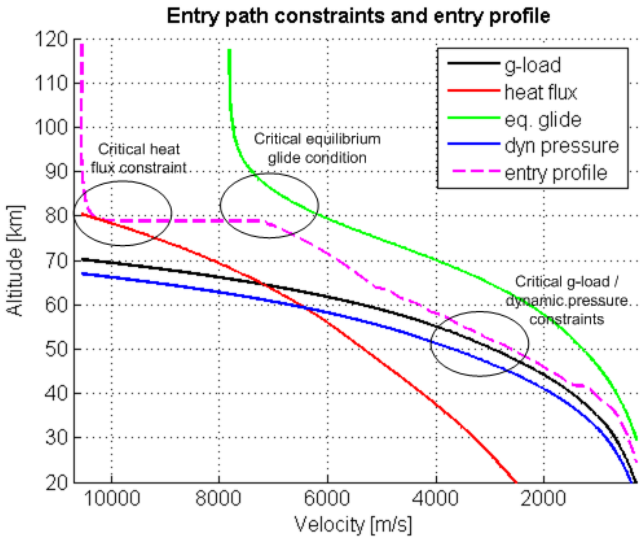

Figure 1.4: Entry corridor path constraints.

Equation (1.7a) represents the constraint in maximum heat flux, where heat flux $\dot{Q}$ is written as $\dot{Q} = C\rho^{\frac{1}{2}}V^{3.15}$, with C a multiplying constant. This expression for heat flux is an approximate expression for convective and radiative heating at stagnation point for a body entering the Earth atmosphere [13, 38]. This constraint is particularly critical in the early stages of re-entry. Equation (1.7b) is the maximum g-load constraint, and states that the aerodynamic acceleration must be lower than a pre-specified maximum g-load, which depends on the vehicle structure, or on the presence of human beings on-board. Equation (1.7c), where $q = \frac{1}{2}\rho V^2$, expresses the constraint on dynamic pressure. Finally, equation (1.7d) is the equilibrium glide condition. This last condition is not a hard constraint, in the sense that it serves to reduce the phugoid oscillations, being more meaningfull at higher altitudes.

1.2.3 Impact of EIP conditions on the re-entry profile

All initial conditions are important for the definition of the entry profile, but some are more relevant than others. Latitude, longitude and heading angle are more related to TAEM targeting and do not influence significantly the re-entry profile: once the range capabilities of the vehicle are determined, the heading angle is usually set in the direction of the landing site, and initial position in terms of latitude and longitude is defined such that final latitude and longitude are met. Altitude, as mentioned before, is an independent initial condition, as it defines the atmospheric layer limits with respect to air density that largely influences the dynamics. Therefore, the initial conditions that have the most impact in the re-entry profile are initial velocity and FPA. EIP velocity is determined by the mission scenario, while EIP FPA is conditioned directly by the re-entry constraints and

RV configuration.

Regarding the mission scenario, two extreme examples can be presented: the case where the RV comes from LEO, with an entry velocity of 7.9 km/s, and the case where the vehicle comes from LTO, with an entry velocity of 11 km/s. Examples of the former are the Shuttle Orbiter and the Soyuz RVs (in fact, all human entries with the exception of the Apollo Mission have been LEO entries), while the Apollo CM and the Phoebus concept vehicle were both designed for the Moon return. The greater the entry velocity, the more sensitive is the capture of the vehicle into atmosphere, and the heat flux and the decceleration that the vehicle will suffer thereafter are necessarily greater. Nonetheless, EIP velocity is fixed *a priori* by the mission scenario, and is not tunable.

The EIP FPA is thus the only EIP condition that is available for tailoring the entry profile (discounting the bank angle σ and the angle of attack α, two control parameters which are discussed in section 1.3), and it should be negative in order to ensure capture. Nonetheless, the shallowness (*i.e.* the FPA being closer to zero) or steepness (*i.e.* the FPA being more negative) of FPA depends on the entry velocity and on the vehicle configuration, and can be tuned accordingly.

As discussed in [13], a shallower EIP FPA results in a smoother re-entry profile, with reduced heat fluxes and acceleration loads. However, re-entry tends to last longer, which implies higher total heat loads[5]. Moreover, if the EIP FPA is too shallow, a skip-out scenario may occur, in which case the vehicle rebound off the atmospheric layer. Steeper FPAs, on the other hand, usually result in harsher and faster re-entries profiles, and usually ensure the capture of the vehicle, with excessive heat fluxes and g-loads associated.

Regarding the dependence of FPA on the entry velocity, typically, the higher the entry velocity, the steeper is the maximum FPA that still ensures capture. This means that for a LEO mission the maximum FPA will be shallower than for a Moon return mission.

Considering the importance of the RV configuration, if it has reduced or even zero L/D (ballistic re-entry), which is the case of the Apollo capsule or the Soyuz, maximum EIP FPA depends only on the entry velocity (in order to avoid skip-out) and minimum EIP FPA depends on the path constraints, *e.g.* maximum heat flux or aerodynamic acceleration. When the RV has an increased L/D, which is the case of the Shuttle Orbiter and Phoebus, it is possible to change lift orientation to enhance capture, which enables shallower FPAs than in the capsule-like case. On the other hand, the minimum FPA in lifting entry is not only conditioned by heat flux and aerodynamic acceleration, but also by the skip-out risk. Once the vehicle is deep in atmosphere, the steeper the FPA is, the higher the lift force will be, which may ultimately result in a rebound off the atmosphere.

In chapter 2, the implications of a slight variation of the EIP velocity and FPA will be further analysed.

1.3 Guidance in re-entry

1.3.1 The Guidance and Control function

The problem of a RV entering the atmosphere is fully bounded by the EIP conditions, the TAEM conditions and the entry corridor constraints. If the real EIP conditions were matched exactly with the desired EIP conditions, and since the re-entry dynamics is known from (1.3), a numerical propagation of the initial conditions would approximately provide the profile flown by the vehicle. The re-entry problem would thus be reduced to a selection, from a pool of EIP conditions, of the ones that would provide re-entry solutions compliant with the entry corridor constraints and the TAEM conditions.

However, this is not possible, as uncertainties are present in all of the re-entry process. Even if the nominal EIP conditions are targeted by the RV when descending from orbit, dispersion will occur and the actual EIP

[5] Because the heat load is the integral with respect to time of the heat flux, longer-duration re-entries have reduced heat fluxes but increased heat loads, while shorter-duration re-entries have higher heat fluxes but lower heat loads.

conditions will be different from those of the nominal case. Moreover, the RV aerodynamic characteristics are not really tested before the RV has performed a number of atmospheric re-entries, which leads to uncertainty in the RV aerodynamic database, and this is even more true when the atmospheric model is considered, for which there is significant uncertainty of the air density, especially at higher altitudes.

The fact that the nominal re-entry configurations suffer from significant uncertainties requires a GC function to be used. The main goals of the GC system are thus to minimize the impact of EIP dispersion on the re-entry profile, ensure that the entry corridor constraints are not violated while accounting for the atmospheric and aerodynamic uncertainties, and guide the RV towards TAEM conditions.

In order to do so, the GC system receives the RV state vector, and produces as outputs the angle of attack α and the bank angle σ, as these are the only variables that are not imposed by the 3-DoF dynamics in (1.4). However, the angle of attack definition is critical to maintain the dynamic equilibrium and stability of the RV during re-entry. Therefore, the angle of attack is usually pre-defined or computed by the inner-loop attitude control algorithms, and kept approximately to its reference values by the outer-loop GC system throughout re-entry, with only minor corrections admitted. The bank angle σ is thus the fundamental output parameter of the outer-loop GC system.

In a 3-DoF setting the RV attitude is not considered, which means that the GC system will only be applied to the outer-loop dynamics of the RV point-mass motion. The GC systems hereafter analyzed comprise a guidance function and a control function, often not clearly separated. The guidance function takes the true state information and produces a reference command, compliant with all entry requirements, that in principle ensures that the desired final conditions will be met. This reference command is then passed to the control algorithm, that also receives the true state information, and uses it to compare against the reference commands. It essays to track this reference by computing and minimizing the error between the reference and the true state space.

From the inversion of (1.4e), the bank angle σ is written as

$$\sigma = \arccos\left\{\frac{\left(V\dot{\gamma} - \frac{V^2}{r} + g\right)}{L}\right\}, \tag{1.8}$$

where it is important to note the direct dependence on the force equilibirum in the numerator, and the presence of the total lift force on the denominator. What is more, the bank angle controls directly the dynamics of $\dot{\gamma}$.

Considering (1.8), the control algorithms aim to find a reference lift force L_{c} that is substituted in the force equilbrium in the numerator of (1.8)

$$\sigma = \arccos\left\{\frac{L_{\mathrm{c}}}{L}\right\}. \tag{1.9}$$

The bank angle command is thus determined. Generally, finding an appropriate guidance solution for a given re-entry scenario and configuration is equivalent to finding an appropriate solution for the bank angle.

The bank angle is used to control the lift force, and the associated drag force, as depicted in figure 1.2. Since this generates lateral deviation from target, bank angle reversals are issued, where the sign of the bank angle is changed (note the cosine function does not provide the sign of the bank angle) but its magnitude is kept the same (in order to keep the vertical lift component as issued by the control algorithm). Crossrange control is seen in figure 1.5.

1.3.2 Review of some guidance solutions

Regarding the different GC system solutions, henceforth simply called guidance solutions, several methods are available, as identified in [28, 43]. In [43] a global distinction between predictor based guidance schemes and

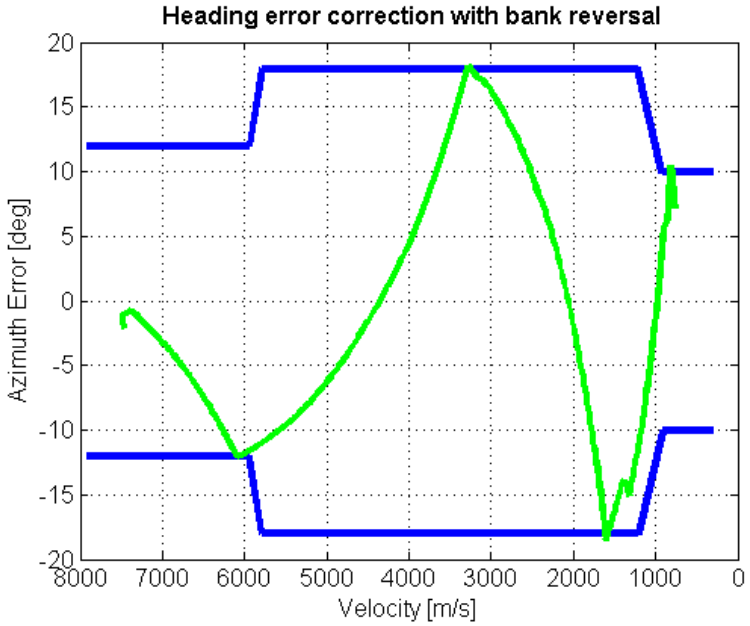

Figure 1.5: Correction of the crossrange error using bank angle sign reversals: the heading error grows up to the point where its derivative sign is changed due to a bank angle reversal command, thus being kept within the pre-defined bounds.

reference trajectory tracking guidance schemes is made and, under these two groups, several entry guidance methods are identified and discussed. Generally, predictor based guidance schemes suffer from being computationally demanding, which is a barrier to its on-board implementation. On the other hand, the bulk of the computation of the reference trajectory tracking algorithms is done off-line, which reduces the required computational loads, but profile adaptability is lost.

In [28] the guidance solutions are grouped into four categories: free profile, which consists of on-board state-space optimisation over the re-entry domain; fixed-shape profile, which uses a pre-defined reference trajectory stored on-board; feedback-like, which makes use of the system dynamics to generate a control solution; flight command law, which directly uses a pre-defined bank angle law. Each of this kind of guidance approach has its advantages and drawbacks: the free profile method is flexible and ensures the existence of a solution, but not of controllability, and is computationally demanding; the fixed-shape profile, the feedback-like approach, and the flight command law all ensure controllability, but not the existence of solution, which should be verified for each case.

Historically[6], the most successful entry algorithms are based on a reference profile generated off-line and stored on-board, which is tracked with gain-scheduled Proportional-Integral-Derivative (PID) controllers [42]. Notable examples of this are the Apollo [3], the Shuttle [17] and the Soyuz [19] Entry Guidance schemes.

Recently, guidance solutions with increased flexibility in reference profile generation and adaptable to uncertainties have been developed. In [10], a controller with scheduled gains, computed with Linear Quadratic Regulator (LQR) theory, is used to track a reference profile where energy is the independent variable. It is proved that the same controller gains can be used for different reference trajectories, provided that the RV is the same. In [34] the Shuttle Entry configuration is used as baseline for the development of an on-board reference trajectory generation algorithm, and a LQR controller based on [10] is used to track the generated reference profile. In [9] an innovative re-entry algorithm developped for a high lift-over-drag RV is presented, where the guidance solution consists of two different methods, feedback linearization through Non-linear Dynamic Inversion technique, and tracking via LQR control of a reference profile generated on-board.

[6]Note that this referes to Earth entry; entry on other planets is usually purely ballistic, which excludes active GC solutions

This last guidance solution is thoroughly presented in section 4.3, as it is extensively used in this work. Furthermore, the Apollo and the Shutte Entry guidance schemes are also thoroughly discussed in section 4.2 and chapter 3, respectively, as they also are an integral part of the work developed.

1.4 Overview of the work developed

The main goal of the work developed was the implementation of a guidance and control design tool, named REACTIVE - Re-Entry guidance and Adaptive ConTrol for Innovative VEhicles. This tool integrates two guidance schemes previously prototyped by GMV, the Apollo Entry Guidance and the Enhanced E-Guide, and a prototypation of the Shuttle Entry Guidance scheme. Furthermore, a procedure for generation of a reference profile for high L/D vehicles was developed, tested, and added to the tool.

The core of the tool is based on a simulation setting implemented in MATLAB, versatile enough in its structure to allow for the addition of several RVs, the inclusion of different guidance schemes, and even of other atmospheric models and planet environments. This simulation setting is organized in four distinct functions: the initialization function, the simulation function, the monte-carlo function, and the post-processing function, being able to run nominal simulations and test scenario and configuration uncertainties.

The guidance and control algorithms were then appended to the tool. The Shuttle Entry guidance was prototyped from scratch, while the Apollo Entry Guidance and the Enhanced E-Guide implementations were re-organized and consolidated, as they had been previously prototyped by GMV for the Highlift project. Moreover, the procedure for profile generation was conceived, developed and prototyped.

The Shuttle Entry Guidance [17] uses a reference profile computed offline and stored on-board, based on a velocity-drag profile mapping, which is tracked via a gain-scheduled PID controller, making use of the moderate lifting capabilities of the Shuttle Orbiter. The profile is constructed based on the expected mission range requirements, and it is possible to make corrections to the original profile in real time, in order to adapt it to slight changes in the range constraints. The implementation of this algorithm, described in chapter 3, was preceded by the modeling of the Shuttle Orbiter, the RV that is used as baseline for the STS Guidance.

The Apollo Entry Guidance consists of two main phases: the atmospheric capture, where the capsule is rotated so as to rotate the lift vector downwards and increase the force that pulls the vehicle into deep atmosphere, and the targeting phase, where a reference profile is tracked using a PID controller.

Enhanced E-Guide is an innovative and adaptive approach that uses feedback linearization through Non-linear Dynamic Inversion (NDI) control [47] in the first entry phases, and a Linear Quadratic Regulator (LQR) gain-scheduled controller [10] for reference trajecotry tracking in the last phase landing site targeting. With this algorithm it is possible to perform mid-entry retargeting, as the last phase reference trajectory is generated on-board at the triggering of the targeting phase.

The previously available algorithms, the Apollo Entry guidance and the Enhanced E-Guide, are suitable for low L/D (capsule-like) and high L/D RVs, respectively. The Shuttle Entry Guidance algorithm was added to provide guidance solutions for moderate L/D RVs, not covered by the others.

The last guidance scheme added to REACTIVE was a semi-analytical procedure for on-board profile generation that enables precise landing site targeting for high L/D RVs. The reason for its development was the mediocre performances of the on-board reference profile generation algorithm implemented in Enhanced E-Guide in the landing site targeting phase, namely its excessive computation times, which would certainly be a barrier to its implementation in on-board software. In that respect, the newly developed solution is computationally lighter and more accurate with respect to the downrange requirement. The procedure generates a reference profile semi-analytically by pre-estimating profiles for altitude and flight-path angle, directly evaluating the equations of motion, and determines the downrange profile by analytical integration of the downrange equation using the linear least squares method [40]. The associated bank angle law is computed so that the

downrange requirement is precisely met. This profile generation algorithm was tested using LQR control for the reference tracking, and it was further validated through Monte-Carlo tests.

REACTIVE thus collects all these guidance schemes and integrates them in one single tool. The associated baseline vehicles, the Apollo CM, the Shuttle Orbiter, and the Plane-shaped Hypersonic Orbital Entry BUS (Phoebus) concept vehicle were also added to REACTIVE's RV database. Furthermore, REACTIVE aims at extending the available guidance schemes to the associated RV L/D class. This means that the prototypations of the guidance schemes, which were tested and validated using the associated baseline vehicles, were generalized and made independent of their baseline vehicles, so that each of the algorithms was made adaptable to different RVs. Therefore, the Apollo Entry Guidance is now suitable for the broader capsule-like RV class, the Shuttle Entry Guidance is suitable for the moderate L/D RV class, and the Enhanced E-Guide is suitable for the high L/D class.

Furthermore, REACTIVE's implementation allows expansions to other environments. Using this feature, the planet Mars environment, for which there are a number of projects under way promoted by ESA and NASA, was added to REACTIVE.

Chapter 2

Re-entry simulator

2.1 Introduction

The simulator setting is the core of the REACTIVE tool, as all the guidance functions will be appended to it. It simulates the free entry motion of the RV from the EIP conditions up to TAEM conditions. If a GC function is further connected, the outputs of the GC system, which are the bank angle and the angle of attack, become control inputs to the simulation equations, and the RV motion during re-entry is controlled.

The re-entry simulator is thus a numerical propagator of the 3-DoF differential equations of motion (1.3a) and (1.3b), *i.e.* only point-mass dynamics are considered, as discussed in chapter 1. It is important to note that this setting is sometimes defined as 4-DoF, because of the bank angle parameter that allows for the rotation of the lift vector and thus adds one extra dimension. However, this convention is not adopted here, as there is no dynamics associated with the bank angle parameter.

In order to propagate the equations of motion, the simulator requires the definition of a planet environment, an atmospheric model, and the RV aerodynamic parameters. These databases are loaded to the simulator when it is initialized, and called at every time-step for evaluation. Furthermore, the simulator is prepared to receive as inputs the signals coming from the actuators, and its output signals are sent to the sensors. However, the dynamics of the actuator and sensor blocks are currently considered to be identities, which means that the simulator receives as inputs the command signals from the GC system (when connected) and outputs the true state-space vector. In this way, the simulator was structured with an architecture similar to the one described in [44].

The simulator was implemented in MATLAB using a collection of routines already available, modified to suit the current implementation, while a few others were prototyped from the beginning. The implementation of the simulator was thus a work of integration, consolidation, and addition of minor adjustments. It relies on four core functions, the initialization, simulation, Monte-Carlo, and post-processing functions, that are managed by a main function.

2.2 Reference frames

There are two main reference frames used in the simulation process: the Earth Centered Earth Fixed (ECEF) reference frame, where the equations of motion are propagated, and the Intrinsic reference frame, used in the definition of the initial and final conditions, of the path constraints, and also appearing in the implementation of most guidance schemes.

The ECEF reference frame, depicted in figure 2.1, is defined as [4]:

1. Origin at the center of the planet;

2. X-axis: aligned with Equatorial plane, pointing to a Prime Meridian;

3. Z-axis: orthogonal to the X-axis, aligned with the Earth's rotation axis pointing towards north;

4. Y-axis: such that the resulting reference frame is an orthogonal right-handed reference frame.

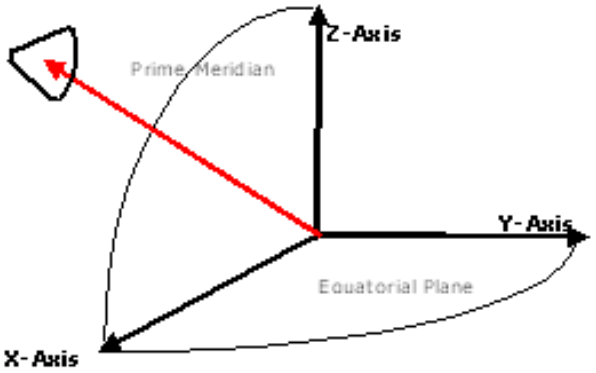

Figure 2.1: Earth Centered Earth Fixed reference frame [4]

This frame accompanies the rotation of the planet, implying that every point on the planet's surface has the same position coordinates, irrespective of the time passed. The position vector $\vec{r}$ and velocity vector $\vec{v}$ define the RV's state space, where $\vec{r}$ is decomposed in $\vec{r}_x$, $\vec{r}_y$, $\vec{r}_z$, with modulus $r = \left(r_x^2 + r_y^2 + r_z^2\right)^{\frac{1}{2}}$, and $\vec{v}$ is decomposed in $\vec{v}_x$, $\vec{v}_y$, $\vec{v}_z$ with modulus V.

The Intrinsic reference frame is defined as [4]:

1. Origin at the body center of mass;

2. X-axis: aligned with the body relative (to the planet) velocity vector;

3. Y-axis: orthogonal to the plane formed by the body position and relative velocity vectors;

4. Z-axis: such that the resulting reference frame is a right-hand orthogonal system.

In this frame the state vector is defined as in (1.5): position components χ, λ, and h, and velocity components V, γ, ψ. Since one of the axis is aligned with the RV velocity vector, the drag and lift forces can be written directly in this frame, along the X-axis and the Z-axis, respectively. This simplifies the writing of the equations of motion and provides more insight to the vehicle motion during re-entry, which justifies why this reference frame is commonly used for the development of guidance solutions.

2.3 Simulation

2.3.1 Equations of motion

The equations of motion for the RV are reduced to translational dynamics, as discussed in chapter 1. Writing explicitly the forces acting on the RV in the ECEF reference frame, equations (1.3a) and (1.3b) become

$$\frac{\mathrm{d}\,\vec{r}}{\mathrm{d}\,t} = \vec{v} \tag{2.1a}$$

$$\frac{\mathrm{d}\,\vec{v}}{\mathrm{d}\,t} = \vec{D} + \vec{L} + \vec{g} + 2\,\vec{\omega} \times \vec{v} + \vec{\omega} \times (\vec{\omega} \times \vec{r}) \tag{2.1b}$$

where $\vec{D}$ and $\vec{L}$ are the drag and lift force vectors per unit of mass. Apart from the aerodynamic and gravitational accelerations, the terms dependent on Earth's angular velocity are present because the reference

frame is not inertial: these are the Coriolis acceleration and centripetal acceleration. Additionally, it should be noted that no thrusting acceleration is considered during re-entry.

For the propagation of the equations of motion, and for the termination of propagation, the definition of the EIP and TAEM conditions is required. Initial conditions for time $t = t_0$, in the intrinsic reference frame, are written as

$$\chi_0 = \chi(t_0), \quad \lambda_0 = \lambda(t_0), \quad h_0 = h(t_0), \tag{2.2a}$$

$$V_0 = \gamma(t_0), \quad \gamma_0 = \gamma(t_0), \quad \psi_0 = \psi(t_0), \tag{2.2b}$$

while final conditions in terms of final velocity are

$$\begin{gathered} V_{\mathrm{f}} = V_{\mathrm{TAEM}}, \\ h_{\mathrm{f}} = h(V_{\mathrm{f}}), \quad s_{\mathrm{f}} = s(V_{\mathrm{f}}), \quad |\Delta\psi_{\mathrm{f}}| \leq \Delta\psi(V_{\mathrm{f}}). \end{gathered} \tag{2.3}$$

The initial and final conditions, written in the intrinsic reference frame definition, are translated and rotated internally to the ECEF reference frame and used to initialize and terminate the propagation of the equations of motion (2.1), which is done in the ECEF reference frame.

2.3.2 Atmospheric and aerodynamic parameters

For the propagation of (2.1) it is necessary to have a model of the atmosphere and of the RV aerodynamic characteristics, which are used to evaluate the aerodynamic forces, lift $\vec{L}$ and drag $\vec{D}$. The norms of these forces per unit of mass are given by

$$L = \frac{1}{2}\rho V^2 \frac{S}{m} C_{\mathrm{L}}, \quad D = \frac{1}{2}\rho V^2 \frac{S}{m} C_{\mathrm{D}}, \tag{2.4}$$

where ρ is the air density, V is the aerodynamic velocity, S/m is the ratio of the vehicle presented area over mass, and C_{L}, C_{D} are the lift and drag coefficients, respectively. An atmospheric model is necessary to determine ρ and a RV aerodynamic database is required to provide C_{L}, C_{D} and S/m.

The model used to approximate Earth's atmosphere is a combination of three atmospheric models, detailed in table 2.1. This model provides a mapping of air density ρ, air temperature, air pressure, and sound speed v_{s} with respect to altitude h.

USSA 76	between 0km and 24km
GRAM 99	between 24km and 100km
MSIS 86	between 100km and 2000km

Table 2.1: Atmospheric model.

The altitude-air density mapping resulting from the models used is depicted in figure 2.2.

The RV aerodynamic database provides the lift and drag coefficients, which are functions of the angle of attack α and the Mach number M, $C_{\mathrm{L}}(\alpha, M)$ and $C_{\mathrm{D}}(\alpha, M)$. The angle of attack is determined by the guidance and control function and the Mach number relation is dependent on the RV velocity and atmospheric sound speed (which is mapped with respect to altitude),

$$M = \frac{V}{v_{\mathrm{s}}(h)}. \tag{2.5}$$

Other RV characteristics required for simulation are also available, namely the S/m ratio, the thermodynamic coefficients, *etc.*

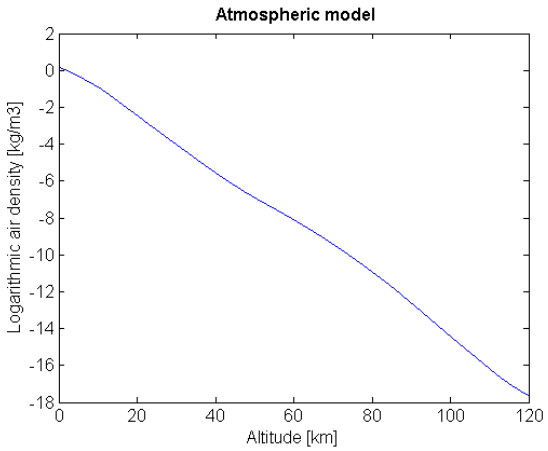

Figure 2.2: Atmospheric model: air density with respect to altitude.

2.3.3 Planet environment

The planet fully determines the acceleration acting on the RV (excepting the aerodynamic accelerations $\vec{L}$ and $\vec{D}$), characterized by the gravity acceleration and the apparent accelerations, the Coriolis and the centrifugal accelerations. These terms, assuming a circular planet model, are given by

$$\vec{g} = -\mu \frac{\vec{r}}{r^3}, \tag{2.6a}$$

$$\vec{a}_{\mathrm{Cor}} = 2\vec{\omega} \times \vec{v}, \tag{2.6b}$$

$$\vec{a}_{\mathrm{Cf}} = 2\vec{\omega} \times (\vec{\omega} \times \vec{r}), \tag{2.6c}$$

where μ is the gravitational parameter. The values of the main environment parameters are depicted in table 2.2 for the case of the Earth [33].

Parameters	Symbol	Units	Values
Gravitational parameter	μ	$[\mathrm{m}^3/\mathrm{s}^2]$	$3.986004418 \times 10^{14}$
Rotation rate	ω	[rad/s]	7.2921150×10^{-5}
Equatorial radius	R	[m]	6378137

Table 2.2: Earth environment parameters.

2.4 Simulator implementation

2.4.1 Main function

The main function main.m is the managing function of the simulator: it interacts with the user, allowing him/her to choose how to proceed in simulation, and calls the functions to initialize, run or process the results of simulation. The flowchart of this main function is depicted in figure 2.3.

2.4.2 Initialization

The initialization function init.m is the first function run by the simulator, when it is required to load a different scenario or configuration setting from the database. All the parameters required for the integration of the equations of motion (discussed in section 2.3), as well as other functional parameters, are loaded so that they

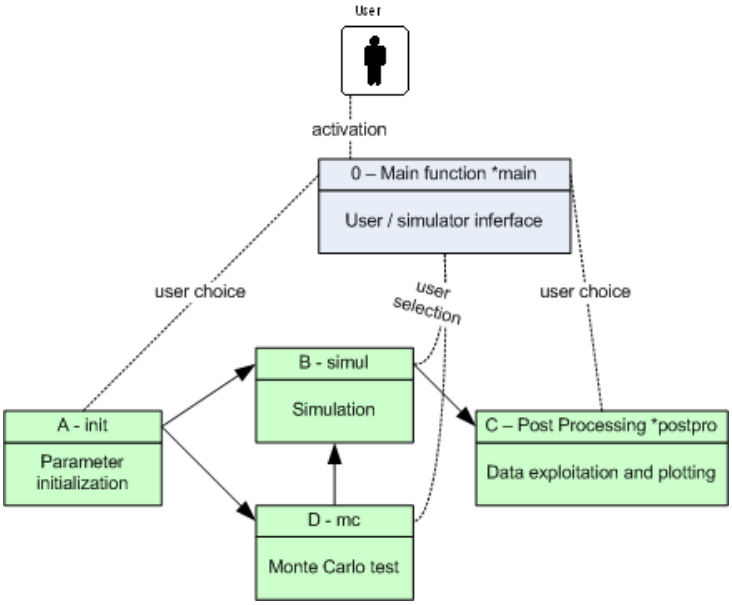

Figure 2.3: Main function algorithm.

are available during simulation. The flowchart asssociated to the initialization function is depicted in figure 2.4.

There are six kind of parameters in the database (figure 2.4):

- General parameters, which are functional parameters, e.g. unit conversion parameters;
- Atmospheric parameters, which are the parameters associated to the atmospheric model, discussed in section 2.3.2;
- Environment parameters, which are the parameters related to the planet environment, discussed in 2.3.3;
- Spacecraft parameters, which are all the parameters related with the RV, particularly the aerodynamic database discussed in 2.3.2;
- Mission parameters, which include EIP conditions, TAEM conditions, and landing site coordinates;
- GNC parameters, which are all the parameters related to the implemented guidance schemes (further discussed in chapters 3 and 6).

These parameters are loaded to three distinct structures, the Dynamics and Kinematics Equation parameter structure, the Mission parameters structure, and the GNC parameters structure, and saved to the SimData.mat file, which is called to load the simulation.

2.4.3 Simulation

The simulation function evaluates the equations (2.1) and integrates them with respect to time, thus simulating the re-entry motion of the RV from EIP conditions up to TAEM. In order to do so, it assesses at every time step the atmospheric properties, the RV aerodynamic values, and the planet environment, and outputs the state-space vector that characterizes the RV at that point. If a GC function is connected, the simulation function receives as inputs the bank angle and angle of attack commands, that are also used to evaluate (2.1). The simulation function further checks if final conditions have been reached or if the path constraints have been violated, so as to terminate or flag the occurrence of such an event.

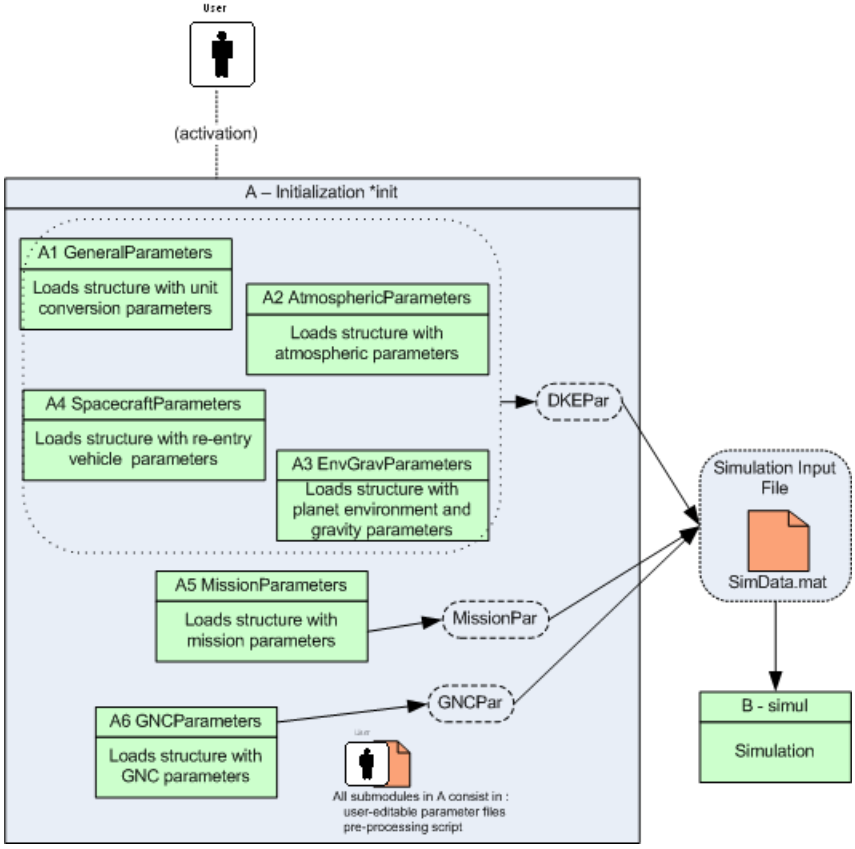

Figure 2.4: Initialization algorithm

The simulation function is initialized with all the parameters and databases in SimData.mat, and saves all the output data in the SimResults.mat. The detailed flowchart asssociated to the simulation function is depicted in figure 2.5.

The propagation of the differential equations of motion uses MATLAB's numeric integration function ode4.m function. While the propagation is performed in the ECEF reference frame, the intrinsic reference frame is used for computation of the aerodynamic variables, which are then converted to the ECEF reference frame. The event control function EOMevents.m regulates the integration process, checking whether limit or final conditions have been reached.

2.4.4 Monte-Carlo setting

The Monte-Carlo test function relies mostly on the simulation function, but adds uncertainties to the initial conditions and to the atmospheric and aerodynamic databases. The flowchart of the Monte-Carlo setting is depicted in figure 2.6.

The uncertainties added to EIP conditions are modeled as

$$\vec{x} = \vec{x}_0 + \mathrm{E}\left[\vec{e}_\mathrm{i}\right] + p\,\sigma\left[\vec{e}_\mathrm{i}\right], \tag{2.7}$$

where $\vec{x}$ is the perturbed intial state-space vector, $\vec{x}_0$ is the nominal initial state-space vector, p is a random number in the interval $[0, 1]$ and $\sigma\left[\vec{e}_\mathrm{i}\right]$ and $\mathrm{E}\left[\vec{e}_\mathrm{i}\right]$ are the standard deviation and mean of the error $\vec{e}_\mathrm{i}$ to be added.

Regarding the uncertainties in atmospheric air density, they are modeled as

$$\rho = \rho_0\left(1 + e_\rho\right), \quad e_\rho = Kp\frac{\rho_\mathrm{u}}{100} \tag{2.8}$$

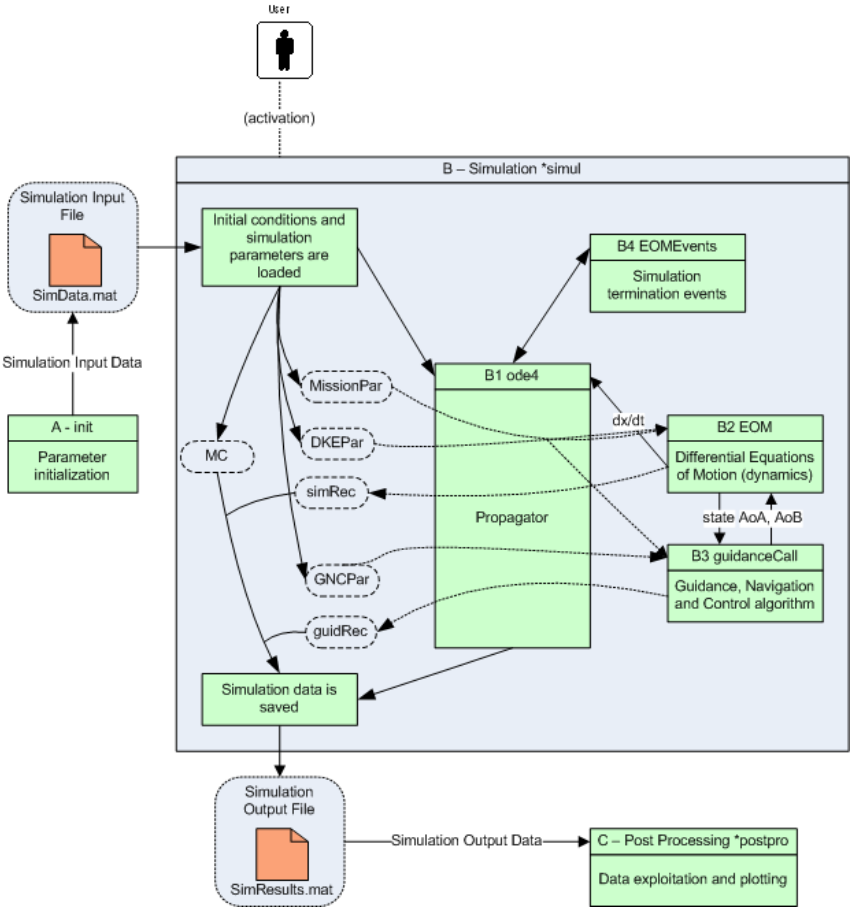

Figure 2.5: Simulation algorithm.

where ρ is the perturbed air density, ρ_0 is the nominal air density value, K is an arbitrary multiplying factor, p is a random number in the interval $[0, 1]$ and ρ_{u} is the atmosphere uncertainty in percentage, which depends on altitude. The reference values for ρ_{u} are shown in figure 2.7 and in table 2.3.

Altitude	[km]	0	8	13	16	20	35	65	85	95	140
Air density uncertainty	[%]	2	2	6	6	10	10	30	30	50	50

Table 2.3: Air density uncertainty.

Finally, the uncertainty model in the aerodynamic database is defined as

$$C_{\mathrm{L,D}} = C_{0\,\mathrm{L,D}} + p\,\sigma\left[\vec{e}_{\mathrm{c}}\right], \tag{2.9}$$

where $C_{\mathrm{L,D}}$ is the perturbed aerodynamic coefficient, $C_{0\,\mathrm{L,D}}$ is the nominal aerodynamic coefficient, p is a random number in the interval $[0, 1]$ and $\sigma\left[\vec{e}_{\mathrm{c}}\right]$ is the standard deviation of the error $\vec{e}_{\mathrm{c}}$ to be added.

2.4.5 Result post-processing

The post-processing function is the simulator's function that processes the input data stored in SimData.m and the output data stored in SimResults.m, and provides the plots and graphics for user interpretation. The flowchart asssociated to the result post-processing function is depicted in figure 2.8.

The post-processing tool allows for viewing separately the true simulation output and the guidance outputs, when available.

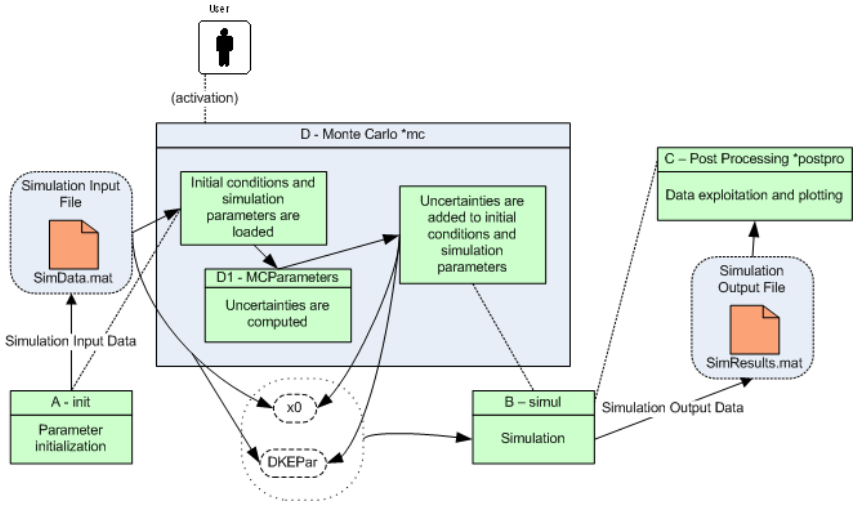

Figure 2.6: Monte-Carlo algorithm.

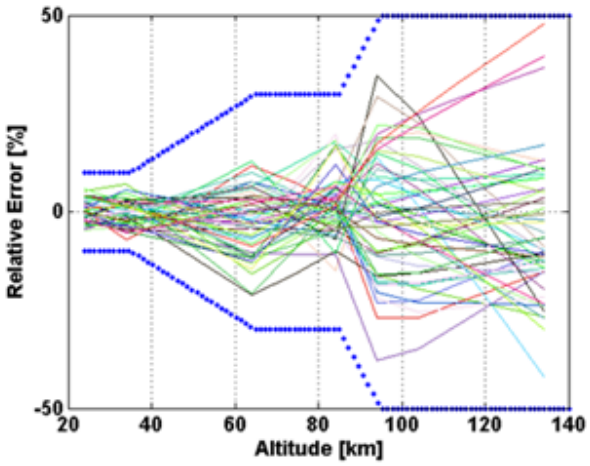

Figure 2.7: Air density uncertainty with respect to altitude [12].

2.5 Tests

2.5.1 Implementation test

The simulator was validated against a previously prototyped simulator. This validation was performed by running simulations with the initialization shown in table 2.4, and the atmospheric and environment databases discussed in sections 2.3.2 and 2.3.3, in both simulators. Nominal simulation was considered, as the aim of the validation was to access the proper implementation of the equations of motion and the associated computations, and an arbitrary moderate L/D RV was used. The results are presented in figures 2.9 to 2.11.

The fact that all state-space variables match exactly the results of the original simulator show that the simulator is working properly, and that it can be used in 3-DoF re-entry simulation.

It is also seen that the peaks in altitude lag behind the peaks in FPA, as the altitude derivative depends on the FPA (1.4a)

$$\dot{h} = V \sin\gamma.$$

Therefore, a maximum FPA will correspond to a maximum in the altitude rate, and a zero in FPA will correspond to a local minimum/maximum in altitude. This also shows why the bank angle is an efficient approach to control the entry motion: since it appears in expression (1.4e) for the evaluation of $\dot{\gamma}$, the bank maneuver impacts directly the evolution of FPA, that itself conditions the altitude profile. Considering that

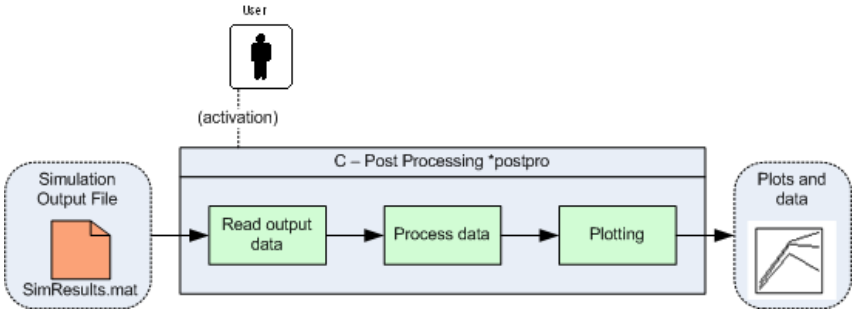

Figure 2.8: Post-processing algorithm.

Initial conditions		
Latitude	[deg]	-30.83
Longitude	[deg]	-164.06
Altitude	[km]	120
Velocity	[m/s]	7450
FPA	[deg]	-1.21
Heading	[deg]	65.60

Table 2.4: Initial conditions used for validation.

the path constraints (1.7) can be mapped in the altitude-velocity plane, it is clear that the selection of the appropriate bank angle allows for keeping the vehicle within the path constraints.

2.5.2 Impact of EIP conditions and L/D in re-entry trajectory

Following the discussion in section 1.2.3 about the importance of EIP velocity and FPA on the re-entry profile, tests were conducted to evaluate this in a simulation setting. The EIP conditions were thus set to values different from nominal, and the results obtained were compared to the nominal scenario.

The considered EIP conditions variation can be found in table 2.5, while the nominal EIP configuration is the same as before (table 2.4). For the first EIP conditions set, only velocity at EIP was varied, while in the second set only FPA at EIP was varied. Six simulation shots were run in total, and the results are shown in figure 2.12.

Nominal EIP FPA	Variation from nominal EIP velocity	[m/s]	-100	0	+100
Nominal EIP velocity	Variation from nominal EIP FPA	[deg]	-1	0	+1

Table 2.5: Variation of EIP conditions for evaluation of its impact on re-entry profile

The results confirm what had been asserted in chapter 1 relative to the importance of EIP FPA. A shallower FPA than nominal allows for a smoother re-entry profile, with less oscillations in the altitude-velocity plane, whereas a steeper FPA induces heavy entry profile oscillations. Note, however, that shallower FPAs than the ones considered here may result in a rebound off the atmosphere, while steeper FPAs might also result in a skip out trajectory due to the surge in the lift force associated to the increase in air density. This is shown in figure 2.12 for the steeper EIP FPA, where there is a peak in altitude after the great dive into the atmospheric layer. Steeper FPAs may also lead to violation of the path constraints, although this is not shown in the graphic plot.

Regarding EIP velocity, it is seen that a slight increase of 100 m/s may result in a skip-out trajectory, where

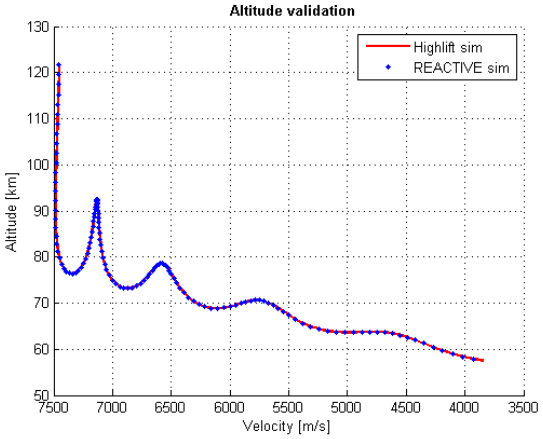

Figure 2.9: Altitude-velocity plot for simulator validation.

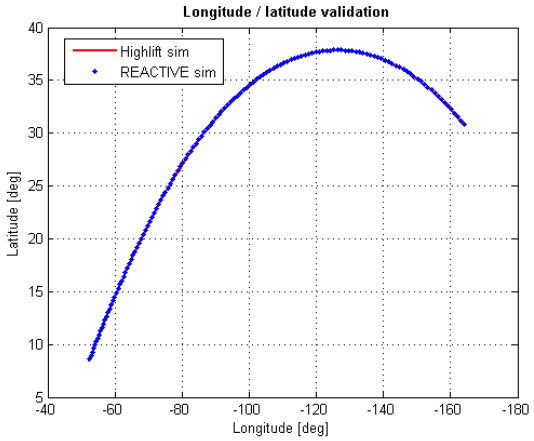

Figure 2.10: Latitude-longitude plot for simulator validation.

the vehicle is not captured, as shown in the profile obtained for the highest entry velocity, where the vehicle is barely kept in atmospheric environment. When the entry velocity is reduced, the re-entry profile becomes more smooth, and the magnitude of the longitudinal oscillations is reduced (though this effect is more noticeable in the case of the shallower EIP FPA).

The impact of the different RV aerodynamic characteristics in the re-entry profile is shown in figure 2.13, where EIP conditions are the same in all cases (table 2.4). For convenience, the re-entry time was limited to be the same time for the three tests, which enables drawing conclusions about the length of re-entry in each case.

It is concluded that the L/D ratio impacts decisively the RV descent rate. While this should be obvious, as more lift per drag implies a greater force in the upward direction capable of sustaining the vehicle in flight during more time, the implications of this are significant. Considering that all three simulations took the same time, it is noted that the low L/D RV, by the time simulation is finished, has decelerated significantly (to about $M = 2$), and is at 30 km of altitude. At the same time, the moderate L/D vehicle is at 60 km of altitude and the high L/D is at 70 km of altitude, which is more than the double, and at $M \approx 10$. This implies that to reach the same conditions as the low L/D RV, more time is required and more range is covered. This last aspect defines the targeting ability of the RV.

Furthermore, the oscillations in the RV phugoid motion are more frequent and more pronounced with higher L/D, as following the dips in atmosphere, the surge in lift (due to increased air density) is more significant. Nonetheless, associated to the longitudinal instability also comes improved controllability, as the bank angle

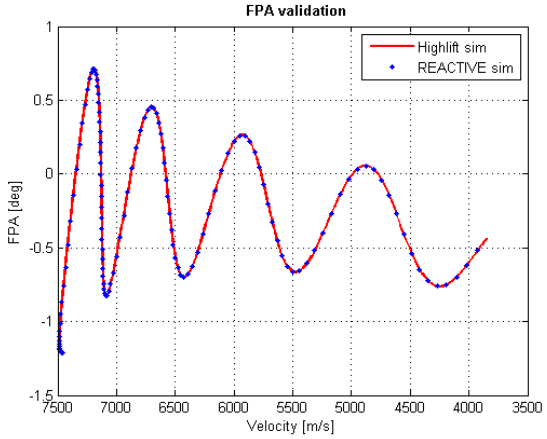

Figure 2.11: FPA-velocity plot for simulator validation.

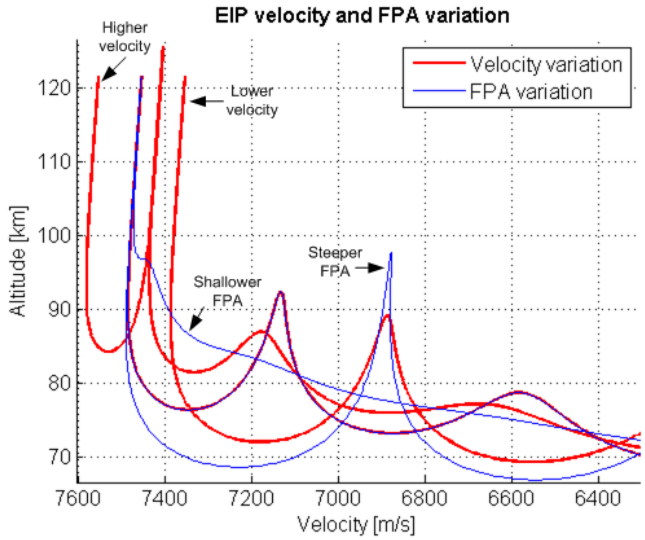

Figure 2.12: Detail of the altitude-velocity entry profile for a moderate L/D RV, with EIP velocity and EIP FPA variation.

commands are able to shape decisively the entry profile due to the higher L/D margins.

2.6 Remarks

The simulator implementation was fully successful, which is demonstrated by its independent validation against another fully validated simulator.

Regarding the reference frames discussed in the first section (section 2.2), it should be added that more reference frames are used in the simulation process, namely intermediate reference frames in the transformation of the intrinsic to the ECEF reference frame. These other reference frames are fully identified in [4], but since they do not provide any additional insight they were omitted in the discussion.

Finally, it is important to remember that the simulator only allows for 3-DoF simulations. While this is acceptable for re-entry profile analysis, as already discussed, it limits the applicability of the simulator to other contexts. The upgrade to 6-DoF setting, as in [44], will be fundamental for the simulator to be applicable to other re-entry simulation settings.

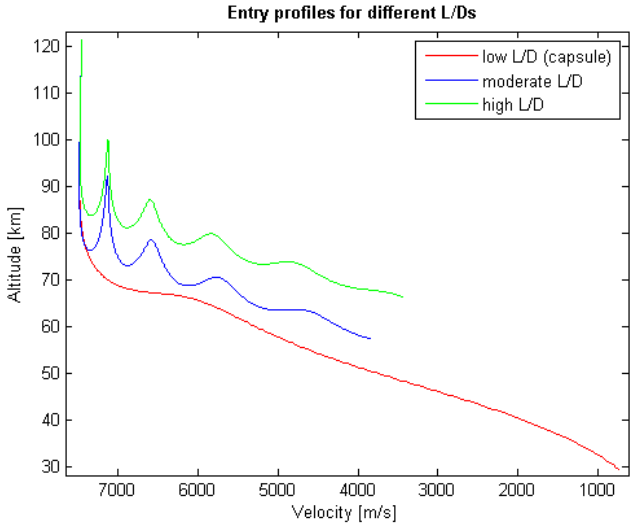

Figure 2.13: Altitude-velocity plot of entry profiles of RVs with different L/Ds.

Chapter 3

Shuttle Entry Guidance scheme implementation

3.1 Introduction

NASA's Space Transportation System (STS) is the state of the art technology for manned missions in space. It is the only reusable winged spacecraft that has been in orbit and re-entered atmosphere successfully several times during the past thirty years [23]. The STS system comprises three main components: the Shuttle Orbiter, which houses the crew, and is the only STS component that eventually re-enters Earth atmosphere, the solid rocket boosters, which power the ascent of the vehicle during launch, and the external fuel tank, the only non-reusable component, which contains the fuel for the main engines during launch.

For de-orbiting, thrusters are used to decelerate the Orbiter from LEO velocity to EIP conditions. The re-entry process lasts about 30 minutes, beginning at an altitude of 400 thousand feet (approximately 122 km) and ending at 45 thousand feet of altitude (approximately 13 km), from which point manual control takes over and steers the vehicle in the direction of the HAC of the primary landing site, the Kennedy Space Center (KSC), or to the secondary landing site available, the Edwards Air Force Base in California [1].

The Shuttle Orbiter enters the Earth atmosphere as a lifting glider, making use of the Shuttle Entry Guidance system [17] to dissipate energy by making a series of banking maneuvers. These bank angle commands are computed by a gain-scheduled PID controller that enables the tracking of an offline generated drag-velocity reference profile, compliant with the range requirements and with the path constraints.

Regarding the REACTIVE tool, that will be discussed in chapter 6, the addition of the Shuttle Entry Guidance algorithm was of particular importance. The algorithms previously available, the Apollo Entry Guidance and the Enhanced E-Guide, which will be discussed in chapter 4, were developed for low $L/D < 0.5$ capsule-like and high $L/D \approx 2$ RVs, respectively, whereas the Shuttle Entry Guidance was designed for the moderate $L/D \approx 1$ Shuttle Orbiter. Therefore, this entry algorithm fills in a missing gap in the coverage of all kinds of RVs classes with different guidance approaches, thus overhauling the capabilities of REACTIVE and turning it into a full-fledged simulator. The generalization of this algorithm is also a critical aspect for its inclusion in the REACTIVE tool, as it will enable REACTIVE to have an algorithm applicable to moderate L/D RVs other than the Shuttle Orbiter.

3.2 Modelling the Shuttle Orbiter re-entry vehicle

The Shuttle Orbiter is the only winged RV that has been used in real operational environment, having been designed for LEO return. It is bigger and heavier than any of the other RVs considered in this work[1]: it has a length of 122.17 ft (37.24 m), a wingspan of 78.06 ft (23.79 m), a presented area of about 250 m^2, and at landing its maximum allowed weight is 230000 lb(104000 kg), while the empty orbiter structure weigths 151205 lb (68585 kg) [23]. Its moderate $L/D \approx 1$ makes it a significantly maneuverable RV, able to cover one quarter of planet turn distance. The vehicle configuration is further depicted in figure 3.1.

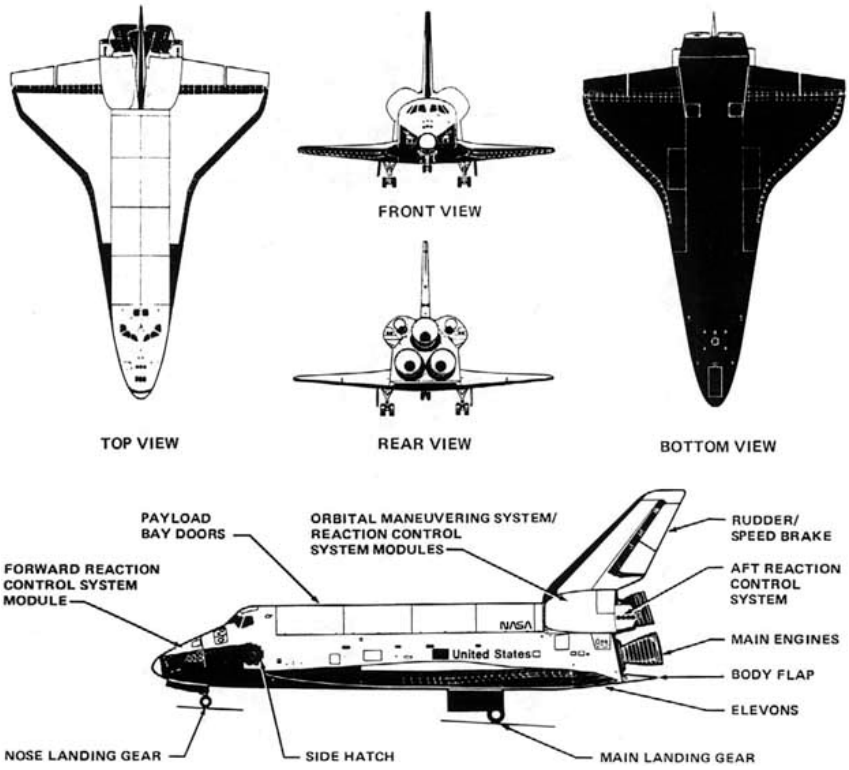

Figure 3.1: Shuttle Orbiter detail [16].

In order to simulate the Orbiter re-entry it was necessary to construct the Orbiter aerodynamic database [25, 25, 25]. The lift $C_{\mathrm{L}}(\alpha, M)$ and drag $C_{\mathrm{D}}(\alpha, M)$ coefficients, which depend on the angle of attack α and the Mach number M, are shown in figure 3.2.

3.3 The Shuttle Entry Guidance scheme

The Shuttle Entry Guidance scheme [17] is based on the tracking of an offline generated drag-velocity reference profile. It does so by comparing the current state of the RV against the reference profile stored on-board, and computing the bank angle and angle of attack commands which ensure that the RV motion will coincide with the pre-defined reference profile, via a PID controller.

3.3.1 The reference profile

The Shuttle reference profile is divided into five different phases [17], where each phase corresponds to an analytical function of drag with respect to velocity $D(V)$, or energy $D(E)$, that take into account the various dynamic regimes which the vehicle experiments during re-entry: the Temperature Control phase, where drag

[1] The other baseline RVs, the Apollo CM and Phoebus, are discussed in chapter 4

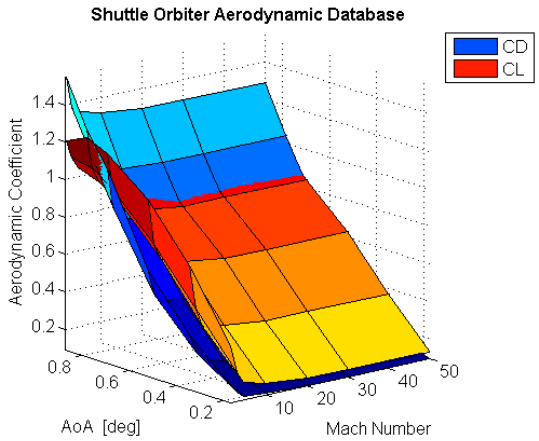

Figure 3.2: Shuttle Orbiter aerodynamic database: $C_{\mathrm{L}}(\alpha, M)$ and $C_{\mathrm{D}}(\alpha, M)$ functions.

is related to velocity via a quadratic relation, the Equilibrium Glide phase, where the FPA time derivative is considered to be zero, the Constant Drag phase, where drag is constant with respect to velocity, and the Linear Energy Transition phase, where drag is mapped with respect to energy via a linear relation. The phases of the reference profile are analytically defined and it is possible to compute the range associated with each phase, that can be added to find the total range.

The reference profile is defined so that the predicted total range matches the mission expected range, without violating the path constraints. For this effect, there are free coefficients in every drag-velocity relation, that are determined so that the range requirement is satisfied. A reference profile [17] is shown in figure 3.3, where the five different phases of the entry profile and the path constraints are identified.

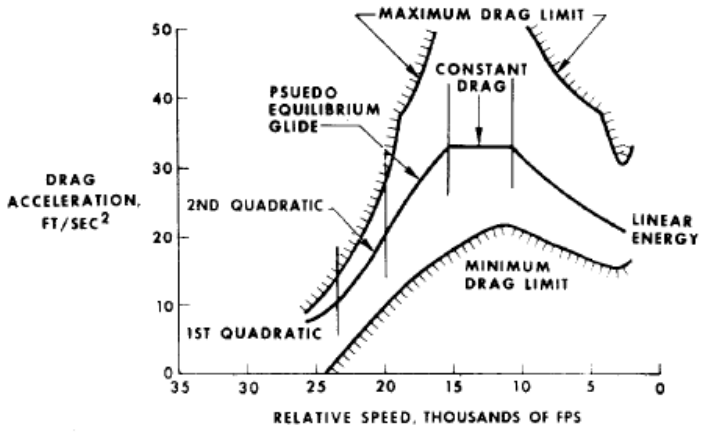

Figure 3.3: Shuttle Orbitar reference entry profile [17], with the path constraints and the different entry phases identified: first and second temperature control, equilibrium glide, constant drag, and linear energy phases.

Below, each of the profile phases is described.

Temperature Control

The Temperature Control phase uses a quadratic relation between drag and velocity

$$D = C_1 + C_2 V + C_3 V^2, \tag{3.1}$$

where C_1, C_2 and C_3 are arbitrary constants.

This phase is composed of two quadratic sub-phases, which means that while the expression for $D(V)$ is

identical (quadratic) in both sub-phases, the coefficients C_1, C_2 and C_3 will be different, implying that the motion of the vehicle in each temperature phase may vary depending on the selected coefficients.

The Temperature Control phase is used in the initial part of reentry, down to a velocity of approximately 18000 ft/s (5500 m/s), and has the goal of not violating the maximum heat flux constraint, the most relevant path constraint in the initial phases of re-entry.

Equilibrium glide

In the Equilibrium glide phase it is assumed that the FPA remains constant and approximately zero, that is, $\dot{\gamma} = 0$ and $\gamma \approx 0$. Using this assumption, (1.4e) becomes

$$D = \frac{\left(g - V^2/r\right)}{L/D} \tag{3.2}$$

which can be written as

$$D = \frac{g}{L/D}\left[1 - \frac{V^2}{V_{\mathrm{S}}^2}\right], \tag{3.3}$$

where V_{S} is an arbitrary constant. The Equilibrium Glide phase lasts from the end of the Temperature Control phase down to a velocity of about 13000 ft/s (4000 m/s), and explicitly avoids violation of the equilibrium glide condition (1.7d).

Constant Drag phase

In the Constant Drag phase the $D\left(V\right)$ expression is

$$D = C_4, \tag{3.4}$$

where C_4 is an arbitrary constant. This phase lasts from the end of the Equilibrium Glide phase down to the velocity of 9000 ft/s (2800 m/s) and avoids exceeding the maximum g-load constraint (1.7b), which is relevant in intermediate phases of re-entry.

Linear Energy Transition phase

The Linear Energy Transition phase is the last phase of the entry profile. It is activated at the end of the Constant Drag phase, and takes the vehicle to TAEM conditions - with a final velocity of 2500 ft/s (750 m/s). $D\left(E\right)$ is considered a linear relation of E,

$$D = D_{\mathsf{F}} + C_5\left(E - E_{\mathsf{F}}\right), \tag{3.5}$$

where C_5 is an arbitrary constant and D_{F} and E_{F} are the desired TAEM drag and energy, respectively.

It is important to note that the independent variable used in this phase is energy, instead of velocity. This change is performed because the small FPA approximation $\gamma \approx 0$ is not valid anymore when the vehicle approaches TAEM conditions, and the controller provides better tracking results in terms of range-to-go when an energy dependent profile is tracked [19, 22].

3.3.2 Reference angle of attack

The angle of attack profile followed by the Shuttle Orbiter is kept to the pre-defined reference values, which is determined in order to ensure RV stability and trimmability. This profile is shown in figure 3.4.

Slight deviations from the reference profile are admitted in order to compensate for drifting when a bank angle reversal command is issued. This issue is further discussed in section 3.3.3.

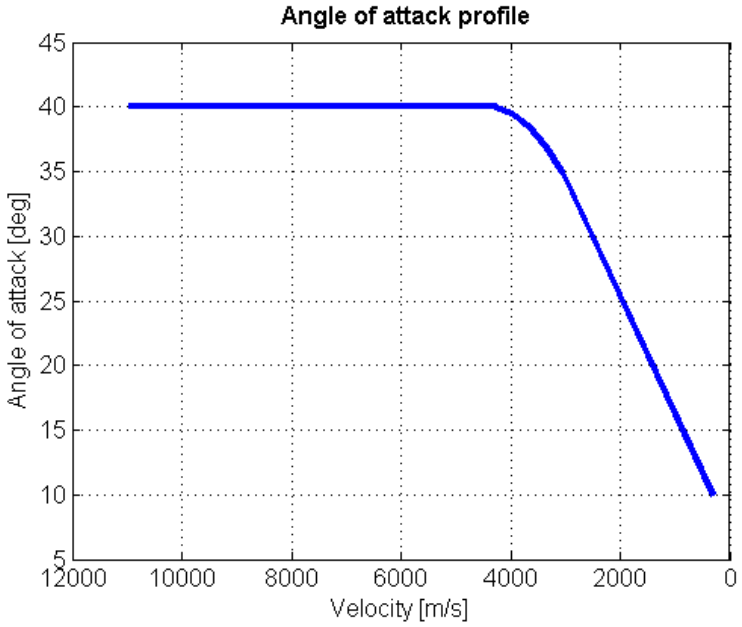

Figure 3.4: Angle of attack reference profile [17], mapped with respect to velocity.

3.3.3 Controller

For the Shuttle Entry Guidance a gain-scheduled PID controller is used to determine the lift over drag ratio command L/D_c. This command is computed using [17]

$$L/D_{\mathrm{c}} = L/D_0 + f_1\left(D - D_0\right) + f_2\left(\dot{h} - \dot{h}_0\right) + f_4 \int \left(D - D_0\right)\mathrm{d}V, \tag{3.6}$$

where the 0 subscript stands for the values associated to the reference profile. The controller gains f_1 and f_2 in (3.6) are taken from a tabled mapping aggainst drag, shown in 3.5.

Note that these gains are dependent on the re-entry phase, meaning that the approach used is a gain-scheduled PID controller. The integrative gain f_4 is arbitrarily set: in this implementation it was set to the constant value that provided the best results in the reference drag-velocity profile tracking.

The bank angle control command is then determined by the expression

$$\sigma_{\mathrm{c}} = \arccos\left(\frac{L/D_{\mathrm{c}}}{L/D_0}\right) + f_{11}\Delta\alpha, \tag{3.7}$$

which has a term dependent on the angle of attack α. This $\Delta\alpha$ term, given by

$$\Delta\alpha = C_{\mathrm{D}_0}\frac{D_0 - D}{f_{10}}, \tag{3.8}$$

where f_{10} and f_{11} are arbitrary gains, is added for improved profile tracking, in order to compensate for lateral motion coupling with longitudinal motion, when a bank angle sign reversal command is issued, as the RV tends to drift from the reference profile to perform the bank reversal maneuver. The variation of the angle of attack $\Delta\alpha$ term is thus added to counteract this deviation.

It should be noted that in the current 3-DoF simulation setting the attitude dynamics is neglected, and therefore the bank angle drifting effect does not occur as it is considered that the bank angle reverses instantaneously. The $\Delta\alpha$ term in equation (3.7) is thus not relevant in the current implementation.

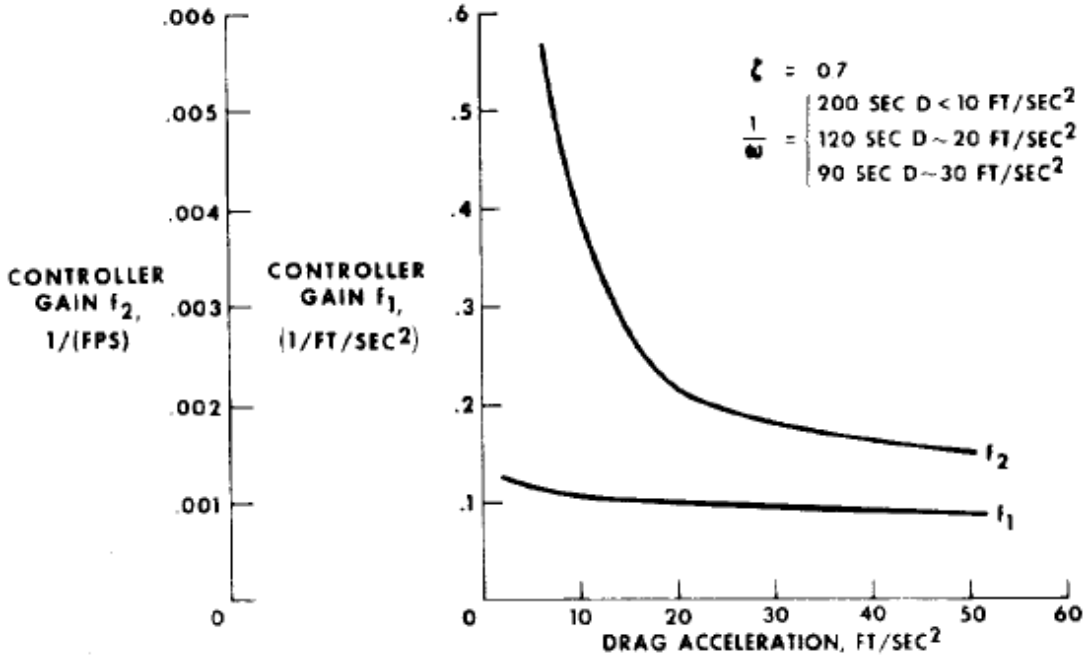

Figure 3.5: Reference gains for Shuttle Orbiter controller: f_1 and f_2 [17].

3.3.4 Crossrange control

The Shuttle Entry Guidance uses simple pre-defined deadband bounds to control the lateral deviation from target. This means that the GC system evaluates at every time step the heading error of the RV, that is, the angle difference between the current heading of the RV and the heading of the landing site. If this heading error exceeds the deadband threshold, the bank angle command sign is reversed (while its magnitude is kept the same), redirecting the lift vector in the symmetric (with respect to the vertical) direction. In this way, the lateral motion of the RV is compensated from one side to the other.

3.4 Implementation notes

The system described above, developed in [17], was implemented in MATLAB.

3.4.1 Tabled equations

The bulk of the re-entry guidance algorithm relies on three sets of equations, taken directly from [17], which are shown in tables 3.1, 3.2, and 3.3.

Range-prediction equations

The first of these is the range prediction equation set, which is depicted in table 3.1. Associated to drag-velocity relation that was established for each phase, it is possible to determine an analytical expression for range. The range expressions are derived from the expression

$$s = -\int \frac{V\cos\gamma}{-D - g\sin\gamma}\,\mathrm{d}V, \tag{3.9}$$

which follows directly from the equations of motion (1.4), and may be reduced to

$$s = \int \frac{V}{D}\,\mathrm{d}V, \tag{3.10}$$

assuming that $\gamma \approx 0$. Substituting the drag $D(V)$ from the second column of 3.1 in 3.10 allows direct integration with respect to V.

Phase	Drag segment form	Range Prediction Equation
Temperature Control	$D = \mathrm{C}_1 + \mathrm{C}_2 V + \mathrm{C}_3 V^2$	$Q = 4\mathrm{C}_3\mathrm{C}_1 - \mathrm{C}_2^2$ If $\mathbf{Q > 0}$ $s_1 = -\frac{1}{2\mathrm{C}_3}\log\left[\frac{\mathrm{C}_1 + \mathrm{C}_2 V_\mathrm{f} + \mathrm{C}_3 V_\mathrm{f}^2}{\mathrm{C}_1 + \mathrm{C}_2 V + \mathrm{C}_3 V^2}\right]$ $+\frac{\mathrm{C}_2}{\mathrm{C}_3\sqrt{Q}}\left(\arctan\left[\frac{2\mathrm{C}_3 V_\mathrm{f} + \mathrm{C}_2}{\sqrt{Q}}\right]\right.$ $\left. - \arctan\left[\frac{2\mathrm{C}_3 V + \mathrm{C}_2}{\sqrt{Q}}\right]\right)$ If $\mathbf{Q < 0}$ $s_1 = -\frac{1}{2\mathrm{C}_3}\log\left[\frac{\mathrm{C}_1 + \mathrm{C}_2 V_\mathrm{f} + \mathrm{C}_3 V_\mathrm{f}^2}{\mathrm{C}_1 + \mathrm{C}_2 V + \mathrm{C}_3 V^2}\right]$ $+\frac{\mathrm{C}_2}{\mathrm{C}_3\sqrt{Q}}\log\left[\frac{\frac{2\mathrm{C}_3 V_\mathrm{f} + \mathrm{C}_2 - \sqrt{-Q}}{2\mathrm{C}_3 V_\mathrm{f} + \mathrm{C}_2 + \sqrt{-Q}}}{\frac{2\mathrm{C}_3 V + \mathrm{C}_2 - \sqrt{-Q}}{2\mathrm{C}_3 V + \mathrm{C}_2 + \sqrt{-Q}}}\right]$
Equilibrium Glide	$D = \frac{g}{L/D}\left[1 - \frac{V^2}{V_\mathrm{s}^2}\right]$	$s_2 = \frac{1}{2}\left[\frac{V_\mathrm{s}^2 - V^2}{D}\log\left(\frac{V_\mathrm{f}^2 - V_\mathrm{s}^2}{V^2 - V_\mathrm{s}^2}\right)\right]$
Constant Drag	$D = \mathrm{C}_4$	$s_3 = \frac{V^2 - V_\mathrm{f}^2}{2\mathrm{C}_4}$
Transition	$D = D_\mathrm{f} + \mathrm{C}_5\,(E - E_\mathrm{f})$	$s_4 = \frac{E - E_\mathrm{f}}{D - D_\mathrm{f}}\log\left[\frac{D}{D_\mathrm{f}}\right]$

Table 3.1: Equations for entry range prediction of the Shuttle Orbiter, divided by phases [17].

When the FPA is large such that $\gamma \approx 0$ is not accurate, (3.10) is no longer valid. In this case, it is possible to write the range with respect to energy, instead of velocity,

$$s = \int \frac{\cos\gamma}{D}\,\mathrm{d}E, \tag{3.11}$$

where even for fairly larger FPAs it may be assumed that $\cos\gamma \approx 1$. Thus, it is written

$$s = \int \frac{1}{D}\,\mathrm{d}E. \tag{3.12}$$

Equation (3.12) provides better results than (3.10) when the FPA is not close to zero [17], which is further confirmed in [22].

For the evaluation of (3.12) it is required to have a drag-energy profile, instead of the drag-velocity profile, which happens for the linear energy transition phase (the last phase). Therefore, both (3.10) and (3.12) are

used to generate the range prediction expressions in table 3.1, the former being used for the first four phases, and the latter being used for the last phase only.

Reference profile equations

The second set of expressions, detailed in table 3.2, refers to the reference trajectory values computation. These are the reference values that show up in the controller equation (3.6): $\dot{h}_0$, D_0, and L/D_0. The expression for D_0 follows directly from the drag-velocity relation for each phase, as discussed in section 3.3.1. The expressions for h_0 and L/D_0 are deduced from the equations of motion, after the manipulation shown in pages 12-14 of [17], assuming small FPA and an exponential atmosphere model.

Phase	D_0	$\dot{h}_0$	L/D_0
Temperature Control	$\mathrm{C}_1 + \mathrm{C}_2 V + \mathrm{C}_3 V^2$	$-\frac{H_\mathrm{s}}{V}\left[2\mathrm{C}_1 + \mathrm{C}_2 V - \frac{\dot{C}_{D_0} V}{C_{D_0}}\right]$	$\frac{g}{D_0}\left(1 - \frac{V^2}{V_s^2}\right) - \frac{4H_\mathrm{s}\mathrm{C}_1}{V^2} - \frac{H_\mathrm{s}\mathrm{C}_2}{V}$
Equilibrium Glide	$\frac{g}{L/D}\left[1 - \frac{V^2}{V_\mathrm{s}^2}\right]$	$-\frac{H_\mathrm{s}}{V}\left[\frac{2D_0}{1 - \frac{V^2}{V_\mathrm{s}^2}} - \frac{\dot{C}_{D_0} V}{C_{D_0}}\right]$	$\frac{g}{D_0}\left(1 - \frac{V^2}{V_s^2}\right) - \frac{4H_\mathrm{s} D_0}{V^2\left(1 - \frac{V^2}{V_\mathrm{s}^2}\right)}$
Constant Drag	C_4	$-H_\mathrm{s}\left[\frac{2D_0}{V} - \frac{\dot{C}_{D_0}}{C_{D_0}}\right]$	$\frac{g}{D_0}\left(1 - \frac{V^2}{V_s^2}\right) - \frac{4H_\mathrm{s} D_0}{V^2}$
Transition	$D_\mathrm{f} + \mathrm{C}_5\left(E - E_\mathrm{f}\right)$	$-H_\mathrm{s}\left[\frac{2D_0 V - \mathrm{C}_5 V^3}{V^2 - 2H_\mathrm{s} g} - \frac{\dot{C}_{D_0} V}{C_{D_0}}\right]$	$\frac{g}{D_0}\left(1 - \frac{V^2}{V_s^2}\right) + \frac{\dot{h}_0}{V} + \frac{g\dot{h}_0^2}{DV^2} + \frac{2V\dot{h}_0 + 2\dot{h}_0\frac{g}{D} + 2D_0 H_\mathrm{s} + \frac{2g\dot{h}H_\mathrm{s}}{V}}{V^2 + 2gH_\mathrm{s}}$

Table 3.2: Expressions for reference trajectory parameters computation of the Shuttle Orbiter, divided by phases [17].

Profile updating equations

Finally, the third set of expressions shown in table 3.3 is related to the refreshing of the reference profile, in case the predicted range differs from the expected range. The profile update is made using the derivatives of range with respect to drag: knowing the difference between predicted and expected range, the derivatives are used to compute the drag variation necessary to correct the range mismatch. This drag variation is then used to update the reference profile.

3.4.2 Prototyped functions

The implementation of the Shuttle Entry Guidance in MATLAB is based on the functions shown in table 3.4. The algorithm works in parallel with simulation, being called every 1.92 seconds [17], and receiving as input the simulation state vector and a structure loaded with user-defined guidance parameters.

As output, the Shuttle guidance scheme provides the bank angle σ and the angle of attack α, which will be used in the propagation of the equations of motion. Moreover, relevant guidance data is recorded, so that the

Phase	Range Equation Constraints	Total Range Prediction	$\mathrm{d}s/\mathrm{d}D$
Temperature Control	$s_4 = \text{Constant}$ $\mathrm{C}_4 = \text{Constant}$	$s_1 + s_2 + s_3 + s_4$	$-\frac{s_1 + s_2}{D_0 \text{ at } V_{\mathrm{B}_1}}$
Equilibrium Glide	$s_4 = \text{Constant}$ $\mathrm{C}_4 = \text{Constant}$	$s_2 + s_3 + s_4$	$-\frac{s_2}{D_0 \text{ at } V_{\text{current}}}$
Constant Drag	$s_4 = \text{Constant}$	$s_3 + s_4$	None, s_3 can be solved directly
Transition	None	s_4	$\frac{D_0 - D_{\mathrm{F}} - (\mathrm{C}_5 D_0 s_4)}{\mathrm{C}_5 D_0 (D_0 - \mathrm{D}_f)}$

Table 3.3: Expressions for the derivative of range with respect to drag of the Shuttle Orbiter, divided by phases [17].

performance of the entry scheme can be assessed in post-processing. The implemented guidance algorithm is shown in figure 3.6.

Function name	Description
ShuttleGuidance.m	Main function: performs the main computations, calls other subfunctions
RangePrediction.m	Computes the range prediction assuming the reference profile is followed
NewProfile.m	The drag-velocity profile is updated depending on the range constraints
RefProfile.m	Reference profile values are evaluated
LateralLogic.m	The sign of the bank angle is determined depending on heading error
gains.m	The PID controller gains f_1 and f_2 are computed

Table 3.4: Functions implemented for the prototyping of the Shuttle Entry Guidance.

The backbone of the implementation is the main function ShuttleGuidance.m: it loads and initializes all the parameters, selects the current phase, calls all the other sub-functions, and computes the guidance output commands, angle of attack α and bank angle σ. The other functions may thus be regarded as auxiliary functions which assist the main function in performing the required calculations.

The functions RangePrediction.m, NewProfile.m, and RefProfile.m are called only after the selection of the entry phase. The range prediction function computes the range predicted for the current phase and for the subsequent phases associated to the reference profile, using the expressions in table 3.1 and adds these together to get a prediction of the total range, using current velocity, and the expected velocity at the beginning of

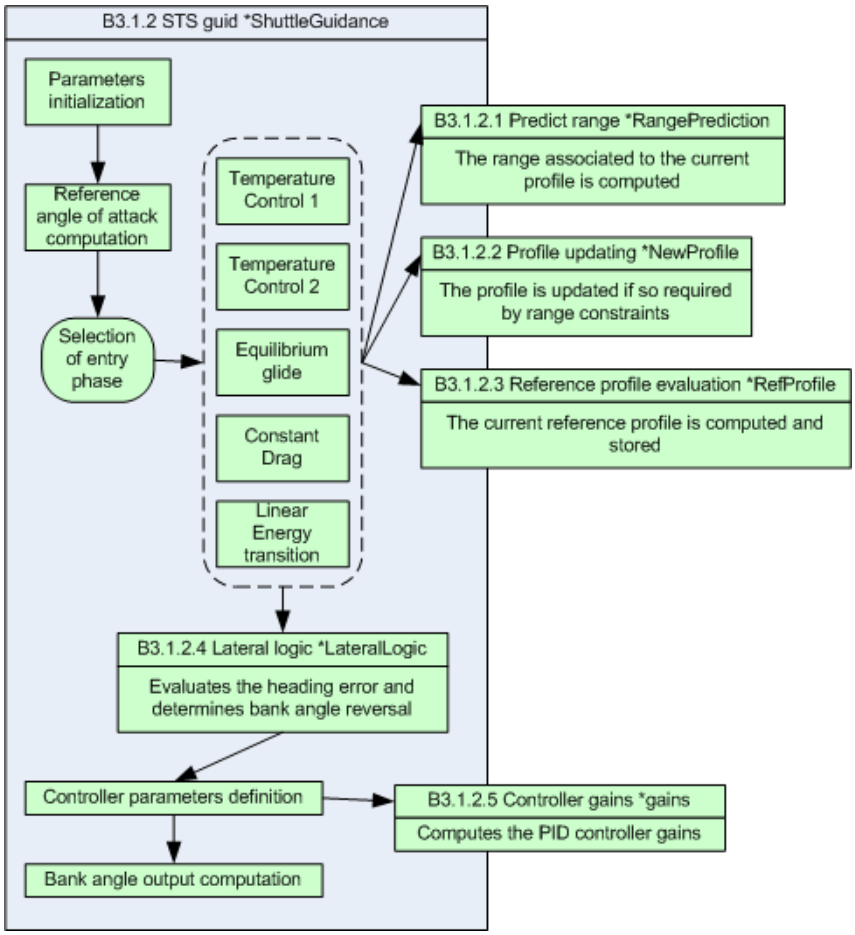

Figure 3.6: Flowchart of the Shuttle Entry Guidance implementation in MATLAB.

each future phase. In the updating profile function, the predicted range (associated to the reference profile) is compared against the estimated real range, and the reference profile is modified, if necessary, in order to match the predicted and estimated ranges. This function uses the range derivatives with respect to drag shown in table 3.3. Finally, the reference profile function implements table 3.2 equations, thus providing as outputs the reference profile values for the controller expression.

The remaining functions, LateralLogic.m and the gains.m, are phase independent. The former evaluates the heading error with respect to target and if it exceeds the pre-defined bounds (as discussed in section 3.3.4) a bank reversal command is issued. The latter computes the gains f_1 and f_2 by taking as input the current drag value and selecting the appropriate gain values from the look-up table, as shown in figure 3.5.

3.5 Testing

The implementation of the Shuttle Entry Guidance algorithm was validated against data taken directly from [17]. The first result, depicted in figure 3.7, shows that the implemented guidance algorithm is able to track the reference profile. The second, shown in figure 3.8[2], compares the bank angle obtained with the current implementation against the results shown in [17].

The most critical part of the reference tracking occurs in the transition from the Equilibrium Glide phase to the Constant Drag phase, where a slight overshoot occurs. In the end of the Linear Energy Transition phase, when the flight path angle becomes relevant, there is also a slight mismatch between actual and reference drag

[2]Note that the original figure from [17] is slightly distorted, which means that the axes of each plot are not an exact match. Therefore, only an approximate match should be expected between the simulated bank angle and the bank angle from [17].

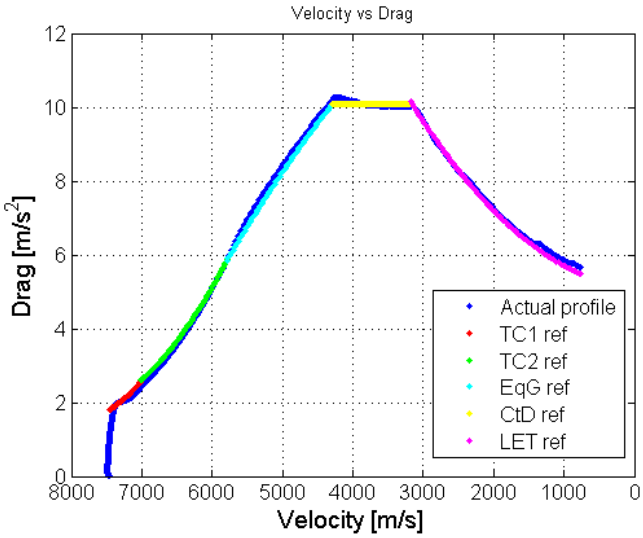

Figure 3.7: Plot of the drag vs velocity reference profile (in different colours) and the actual (flown) drag vs velocity profile (in dark blue).

profiles. However, the global performance is satisfactory, and provew that the current concept implementation is working. Further tests will be made in chapter 6.

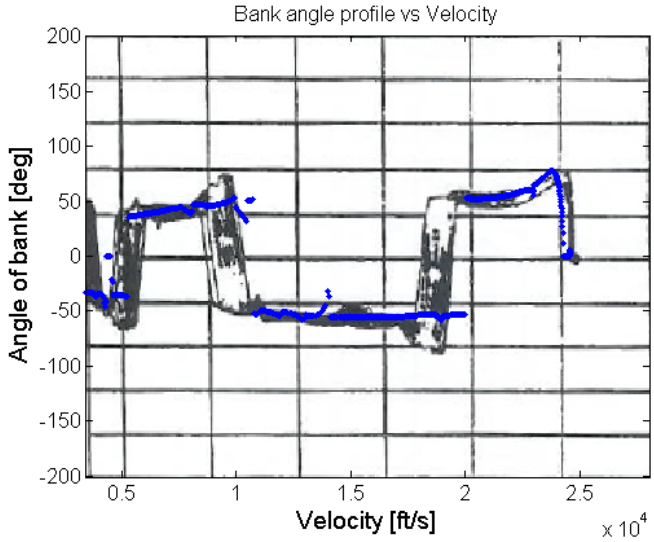

Figure 3.8: Plot of the bank angle vs velocity profile in [17] (in black) and of the bank angle profile obtained with the STS implementation.

From figure 3.8 it is possible to conclude that the bank angle resulting from the current algorithm implementation closely matches the bank angle results in [17], while the bank reversals occur approximately at the same speeds. However, it is clear that because the propagated dynamics is limited to 3-DoF (and not 6-DoF as is the case of the results in [17]), there are discontinuities in the simulated bank angle output.

3.6 Generalization of the Shuttle Entry guidance

The Shuttle Entry Guidance relies on reference profile tracking: extension of this algorithm to other RVs thus requires scheduled gain computation depending on the RV aerodynamic characteristics. Furthermore, the entry profile itself can be made user-defined, which allows for direct adaptation to the entry profiles of similar RVs.

Two functionalities were added to generalize the Shuttle Entry guidance in REACTIVE: the arbitrary definition of the drag-velocity profile and the analytic scheduled gain computation, so as to make this algorithm adaptable and reconfigurable to different RVs.

Regarding the definition of the profile, from the discussion in chapter 3 it is known that the Shuttle Guidance drag profile is analytically expressed in terms of the independent variable velocity for each phase (*e.g.* Temperature Control, Equilibrium Glide, Constant Drag, except for the last phase, where the independent variable becomes energy), with most coefficients in the analytical expressions being arbitrary.

In REACTIVE, instead of being constrained to the reference profile presented in [17], it is possible to set the expressions' coefficients at will, by selecting a set of points for each phase. In this way, flexibility in the design of the entry profile is achieved, while the analytical drag-velocity expressions relations for each phase are retained, as are all the other expressions derived thereof. In figure 3.9 the reference profile and a new profile constructed in REACTIVE are shown.

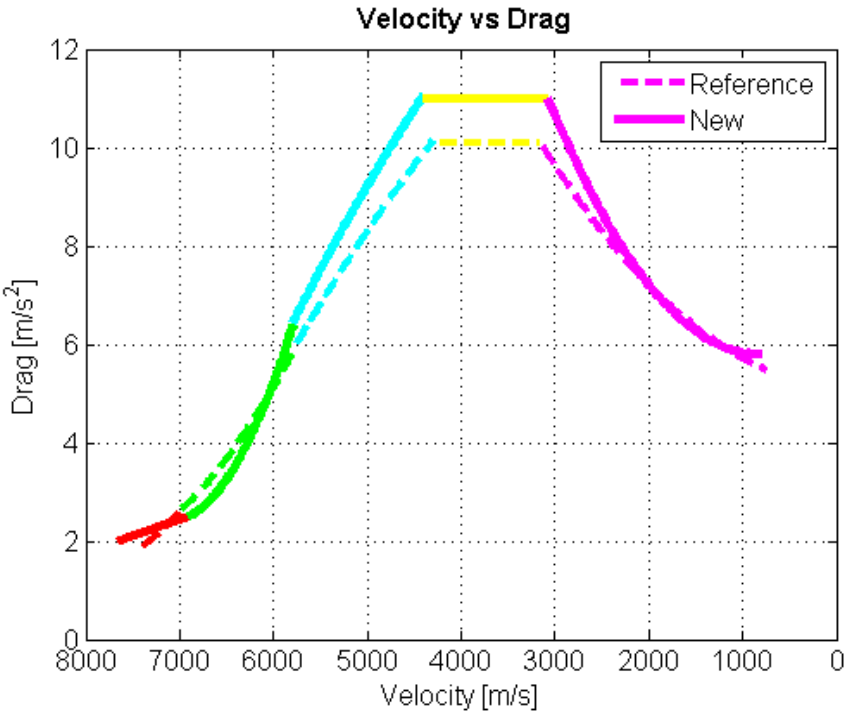

Figure 3.9: Reference profile for moderate L/D RV and newly constructed profile.

Regarding the gain computation, the analytical relations for gains f_1 and f_2 derived in [17] are used

$$f_1' = \frac{H_s}{D_0^2}\left[\omega_0^2 + 3\dot{D}_0\left(\frac{1}{V_0} - \frac{\dot{D}_0}{D_0^2}\right) + \frac{1}{H_s}\left(\frac{V_0^2}{r_0} - g\right) - \frac{4D_0^2}{V_0^2} + \frac{2\ddot{D}_0}{D_0} + \frac{\dot{C}_{D_0}^2}{C_{D_0}^2} + \frac{\ddot{C}_{D_0}^2}{C_{D_0}}\right]$$

$$f_2' = \frac{H_s}{D_0^2}\left[2\xi\omega_0 + \frac{2\dot{D}_0}{D_0} - \frac{3D_0}{V_0}\right]$$

$$f_1 = f_1' - f_2'\left(\frac{\dot{h}_0}{H_s} + \frac{4D_0}{V_0} - \frac{\dot{C}_{D_0}}{C_{D_0}}\right) \tag{3.13a}$$

$$f_2 = -f_2'\frac{D_0}{H_s}, \tag{3.12b}$$

instead of the tabled values in figure 3.5. In 3.12b the subscript '0' refers to the reference profile values that are store on-board, while ξ and ω_0 are the damping ratio and the natural frequency of the second-order dynamics assumed for the controller.

For the evaluation of these equations the derivative of the drag coefficient is evaluated analytically in order to generalize the Shuttle guidance to other vehicles. In [17] it is suggested that C_{D_0} $\dot{C}_{D_0}$ are approximated by

$$C_D = \mathrm{K}_1 + \mathrm{K}_2\alpha + \mathrm{K}_3\alpha^2 + \mathrm{K}_4 \exp\left(-\frac{V - \mathrm{K}_5}{\mathrm{K}_6}\right)$$
$$\dot{C}_D = \mathrm{K}_7\left(D + g\frac{\dot{h}}{V}\right)\exp\left(-\frac{V - \mathrm{K}_5}{\mathrm{K}_6}\right) + \dot{\alpha}_0\left(\mathrm{K}_8\alpha_0 + \mathrm{K}_9\right),$$

which uses a second order polynomial to model the C_D dependence on the angle of attack α, and an exponential relation to model the C_D dependence on the Mach number. However, in order to make this implementation more flexible, the approximation of C_D used in REACTIVE uses a combination of two polynomial expressions of arbitrary order, one dependent on the angle of attack and the other of the Mach number. In REACTIVE, the drag coefficient and its derivative are computed using

$$C_D = \mathrm{K}_{0_\alpha} + \mathrm{K}_{1_\alpha}\alpha + \cdots + \mathrm{K}_{n_\alpha}\alpha^{n_\alpha} + \mathrm{K}_{0_M} + \mathrm{K}_{1_M}M + \cdots + \mathrm{K}_{n_M}M^{n_M} \tag{3.13a}$$
$$\dot{C}_D = \dot{\alpha}\left(\mathrm{K}_{1_\alpha} + 2\mathrm{K}_{2_\alpha}\alpha + \cdots + n\mathrm{K}_{n_\alpha}\alpha^{n_\alpha - 1}\right) + \dot{M}\left(\mathrm{K}_{1_M} + 2\mathrm{K}_{2_M}M + \cdots + n\mathrm{K}_{n_M}M^{n_M - 1}\right), \tag{3.13b}$$

where n_α and n_M are the arbitrary order of the polynomial. Equation 3.13b enables the evaluation of $\dot{C}_D$ for any RV.

3.7 Remarks

The Shuttle Entry Guidance most critical aspect is the design of the reference profile, as it must take into account path constraints and the range requirements for the determination of the different free parameters in the $D(V)$, $D(E)$ relations. However, since there are more free parameters than constraints, the final solution is open, requiring iteration and design experience. This is most felt when attempting to design entry profiles different from the one suggested in [17]. Nonetheless, if this difficulty is surpassed, the STS guidance scheme may be applied to different scenarios and configurations, as all the guidance parameters can be freely tuned.

Regarding the algorithm implementation, the results in section 3.5 suggest that the STS guidance scheme was successfully implemented.

Chapter 4

The Apollo Entry Guidance and the Enhanced E-Guide

4.1 Introduction

Apart from the Shuttle Entry Guidance, two other guidance algorithms that had been prototyped by GMV are used in REACTIVE: the Apollo Entry Guidance and the Enhanced E-Guide.

The Apollo Entry Guidance is associated with one of the greatest humanity achievements: the landing on the Moon in the year of 1969. Likewise, it was designed for LTO re-entry, the most demanding re-entry scenario, where entry velocities exceed 8.5 km/s. The guidance scheme consists of two most important phases: RV atmospheric capture and landing site targeting. In atmospheric capture, the lift vector is directed downwards (which means that the bank angle is set to $\sigma = 180$ deg) at EIP so as to increase the force that pulls the vehicle down to the planet surface. Once sufficient energy has been dissipated, which may require an additional constant drag segment or skip-entry, the targeting phase is triggered. In this phase, a reference profile mapped with respect to velocity is tracked using a LQR controller, and the RV eventually reaches TAEM conditions.

The vehicle for which the Apollo Entry Guidance was designed is the Apollo CM, a low L/D capsule-like vehicle. As such, it performs an approximately ballistic re-entry.

The Enhanced E-Guide is an innovative and adaptive approach developed for high L/D RVs, that divides the entry process in three phases: in the first phase, the vehicle follows a reference altitude, progressively reducing the bank angle in order to increase lift and thus keep the same constant altitude [9]; in the second phase, the RV tracks a constant heat flux [47], which allows it to be compliant with the maximum heat flux and g-load constraints; finally, at moderate entry velocities ($V \approx 5300$ m/s) and intermediate altitude ($V \approx 64$ km), the targeting phase is triggered, with a reference profile being generated on-board and tracked using a LQR controller.

For the first two phases, Enhanced E-Guide uses NDI control, and the tracking of the reference profile uses a scheduled gain controller, where its gains are computed using Linear Quadratic Regulator (LQR) [10]. The fact that the reference trajectory is generated on-board at the triggering of the targeting phase further allows for mid-entry retargeting.

For the development of the Enhanced E-Guide guidance solution, the definition of the baseline vehicle configuration was required. The chosen RV concept resulted from a trade-off analysis of several existing low to high lift-over-drag (L/D) vehicle concepts, proposed by another project partner, the OHB team [12]. Among the entry vehicles that were analysed, there were the Soyuz spacecraft, the Apollo capsule, the ORION Crew Exploration Vehicle (CEV, a NASA prototype), the Space Shuttle Orbiter, the X-38 Crew Return Vehicle (CRV), and various configurations of the Plane-shaped Hypersonic Orbital Entry BUS (Phoebus) concept.

Finally, the choice fell on the Phoebus vehicle with the HL-3A configuration, a high L/D RV, compliant with all project requirements.

The implementation of these algorithms in REACTIVE consisted not only of consolidating the algorithms available, but also aimed at generalizing the application of these algorithms (similarly to what was done in chapter 3 with respect to the Shuttle Entry Guidance) to general low (in the case of the Apollo Entry Guidance) or high (in the case of Enhanced E-Guide) L/D RVs. Hence, this generalization was performed on both algorithms with relative success.

4.2 The Apollo prototypation

4.2.1 Apollo Commmand Module

The Apollo Command Module, shown in figure 4.1, is a cone-shaped capsule-like RV [27] which has an height of 10 ft 7 in (3.226 m), a cone base diameter of 12 ft 10 in (3.912 m), and a presented area of 12.56 m^2, being able to support a crew of three astronauts. Its total mass amounts to 13000 lb (5897 kg) at EIP, and is reduced to 11700 lb (5307 kg) at splashdown, while its ballistic coefficient varies from $B_{\mathrm{C}} \approx 350$ at EIP to as much as $B_{\mathrm{C}} \approx 530$ at splashdown [31] (however, the for most of re-entry it remains $B_{\mathrm{C}} \approx 370$).

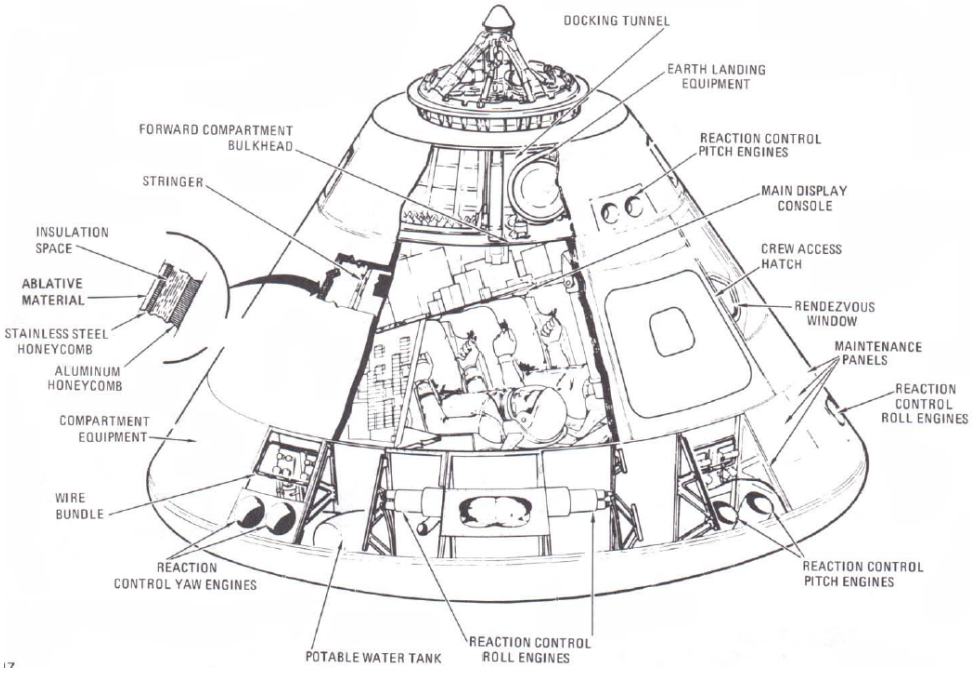

Figure 4.1: Apollo Command Module detail [27].

The L/D of the Apollo CM is around $L/D \approx 0.3$[1], which limits maneuverability and travelled distance (about one eighth of planet turn). During re-entry, the Apollo CM is trimmed to an almost constant angle of attack, in the order of $\alpha_{\mathrm{T}} \approx 156$ deg[2]. At the base of the cone, which has a curvature radius of 4.7 m, there is an ablative shield that enables the RV of sustaining high entry heat fluxes, of more than 2 MW/m^2.

4.2.2 Apollo Entry Guidance

The Apollo Entry Guidance [3] uses a main navigation filter, associated to a targeting function, to evaluate at all time steps the positions of the vehicle and of the landing site. Its guidance scheme is divided into different

[1] The Apollo is able to perform bank angle maneuvers by using its reaction control engines.

[2] This angle of attack value is due to the body reference frame definition, which aligns the x-axis along the vertex of the capsule's conical shape, while during re-entry it is the capsule's bluntest part, the cone base, that faces incoming airflow.

phases, which are selected depending on the current state of the vehicle:

- Initial Roll phase
- Constant Drag phase (optional)
- Up Control phase + Ballistic phase (optional)
- Targeting phase

The schematic depicting the Apollo Entry Guidance algorithm structure is shown in figure 4.2.

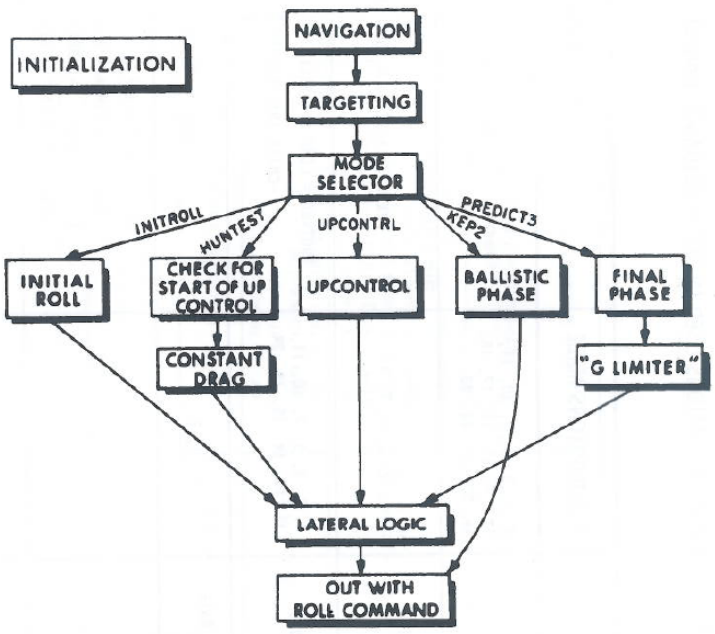

Figure 4.2: Schematic of the Apollo Entry Guidance [3]

The first phase of the guidance scheme is the Initial Roll. In this first phase, the lift vector is rotated downwards, by banking the capsule by 180 deg, in order to maximize the force that pulls down the vehicle and ensure that the vehicle is captured. This phase lasts until a maximum altitude rate is reached, at which point a significant amount of energy has been dissipated, in order to avoid skipping, while enough remains so that the vehicle is still able to reach the final target.

The following optional phases, Constant Drag, Up Control, and Ballistic, allow additional dissipation of energy and correct for range until the predicted miss (that is, the distance between the landing site and the predicted landing point) is less than a pre-specified value. These are only used to adjust the vehicle position and energy to the values required for the triggering of the Targeting phase.

In the Constant Drag phase, a constant drag value is tracked. The Up Control and Ballistic phases allow to perform a skip-entry[3], where the RV is controlled in an upward trajectory, and projected out of the atmosphere with a certain velocity and flight path angle. The Ballistic Phase is activated until the RV returns again to atmospheric environment, expectedly at a satisfactory range from target.

When the RV is at approximately the desired range from target and has an acceptable energy level, the Targeting Phase is activated. In this final phase, the RV aims at landing site targeting. It does so by tracking a reference trajectory generated offline, using a gain-scheduled PID controller whose gains are the derivatives of range with respect to altitude rate $F2\,(V)$, drag $F1\,(V)$, and lift to drag ratio $F3\,(V)$, also stored on-board.

[3]This approach was never used.

The expression used to predict range in this final phase is [3]

$$s_{\text{pred}} = s_{\text{ref}}(V) + F2(V)\left[\dot{h} - \dot{h}_{\text{ref}}(V)\right] + F1(V)\left[D - D_{\text{ref}}(V)\right], \tag{4.1}$$

where s is the range, h is altitude and D is drag, and the subscripts 'pred' and 'ref' stand for 'predicted' and 'reference'. Note that the reference values are all taken from the entry profile stored on-board, and are mapped with respect to velocity V. The predicted range thus computed is plugged into the computation of the desired L/D [3],

$$L/D = L/D_{\text{ref}} + 4\frac{(s_{\text{des}} - s_{\text{pred}})}{F3(V)}, \tag{4.2}$$

where the 'des' subscript stands for 'desired'. The desired range s_{des} is determined by the navigation and targetting functions of the Apollo algorithm.

Success of the Targeting phase is further ensured by the G-Limiter, which at every time step computes the current aerodynamic acceleration of the vehicle and compares it with the maximum g-load allowed.

In the Apollo guidance scheme the Lateral Logic function is called to ensure lateral guidance control in all phases. Lateral control is performed by reflecting the horizontal component of lift about the vertical axis, either to the right or to the left, which therefore takes the RV into any of the two directions, via determination of a bank angle control command σ_{c}. This is done with the expression [3]

$$\sigma_{\text{c}} = K2 \arccos\left(\frac{L/D}{L/D_{\max}}\right) + 2\pi K1, \tag{4.3}$$

where $K1$ and $K2$ are indicators for switching the bank angle sign, and $L/D_{\max}$ is the maximum lift-over-drag ratio. Note that this maximum value is a constant, and that the argument of the $\arccos$ function comes from the result of (4.2), in the final phase of the entry guidance algorithm.

The orientation of the lift reflection, that is, the values of $K1$ and $K2$, is determined based on the predicted cross range miss: if it exceeds a predetermined fraction of the vehicle cross range capability, the direction of the lift vector is changed.

4.2.3 Apollo derivatives computation

The core of the Apollo Entry Guidance relies on the tracking of the reference trajectory using a gain-scheduled PID controller. In order to make this algorithm suitable for any capsule-like vehicle, and assuming that a reference trajectory associated to the RV is available, it is necessary to compute the scheduled gains in a systematic manner.

In the landing site targeting phase of the original Apollo Guidance scheme, discussed in chapter 4, a reference trajectory stored on-board is tracked using a PID controller. The PID scheduled gains are derived from the re-entry dynamics, and stored alongside the reference trajectory in a mapping with respect to velocity. In particular, because precise landing site targeting is required, the gains are derived from the derivatives of range with respect to the control variables. In the expressions for the Apollo controller, (4.1) and (4.2), the gains F_1 (the derivative of range with respect to atmospheric drag), F_2 (the derivative of range with respect to vertical velocity), and F_3 (the derivative of range with respect to the L/D) are

$$F_1 = \frac{\mathrm{d}s}{\mathrm{d}D}, \quad F_2 = \frac{\mathrm{d}s}{\mathrm{d}\dot{h}}, \quad F_3 = \frac{\mathrm{d}s}{\mathrm{d}L/D} \tag{4.4}$$

In table 4.1, the reference trajectory taken from [3] is presented.

In table 4.1 the first three columns and the sixth column are part of the reference trajectory, while the fourth, the fifth and the seventh columns, identified by F_2, F_1 and F_3, respectively, are the reference scheduled gains for the PID controller.

V_{REF} FPS	$\dot{R}_{\mathrm{REF}}$ FPS	$\dot{D}_{\mathrm{REF}}$ FPSS	$\mathrm{d}R/\mathrm{d}\dot{R}$ (F_2) NM/FPSS	$\mathrm{d}R/\mathrm{d}\dot{D}$ (F_1) NM/FPSS	R_{TOGO} NM	$\mathrm{d}R/\mathrm{d}L/D$ (F_3) NM
0	-331	34.1	0.0	-0.02695	0.0	1.0
337	-331	34.1	0.0	-0.02695	0.0	1.0
1080	-693	42.6	0.002591	-0.03629	2.7	6.44 x 2
2103	-719	60.0	0.003582	-0.05551	8.9	10.91 x 2
3922	-694	81.5	0.007039	-0.09034	22.1	21.64 x 2
6295	-609	93.9	0.01446	-0.141	46.3	48.35 x 2
8531	-493	98.5	0.02479	-0.1978	75.4	93.72 x 2
10101	-416	102.3	0.03391	-0.2372	99.9	141.1 x 2
14014	-352	118.7	0.06139	-0.3305	170.9	329.4
15951	-416	125.2	0.07683	-0.3605	210.3	465.5
18357	-566	120.4	0.09982	-0.4956	266.8	682.7
20829	-781	95.4	0.1335	-0.6483	344.3	980.5
23090	-927	28.1	0.2175	-2.021	504.8	1385.0
23500	-820	6.4	0.3046	-7.569	643.0	1508.0
35000	-820	6.4	0.3046	-7.569	643.0	1508.0

Table 4.1: Apollo reference trajectory and associated range derivatives [3].

In order to perform the generalization of the Apollo Guidance, in REACTIVE the F_1, F_2, and F_3 derivatives are analytically computed. In this respect, three assumptions are made, following the rationale in the appendix of [3]:

- lateral motion is neglected;
- the effect of the Earth rotation is neglected;
- the atmospheric air density is given by the exponential relation $\rho = \rho_0 \exp\left(-h/H_{\mathrm{s}}\right)$;
- FPA γ is small so that $\cos\gamma = 1$ and $\sin\gamma = \gamma$ (or zero).

From (1.4)

$$\dot{h} = V\sin\gamma \tag{4.5a}$$

$$\dot{V} = -D - g\sin\gamma \tag{4.5b}$$

$$V\dot{\gamma} = \left(\frac{V^2}{r} - g\right)\cos\gamma + L, \tag{4.5c}$$

while range (5.4) is

$$\frac{\mathrm{d}s}{\mathrm{d}t} = -\frac{R}{R+h}V\cos\gamma. \tag{4.6}$$

where $\dot{h}$, $\dot{V}$, and $\dot{\gamma}$ are the time derivatives of altitude, velocity, and FPA, respectively.

Derivative F_1 is the derivative of range with respect to aerodynamic drag. Combining (4.6) and the

derivative with respect to time of drag D

$$F_1 = \frac{\frac{\mathrm{d}s}{\mathrm{d}t}}{\frac{\mathrm{d}D}{\mathrm{d}t}} = \frac{\mathrm{d}s}{\mathrm{d}D}. \tag{4.7}$$

From the appendix of [3],

$$\frac{\mathrm{d}D}{\mathrm{d}t} = -\frac{D}{H_S}\dot{h} + 2\frac{\dot{V}}{V}D \tag{4.8}$$

and thus F_1 is given by

$$F_1 = \frac{V^2\cos\gamma}{V\frac{\dot{h}}{H_s} + 2\left(-D - g\sin\gamma\right)}\frac{1}{D}\frac{\mathrm{ATK}}{R}, \tag{4.9}$$

where ATK/R is a multiplying constant, and $\dot{V}$ was substituted by (4.5b).

Derivative F_2 is the derivative of range with respect to altitude rate. Combining (4.6) and the derivative with respect to time of $\dot{h}$

$$F_2 = \frac{\frac{\mathrm{d}s}{\mathrm{d}t}}{\frac{\mathrm{d}\dot{h}}{\mathrm{d}t}} = \frac{\mathrm{d}s}{\mathrm{d}\dot{h}} \tag{4.10}$$

The derivative of $\dot{h}$ with respect to time, using the assumptions relative to FPA, is

$$\frac{\mathrm{d}\dot{h}}{\mathrm{d}t} = \dot{V}\sin\gamma + V\dot{\gamma}\cos\gamma \approx V\dot{\gamma}. \tag{4.11}$$

where it is possible to substitute for 4.5c. F_2 is thus given by

$$F_2 = \frac{V\cos\gamma}{\left(\frac{V^2}{r} - g\right)\cos\gamma + D\frac{L}{D}}\frac{\mathrm{ATK}}{R} \tag{4.12}$$

Finally, F_3 is computed simply by dividing the reference range to go with respect to the reference L/D:

$$F_3 = \frac{s_{\mathrm{ref}}}{L/D} \tag{4.13}$$

Expressions (4.9), (4.12), and (4.13) are evaluated using the reference trajectory values in table 4.1, and compared against the reference results shown in that table in figures 4.3 to 4.5.

The tabled numerical derivatives F_1 and F_3 are closely matched by the derived analytical results, while F_2 is slightly mis-approximated. This difference may be a consequence of mismatches in the atmospheric model and in the RV aerodynamic model. However, the implementation of the analytically computed gains in REACTIVE provide satisfactory results.

It is important to note that the generalization of the Apollo targeting approach to other capsule-like RVs requires that a reference entry profile associated to the RV is available. If so, (4.9), (4.12),(4.13) can be used to evaluate the controller gains and track this reference profile.

4.3 Highlift vehicle and guidance solution

4.3.1 Phoebus vehicle

The selected configuration for Phoebus [12], depicted in figure 4.6, uses a cylindrical fuselage nose, and the wing's leading edges, in delta shape, have a curvature radius of 5 cm. Its mass is about 5000 kg, with a center of gravity at 7.54 m (64.9% of the full vehicle length, $L = 11.6$ m) of the nose leading edge. The reference presented area is 61.6 m^2, which corresponds to a wing loading of 81.1 kg/m^2.

Regarding re-entry constraints, the Phoebus RV has an high $L/D \approx 2$, and is able to sustain a maximum

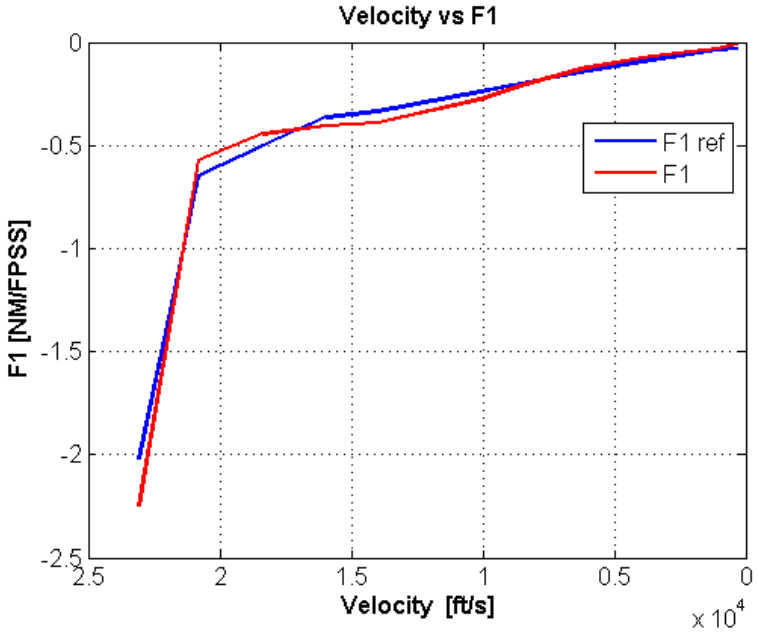

Figure 4.3: Tabled F_1 derivative in blue against analytical F_1 derivative in red.

heat flux in the leading edge of 2 MW/s and a maximum g-load of 6 g's. Its high L/D further enables entry trajectory flexibility, enhanced maneuverability, and looser range capabilites (about one-planet turn). Moreover, re-entry time duration is prolonged, which reduces peak loads in acceleration and heat flux.

4.3.2 Enhanced E-Guide

The Enhanced E-Guide is an innovative entry guidance scheme, tailored for a high L/D RV. It consists of three different entry phases:

- Feedback linearization with Non-linear Dynamic Inversion (NDI) technique for constant reference altitude tracking with PID control;
- Feedback linearization with NDI technique for constant reference heat flux tracking with PID control;
- On-board-generated reference profile tracking with Linear Quadratic Regulator (LQR) gain-scheduled controller for landing site targeting.

These three phases are made explicit in figure 4.7, in a Phoebus nominal entry profile.

In the two phases with NDI implementaion, the controller aims at tracking a constant altitude or constant heat flux by producing a suitable bank angle law [47]. The dynamics of the bank angle is taken to be

$$\sigma = \arccos\left\{\frac{\left(\dot{\gamma} - \frac{V}{r} + \frac{g}{V}\right)\frac{V}{D}}{L/D_{\text{est}}}\right\}, \tag{4.14}$$

where L/D_{est} is the estimated L/D.

Because both the altitude and heat flux can be expressed as a function of FPA as the control input [7,9,47], it is possible to write

$$\dddot{Q} = a_Q + b_Q\dot{\gamma}, \quad \ddot{h} = a_h + b_h\dot{\gamma}, \tag{4.15}$$

where a and b are the system state and input matrices, respectively, for each of the tracked variable. Selecting a second order dynamics associated to the PID controller used to track the reference variables, which in the

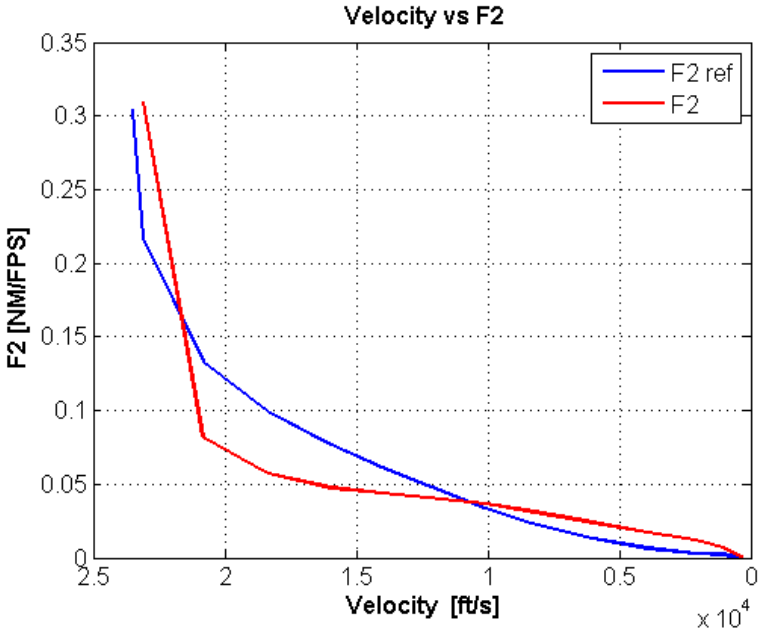

Figure 4.4: Tabled F_2 derivative in blue against analytical F_2 derivative in red.

first phase is altitude h and in the second phase is heat flux $\dot{Q}$,

$$\dddot{Q} + \xi\omega_0\ddot{Q} + \omega_0^2\left(\dot{Q} - \dot{Q}_{\text{ref}}\right) = 0, \quad \dddot{h} + \xi\omega_0\ddot{h} + \omega_0^2\left(h - h_{\text{ref}}\right) = 0, \tag{4.16}$$

with ξ and ω_n the damping ratio and the natural frequency, respectively, the flight path angle derivative is written as

$$\dot{\gamma} = \frac{\ddot{Q}_{\text{ref}} - a_Q}{b_Q}, \quad \dot{\gamma} = \frac{\ddot{h}_{\text{ref}} - a_h}{b_h}. \tag{4.17}$$

This FPA is then plugged into (4.14) and the bank angle command is found.

By tracking constant altitude and a constant heat flux using this approach, the RV avoids the initial excessive heat fluxes and aerodynamic accelerations, and further ensures that the RV is kept within the corridor bounds.

In the targeting phase, which is the last phase of Enhanced E-Guide, the guidance scheme tracks a reference profile to reach the pre-specified TAEM conditions. This reference profile is generated on-board, using a pre-specified linear bank angle law

$$\sigma\left(t\right) = \sigma_0 + \sigma_i t \tag{4.18}$$

whose constant parameter σ_0 and slope parameter σ_i, both constant, are determined by means of a shooting method [37], which is a numeric optimisation method. The bank angle law thus determined is used to generate a reference profile on-board, which takes as initial conditions the state-space vector at the moment of transition from the previous phase and as final conditions the TAEM conditions.

The on-board generated reference profile is then tracked by a gain-scheduled LQR controller, using the method explained in [10], whose gains are computed offline using the LQR technique via the optimisation of the cost function

$$J = \int_{t_0}^{\infty} \left(x^T Q x + u^T R u\right) \mathrm{d}t, \tag{4.19}$$

whose control solution is found by solving the Ricatti equation. A reference profile is generated offline, and the system is lineared about this reference, using energy as the independent variable. This change of independent variable, from velocity to energy, is justified by improved controllability results with respect to downrange when

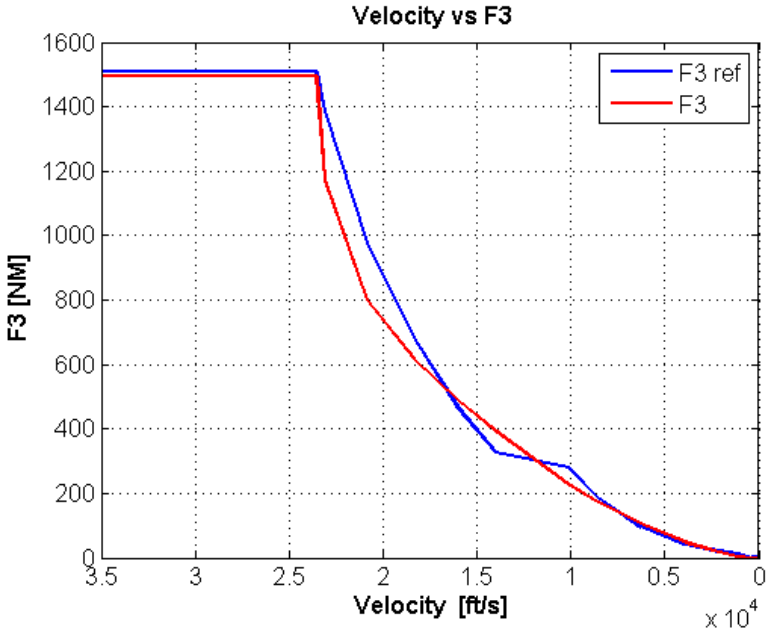

Figure 4.5: Tabled F_3 derivative in blue against analytical F_3 derivative in red.

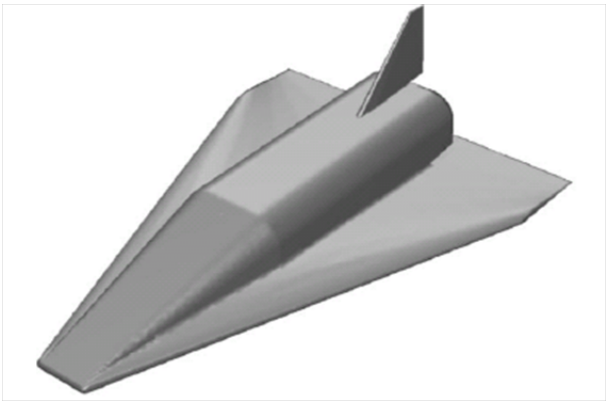

Figure 4.6: Phoebus vehicle concept drawing [12]

the FPA is large, as discussed in [19, 22]. The linear perturbation model around a nominal entry trajectory is

$$\begin{bmatrix} \delta\dot{s} \\ \delta\dot{h} \\ \delta\dot{\gamma} \end{bmatrix} = A \begin{bmatrix} \delta s \\ \delta h \\ \delta\gamma \end{bmatrix} + B \begin{bmatrix} \delta\sigma \\ \delta\alpha \end{bmatrix}, \tag{4.20}$$

where $\delta s = s - s_{\text{ref}}$, $\delta h = h - h_{\text{ref}}$, and $\delta\gamma = \gamma - \gamma_{\text{ref}}$ (with the subscript 'ref' indicating values from the reference trajectory).

The fact that in the last phase the profile is generated on-board allows for greater flexibility in the landing site targeting: it is possible to change the final landing site when the targeting phase is triggered, simply by providing different TAEM conditions to the optimiser.

The lateral guidance algorithm used in Enhanced E-Guide uses the same logic as the one implemented in Apollo (see the end of section 4.2).

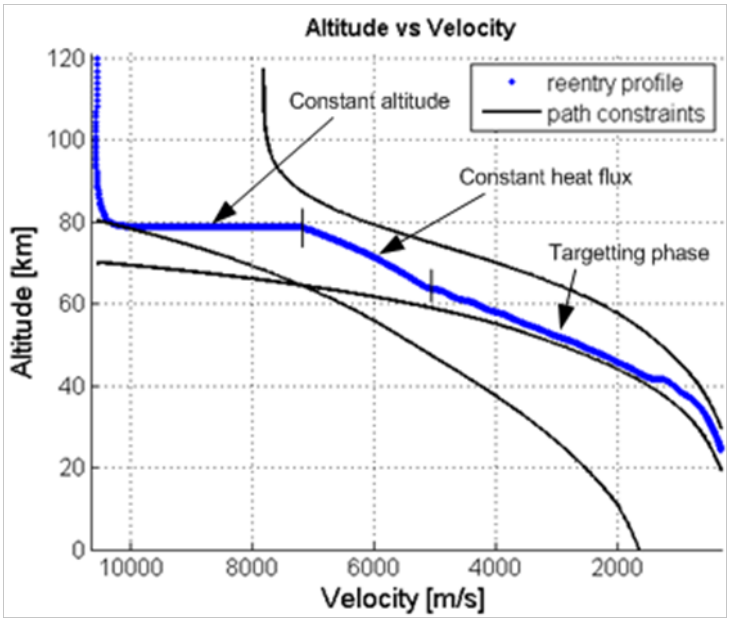

Figure 4.7: Phoebus nominal re-entry profile, with the different phases identified, and corridor bound constraints.

4.3.3 Flexibilization of Enhanced E-Guide

The NDI implementation is adaptable to different RV configurations. However, the selection of the reference commands for the NID phases and the phase changing policy, which were pre-determined and unchangeable, may be made user-definable.

The Enhanced E-Guide relies on Non-Linear Dynamic Inversion control and onboard numerical trajectory generation for guidance and control of the vehicle. This kind of algorithms are highly adaptable to different RV characteristics, as the computation of the guidance law takes directly into account the vehicle dynamics.

Therefore, the changes made to Enhanced E-Guide were concerned with turning the constant reference altitude and the constant heat flux that are to be tracked by the NDI controller, as well as the phase changing method, into user-definable parameters (figure 4.8). The bank angle parameters for the targetting phase optimiser were also made user-definable.

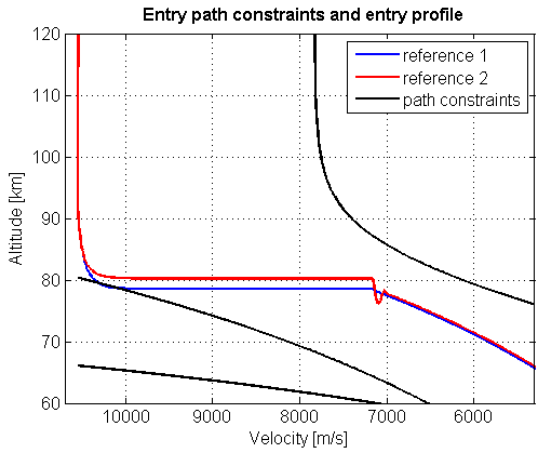

(a) Different altitude and heat flux references are tracked;

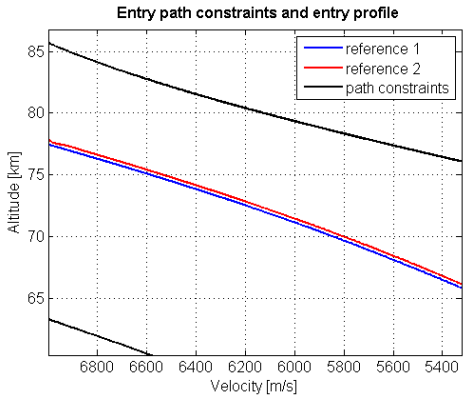

(b) Detail of the heat flux tracking: two heat flux references are followed;

Figure 4.8: High L/D RV on Enhanced E-Guide, following two different altitude and heat flux references.

In this way, the Enhanced E-Guide can be tailored to different high L/D vehicles. Note that it is possible

to omit one of the phases, if desired, or interchange its order. Ultimately, REACTIVE's generalization of Enhanced E-Guide can be seen as three independent guidance schemes, which can be concatenated at will, depending on the RV characteristics and on the re-entry profile desired: altitude tracking with NDI, heat flux tracking with NDI, and tracking of onboard-generated reference profile.

4.4 Remarks

The Apollo Entry Guidance generalization was successful in the sense that the tabled derivatives were conveniently approximated by the analytical expressions derived. This will be further confirmed in chapter 6, where tests are performed on general low L/D vehicles.

Regarding the Enhanced E-Guide, two issues that should be noted. The first concerns the shooting method used to generate the reference profile at the triggering of the targeting phase. In fact, this approach is computationally demanding, as the internal numerical propagation and the required iterations for these method consume considerable time. This will be further discussed in chapter 5.

The second issue is related to fact that the LQR scheduled gains used in the targeting phase of Enhanced E-Guide were not generalized. Enhanced E-Guide uses the same LQR computed gains for different trajectories as shown in [10], but these results do not guarantee that the same gains can be used for different RVs (in fact it is stated in [10] that the results are only applicable if the same RV is considered). However, the generation of the gain look-up table is not trivial to generalize, as it involves the local linearization of the reference trajectory along several points. This was clearly beyond the scope of the current work.

Chapter 5

Guidance for landing site targeting

5.1 Introduction

In this chapter a newly developed guidance approach, that solves semi-analytically the TBVP (defined by the equations of motion (1.4) and the initial and final conditions) of the targeting phase of Enhanced E-Guide, is presented. The proposed approach enables precise landing site targeting for a high L/D RV by generating a reference profile that meets the inital and final conditions, the range requirements, and is further compliant with the path constraints.

In Enhanced E-Guide, the targetting phase is triggered at some point during re-entry (typically at velocities between 5 km/s to 6 km/s), where the state vector is assumed to be known. The shooting method [37] is then used to solve the TBVP, by finding the free parameters σ_0 and σ_i of the linear bank angle law

$$\sigma(t) = \sigma_0 + \sigma_\mathrm{i} t, \tag{5.1}$$

and the associated entry reference profile that meets the TAEM conditions without violating the path constraints. However, this approach involves iterative propagation of the equations of motion, which deems it computationally demanding. Hence the rationale for developing a different solution, able to find a reference profile and the associated bank angle law, but that is computationally less demanding.

Several approximate analytical methods were analysed. In particular, the approach using Hamilton-Jacobi theory to solve TBVPs [15] proved inadequate, as the re-entry dynamics cannot be framed in a Hamiltonian system. Two other approaches, the homotopy analysis method [21], which proposes solving TBVPs in finite domains using polynomials as the base functions for the solution, and the differential transformation method [6], that defines a differential transformation operator, based on the Taylor series expansion, to rewrite the TBVP in another function space and solve it, were also considered. However, the implementation of any of these methods has two drawbacks: the first is that they are mainly suitable for polynomial differential equations, as the natural space function solutions for these approches are polynomials, and these are not ideal base solutions for the re-entry TBVP; the second problem arises from the difficulty of implementing, testing, validating and applying any of these methods to the re-entry TBVP, which would require too much time being consumed without guarantee of results. Therefore, the followed approach takes on the insights in entry dynamics provided by the Apollo Guidance scheme [3], the Shuttle Entry Guidance [17] and [34], which proposes a method for 3-DoF reference trajectory on-board generation.

A bank angle law dependent on the velocity $\sigma(V)$ (as opposed to the bank angle law depending on time $\sigma(t)$ in (5.1)) that meets initial and final conditions, as well as the range requirements, is sought. To ensure

compliance with the downrange requirement, the downrange equation

$$\frac{\mathrm{d}s}{\mathrm{d}V} = -\frac{R}{R+h}\frac{V\cos\gamma}{-D-g\sin\gamma} \tag{5.2}$$

must also be integrated and taken into consideration.

In a first approach, approximations are made to the equations of motion (1.4), and a relation between the downrange, velocity and bank angle, based on (5.2), is obtained. This relation is integrated analytically with respect to the velocity V, and a constant bank angle solution is found. However, the accuracy of the final solution is hampered by the approximations introduced.

In order to improve these results, another approach was developed, where the downrange expression (5.2) is instead approximated by a polynomial depending on the velocity V whose coefficients are determined via the least-squares method [40]. Once the least squares polynomial approximation is found, downrange can be determined by analytical integration of this polynomial with respect to V. In order to perform this approximation, it is required to evaluate (5.2), which implies having approximations of the altitude, FPA, and the bank angle profiles.

The altitude profile is approximated by a linear combination of two altitude estimates depending only on velocity, where one estimate respects the initial conditions and the other respects the final conditions, using the analytical collocation method [48]. Once the altitude profile is approximated, the FPA profile approximation is determined by deriving the altitude profile. Regarding the bank angle, a $\sigma(V)$ law with three degrees of freedom is constructed, where two degrees of freedom are constrained by the initial and final conditions (the bounds of the TBVP), and the third is set so that the downrange requirement is met. In this way, the Reference Profile Generation (RPG) procedure ensures that initial and final conditions, as well as the downrange requirement, are satisfied.

5.2 TBVP identification

5.2.1 Equations of motion

The 3-DoF equations of motion (1.4) can be simplified by ignoring the terms related to the angular acceleration of the Earth ω, as the ficticious forces are small when compared to the drag force. Under this condition equations (1.4b), (1.4c), (1.4f), referring to the lateral motion, become decoupled from equations (1.4a), (1.4d), (1.4e), which are related to the RV's longitudinal motion. This allows for the separation of the equation set in two subsets, and enables the evaluation of longitudinal dynamics independently (after which the solution obtained can be plugged in the lateral motion equations to solve for χ, λ and ψ).

Considering the longitudinal motion equation set, the independent time variable t is replaced by velocity V, which is monotonously decreasing with respect to time during the targeting phase. This change is performed using the identity

$$\frac{\mathrm{d}}{\mathrm{d}t} = \frac{\mathrm{d}}{\mathrm{d}V}\frac{\mathrm{d}V}{\mathrm{d}t},$$

and allows reducing the number of state variables.

The transformed longitudinal set of equations written with V as independent variable is:

$$\frac{\mathrm{d}h}{\mathrm{d}V} = \frac{V\sin\gamma}{-D-g\sin\gamma}, \tag{5.3a}$$

$$\frac{\mathrm{d}\gamma}{\mathrm{d}V} = \frac{1}{V\left(-D-g\sin\gamma\right)}\left[\left(\frac{V^2}{r}-g\right)\cos\gamma + L\cos\sigma\right]. \tag{5.3b}$$

Another important expression is the downrange relation [13]

$$\frac{\mathrm{d}s}{\mathrm{d}t} = -\frac{R}{R+h} V \cos\gamma \cos\Delta\psi, \tag{5.4}$$

which is independent from equations (1.4) and can be determined once a solution is found for the state-space variables[1]. Performing the substitution of t for V as before, and neglecting the lateral motion term by assuming $\cos\Delta\psi \approx 1$, (5.2) is obtained.

5.2.2 Boundaries

The TBVP is fully defined by (5.3), (5.2), and the initial and final conditions that must be satisfied. The initial conditions are directly taken from the state-space vector at the triggering of the targeting phase, which typically occurs for velocities close to $5\ \mathrm{km/s}$. Considering (5.3) and setting V_0 as the velocity at which the targeting phase is triggered, the initial conditions for the state-space and control input vectors are

$$h_0 = h\left(V_0\right), \quad \gamma_0 = \gamma\left(V_0\right), \quad s_0 = s\left(V_0\right) \tag{5.5a}$$

$$\sigma_0 = \sigma\left(V_0\right), \quad \alpha_0 = \alpha\left(V_0\right). \tag{5.5b}$$

The final conditions of the problem are taken from the TAEM conditions, and written considering velocity V as the independent variable:

$$\begin{gathered} V_\mathrm{f} = V_\mathrm{TAEM}, \\ h_\mathrm{f} = h\left(V_\mathrm{f}\right), \quad \gamma_\mathrm{f} = \gamma\left(V_\mathrm{f}\right), \quad s_\mathrm{f} = s\left(V_\mathrm{f}\right). \end{gathered} \tag{5.6}$$

Note that the HAC constraint is not considered because the profile generation procedure does not deal with lateral motion.

The TBVP problem is also subject to the constraints that limit the solution state-space (1.7). The constraints (1.7) are mapped in the altitude-velocity plane in figure 1.4, alongside a nominal re-entry profile, using the requirements for the high lift-over-drag RV Phoebus [8, 12].

The most relevant constraint for the TBVP under analysis is the maximum aerodynamic acceleration, as for targeting phases velocities the heating flux becomes negligible, and it is not necessary to enforce the equilibrium glide condition at this stage of re-entry.

5.3 Approximate analytic bank angle solution

5.3.1 Obtaining the approximate analytical solution

This first approach takes on equation (5.2), and finds an approximate analytical expression relating the downrange s, the velocity V, and the bank angle σ. This is performed by simplifying (5.2), noting that for a high L/D RV the derivative of the FPA in this phase is small, in the order of 10^{-4}. It is thus assumed that the FPA is constant value (zero derivative), which commonly defines the equilibrium glide condition (as in (1.7d)), and is often valid in an intermediate phase during re-entry, as discussed in chapter 3, or in [34]. Equation (5.3b) is thus simplified and solved for lift L

$$0 = \frac{1}{V}\left[\left(\frac{V^2}{r} - g\right)\cos\gamma + L\cos\sigma\right] \Leftrightarrow L = \frac{g - \frac{V^2}{r}}{\cos\sigma}\cos\gamma, \tag{5.7}$$

[1] It is noted that the work here developed concerns longitudinal motion only, leaving aside crossrange considerations.

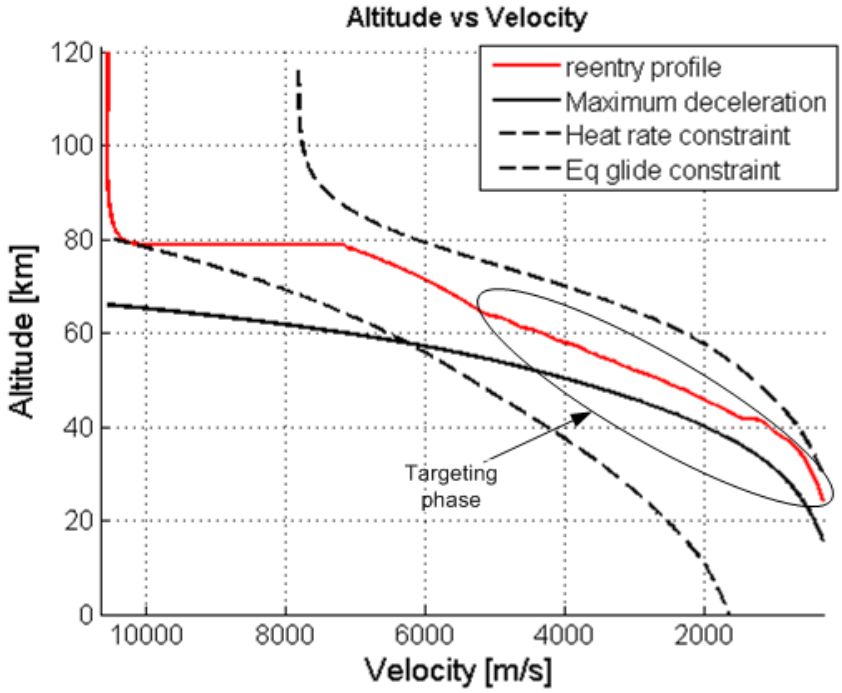

Figure 5.1: Nominal re-entry profile with targeting phase identified, and corridor constraints: the only hard constraint relevant for the targeting phase is the maximum deceleration constraint (1.7b).

which is used to replace the drag D in (5.2) via the relation

$$D = L\frac{C_D}{C_L}. \tag{5.8}$$

Substituting (5.7) and (5.8), (5.2) can be written as

$$\frac{\mathrm{d}s}{\mathrm{d}V} = R\frac{C_L}{C_D}\cos\sigma\frac{V}{V^2 + gr\left(\tan\gamma\frac{C_L}{C_D}\cos\sigma + 1\right)}, \tag{5.9}$$

after the terms are rearranged.

For integration of this expression, three other assumptions are required. Firstly, the distance to Earth center r is assumed to be constant, which implies that gravity $g = \frac{\mu}{r^2}$ is also constant. This is approximately valid noting that $r = R\left(1 + \frac{h}{R}\right)$ and that $h << R$. Another assumption considers that the L/D is constant. Note that this is the most delicate assumption, as for the high L/D RV considered, the targeting phase L/D variations are in the $[2.0,\ 2.5]$ interval. The effects of this coarse assumption can be mitigated by considering a piece-wise constant L/D instead, dependent on downrange. Finally, the bank angle must also be assumed constant, which is a limitation to the solution of the problem, rather than a simplification, as the bank angle is a free control parameter. The assumptions are summarized as:

- FPA is constant throughout the targetting phase;
- Distance to center of planet $r = R + h$ is constant;
- L/D is constant;
- Bank angle σ is constant.

Using these assumptions it is thus possible to integrate analytically (5.9),

$$s - s_0 = \frac{R}{2}\cos\gamma\frac{C_L}{C_D}\cos\sigma\log\left[\frac{V^2 + gr\left(\tan\gamma\frac{C_L}{C_D}\cos\sigma + 1\right)}{V_0^2 + gr\left(\tan\gamma\frac{C_L}{C_D}\cos\sigma + 1\right)}\right]. \tag{5.10}$$

Expression (5.10) provides a relation between downrange s and bank angle σ, with velocity as the independent variable. In order to write the bank angle in terms of downrange, inversion of this non-linear relation is required. Rewriting (5.10) in terms of bank angle

$$\begin{aligned} V^2 + gr = &\exp\left[\frac{1}{\cos\sigma}\frac{(s-s_0)}{\frac{R}{2}\cos\gamma\frac{C_L}{C_D}}\right](V_0^2 + gr) \\ &+ \exp\left[\frac{1}{\cos\sigma}\frac{(s-s_0)}{\frac{R}{2}\cos\gamma\frac{C_L}{C_D}}\right]\left(\tan\gamma\frac{C_L}{C_D}\cos\sigma\right) \\ &- gr\tan\gamma\frac{C_L}{C_D}\cos\sigma, \end{aligned} \tag{5.11}$$

it is noted that this expression is of the form

$$\mathrm{k}_1\exp\left[\frac{\mathrm{p}_1}{x}\right] + \mathrm{k}_2\exp\left[\frac{\mathrm{p}_1}{x}\right]x + \mathrm{k}_3 x = \mathrm{k}_4,$$

which can be solved with respect to x, using the method proposed in [41], or [26]. Hence the constant bank angle σ is computed (numerically) for a given downrange requirement.

Note that is possible to simplify (5.11) if it is further assumed that FPA is also small enough so that $\sin\gamma \approx 0$, $\cos\gamma \approx 1$, which is the case most of the time. Then (5.11) is reduced to

$$\cos\sigma = \frac{(s-s_0)}{\frac{R_E}{2}\cos\gamma\frac{C_L}{C_D}}\log\left[\frac{V^2 + gr}{V_0^2 + gr}\right]^{-1}, \tag{5.12}$$

which is a closed analytical relation between bank angle, the downrange requirement, and velocity.

5.3.2 Limits of validity

In obtaining (5.11) and (5.12) only the downrange requirement was taken into account. The other final conditions were not enforced but rather frozen in the assumptions made: when the FPA and FPA derivative are set to zero, and r is made constant, a profile for FPA (constant and zero) and altitude (constant) are implicitly assumed. Obviously, neither of these assumptions is true when the landing site is approached. Furthermore, the L/D is not constant either. As discussed before, it varies in the $[2.0,\ 2.5]$ interval, and will be another source of error. As a result of this approximation, it is expected a loss in the accuracy of the solution in terms of downrange, even though the final downrange constraint was strictly imposed.

To verify this hypothesis, (5.12) was tested in the simulation environment described in chapter 2. Nominal targeting phase triggering conditions were assumed as initial conditions, and TAEM conditions were used to terminate simulation, as shown in table 5.1. The result is shown in figure 5.2.

It is concluded that this approach enables a nominal final accuracy within $10 - 20$ km of the desired TAEM condition. While this is by no means satisfactory for a nominal test, the results were better than expected, as it is a simplified approach. It should be further noted that this result discards the need for more detailed Monte-Carlo testing, as the introduction of uncertainties would only deteriorate the performance of this analytical approach.

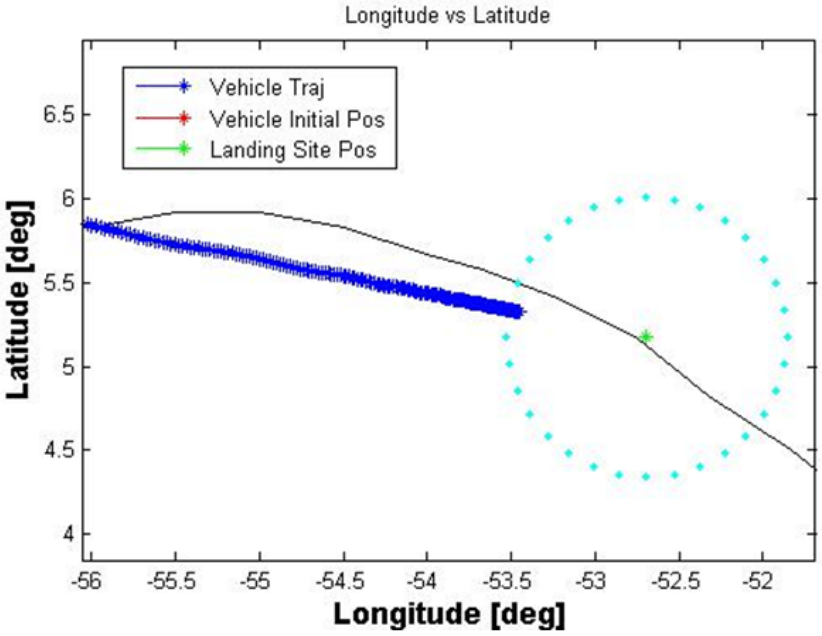

Figure 5.2: Detail of TAEM (indicated by the circle) targeting using the approximate analytical bank angle solution: the RV trajectory is given by the blue line.

5.4 Reference profile generation procedure

5.4.1 General description

The simplified analytical solution obtained in section 5.3 has shortcomings intrinsically related with the approximations performed on the set of differential equations that model the system dynamics. The approximations had as main goals the decoupling and linearization of the equations, so as to enable integration. Ultimately they resulted in a loss of accuracy in meeting final conditions.

For the Reference Profile Generation (RPG) procedure, simplifications to the set of differential equations are also made (otherwise the problem would be impossible to solve analytically). Nonetheless, these simplifications will be less restrictive and will try to capture the evolution of each state variable. Therefore, instead of simplifying (5.2) to enable integration, the RPG procedure approximates this expression by a polynomial depending on the velocity V, which is then integrated with respect to V to obtain $s(V)$. The approximation is performed using the least squares technique [40], which requires the evaluation of (5.2). For this evaluation, approximate altitude and FPA profiles, and a bank angle law, are necessary. Therefore, the RPG procedure initially selects a bank angle law, subsequently determines the altitude and FPA profiles, and finally evaluates (5.2), approximates it to a polynomial depending on velocity using least squares [40] and analytically integrates the polynomial obtained.

In this process the bank angle law is selected prior to downrange evaluation. However, the central problem is to find a bank angle that satisfies the downrange requirement, and not a bank angle law that imposes a downrange. To solve this, the procedure just described is repeated a pre-defined number of times, *e.g.* 10 or 20 (depending on the desired accuracy), for different bank angle laws, and a mapping $\sigma(s_{\mathrm{t}})$ between the bank angle σ and the total downrange s_{t}

$$s_{\mathrm{t}} = s(V_0) - s(V_f). \tag{5.13}$$

is determined. This mapping allows to find the bank angle by evaluating $\sigma(s_{\mathrm{t}})$ for the total downrange requirement, $s_{\mathrm{t_D}}$.

It is important to note that the shape of the bank angle laws must be kept constant, with only one varying

parameter, to ensure a univocal relation between σ and s_{t}. For example, if constant bank angle is considered, the higher the bank angle the lower is the total downrange covered, implying that the mapping $\sigma\left(s_{\mathrm{t}}\right)$ should be monotonous decreasing. Therefore, defining a maximum and minum admissible bank angles for the RV, the downrange results obtained will be the minimum and maximum downrange that the vehicle is able to cover, respectively. Every $s_{\mathrm{t_D}}$ should thus be inside this interval:

$$\left[\sigma_{\min}, \sigma_{\max}\right] \mapsto \left[s_{\mathrm{t,min}}, s_{\mathrm{t,max}}\right], \text{ then } s_{\mathrm{t_D}} \in \left[s_{\mathrm{t,min}}, s_{\mathrm{t,max}}\right] \Rightarrow \sigma_{\mathrm{D}} \in \left[\sigma_{\min}, \sigma_{\max}\right], \tag{5.14}$$

which is true for a constant bank.

However, in the TBVP the initial and final boundary conditions impose initial σ_0 and final σ_{f} bank angles. If a constant bank angle solution was adopted for solving the TBVP, the bank angle would be frozen and there would be no margin for downrange control. Therefore, a bank angle solution with three free parameters should be used: two parameters are used to ensure that the bank angle law satisfies the initial and final conditions boundaries, and the third parameter is selected so that the downrange requirement is met. The bank angle law, which is defined as being depending on velocity, has thus the free parameters p_1, p_2, p_3, and is of the form

$$\sigma\left(V, p_n\right) = p_1 \cdot f_1\left(V\right) + p_2 \cdot f_2\left(V\right) + p_3 \cdot f_3\left(V\right), \tag{5.15}$$

where f_{n} are different functions depending on V. Note that since the bank angle in the end only has one free parameter (the other two are determined by the initial and final conditions), the mapping in 5.14 applies with respect to this free parameter in the bank angle law. It is determined by selecting an intermediate bank angle σ_{i}, and varying the values only of σ_{i} in the bank angle law, to find a $\sigma_{\mathrm{i}}\left(s_{\mathrm{t}}\right)$ mapping.

Regarding the approximate determination of the altitude h and FPA γ profiles, which are used to evaluate (5.2), this is made in two steps: the estimation of the state-variables appearing in the equations of motion, and the direct evaluation of the equations of motion by using the estimated variables.

In both steps, the inverted set of (5.3) is used. This inversion consists in rewriting equation (5.3b) in terms of air density ρ and (5.3a) in terms of FPA γ:

$$\rho = \left[\left(-\frac{V^2}{r} + g\right)\cos\gamma - g\sin\gamma\frac{\mathrm{d}\gamma}{\mathrm{d}V}V\right]\left[D_{\mathrm{c}}\frac{\mathrm{d}\gamma}{\mathrm{d}V}V^3 + L_{\mathrm{c}}V^2\cos\sigma\right]^{-1}, \tag{5.16a}$$

$$\gamma = \arcsin\left[-D\frac{\mathrm{d}h}{\mathrm{d}V}\left(g\frac{\mathrm{d}h}{\mathrm{d}V} + V\right)^{-1}\right], \tag{5.16b}$$

where lift and drag forces per unit of mass are written as

$$L = \frac{1}{2}C_L\frac{S}{m}\rho V^2 = L_{\mathrm{c}}\rho V^2 \tag{5.17a}$$

$$D = \frac{1}{2}C_D\frac{S}{m}\rho V^2 = D_{\mathrm{c}}\rho V^2, \tag{5.17b}$$

with $L_{\mathrm{c}}\left\{D_{\mathrm{c}}\right\} = \frac{1}{2}C_L\left\{C_D\right\}\frac{S}{m}$. Note that expressions (5.16) and (5.17) are exactly the same as the original equations and have not suffered any simplification.

For the estimation of the profiles, it is assumed that both (5.16) and (5.17) are depending on velocity only, while the other variables appearing in the two expressions, *e.g.* r, g, $\mathrm{d}\gamma/\mathrm{d}V$, γ, $\mathrm{d}h/\mathrm{d}V$, are considered to be parameters depending on velocity that must be estimated. This is an important assumption that reduces the complexity of the problem, as the equations are 'integrated' and become decoupled. Moreover, in order to ensure that initial and final boundary conditions are exactly satisfied, the boundary conditions are strictly enforced in the estimation process, using a simple implementation of the collocation method [48].

When (5.16) is evaluated using the estimated parameters, the altitude and FPA profiles obtained meet exactly all the boundary conditions, and are used to evaluate (5.2). Additionally, these profiles also come for

free as outputs of the RPG procedure, describing the full longitudinal profile of the RV motion. The procedure thus produces the solution to the reduced state-space vector and the associated control input

$$\vec{x} = \begin{bmatrix} h(V) \\ \gamma(V) \\ s(V) \end{bmatrix}, \quad u = \sigma(V) \tag{5.18}$$

for all the velocity range, which meet exactly the initial (5.5) and final (5.6) boundary conditions of the TBVP (including the downrange requirement).

For the derivation of the RPG procedure, it is considered that:

- Initial conditions (2.2) and final conditions (2.3) are known exactly;
- There is one atmospheric database which maps air density and sound speed to altitude;
- There is one aerodynamic database available which maps drag and lift coefficients to Mach number and angle of attack.

These are usual requirements in the derivation of any guidance solution. Other common assumptions, that are also required for the RPG procedure, are:

- The TBVP problem defined by (5.3), (2.2) and (2.3) has at least one state-space region which is a feasible solution to the problem;
- The region of solutions does not violate the constraint equations (1.7);
- An angle of attack law, mapped with respect to velocity, is known.

Note that due to the last assumption, the profile generation procedure only deals with generating the reference command σ. As discussed before, keeping the angle of attack α to its reference values is common practice in outer loop guidance solutions, to ensure stability and trimmability of the RV motion.

5.4.2 Determination of the altitude and FPA profiles

Estimation of the state-variables

The evaluation of equations (5.16) and (5.17) requires the estimation of the variables appearing in the right side of the equations. These variables are $\hat{h}$, $\hat{\gamma}$ and $\hat{\dot{\gamma}}$ (where $\dot{x}$ is the derivative of x with respect to velocity), while the distance to Earth center r, gravity g and the D_c, L_c parameters are all approximately determined once $\hat{h}$ is known. In the estimation process it is assumed that the state variables are depending on velocity only, which implies that they are decoupled from one another.

The estimation procedure uses directly equation set (5.16). Equation (5.17) can be used for estimating $\hat{\gamma}$, while (5.16) can be used to estimate $\hat{h}$ if the exponential atmospheric approximation

$$\rho = \rho_0 \exp\left(-\frac{h}{H_S}\right) \Leftrightarrow h = -H_S \log\left\{\frac{\rho}{\rho_0}\right\} \tag{5.19}$$

is considered:

$$h = -\frac{1}{H_S}\log\left\{\frac{\frac{1}{\rho_0}\left[\left(-\frac{V^2}{r}+g\right)\cos\gamma - g\sin\gamma\frac{\mathrm{d}\gamma}{\mathrm{d}V}V\right]}{D_c\frac{\mathrm{d}\gamma}{\mathrm{d}V}V^3 + L_c V^2\cos\sigma}\right\}. \tag{5.20}$$

Estimation of the altitude profile $\hat{h}$ allows for estimating the FPA profile $\hat{\gamma}$ by derivating the altitude with respect to velocity $\hat{\dot{h}}$ and evaluating (5.17). Likewise, an estimate for FPA $\hat{\gamma}$ allows for the computation of the altitude profile estimate by derivation of γ with respect to velocity $\hat{\dot{\gamma}}$ and evaluation of (5.20). From (5.20)

it is seen that the relation of altitude with respect to air density is approximately given by a logarithm. The approximation errors introduced in the ρ profile will thus be mitigated by the logarithm effect. On the other hand, the FPA profile is extremely sensitive to the altitude derivative wrt V. Any error introduced in $\hat{\dot{h}}$ will appear in $\hat{\gamma}$. Minimization of the impact of the errors present in the estimated variables makes the case for estimating the alitude profile $\hat{h}$ first, and then use this profile for the subsequent estimation steps. Further advantages of estimating $\hat{h}$ first is that it allows for the evaluation of C_D (using the aerodynamic databases as detailed in section 2.3.2) as well as of the gravitic acceleration g, which are both used in $\hat{\gamma}$ determination.

Estimation of $\hat{h}(V)$ uses equation (5.20) and considers V as the independent variable, while the other variables are considered to be constant, and equal to their values at initial and final conditions:

$$r_0 = r(V_0), \quad g_0 = g(V_0), \quad \gamma_0 = \gamma(V_0), \quad \dot{\gamma}_0 = \dot{\gamma}(V_0), \quad L_{c_0} = L_c(V_0), \quad D_{c_0} = D_c(V_0) \tag{5.21a}$$

$$r_f = r(V_f), \quad g_f = g(V_f), \quad \gamma_f = \gamma(V_f), \quad \dot{\gamma}_f = \dot{\gamma}(V_f), \quad L_{c_f} = L_c(V_f), \quad D_{c_f} = D_c(V_f) \tag{5.21b}$$

Substituting the constant values (5.21a) and (5.21b) in equation (5.20) with $V \in [V_f, V_0]$ as independent variable results in two different profiles for altitude, $\hat{h}_0(V)$ and $\hat{h}_f(V)$, which meet initial conditions and final conditions, respectively (figure 5.3). These two altitude profiles are then linearly combined by means of two weighting functions $w_0(V)$ and $w_f(V)$, similarly to what is done in the analytical collocation method [48]

$$h(V) \approx \hat{h}(V, w_{\mathrm{i}}) = \sum_{i=0}^{n} w_{\mathrm{i}}(V)\, h_{\mathrm{i}}(V). \tag{5.22}$$

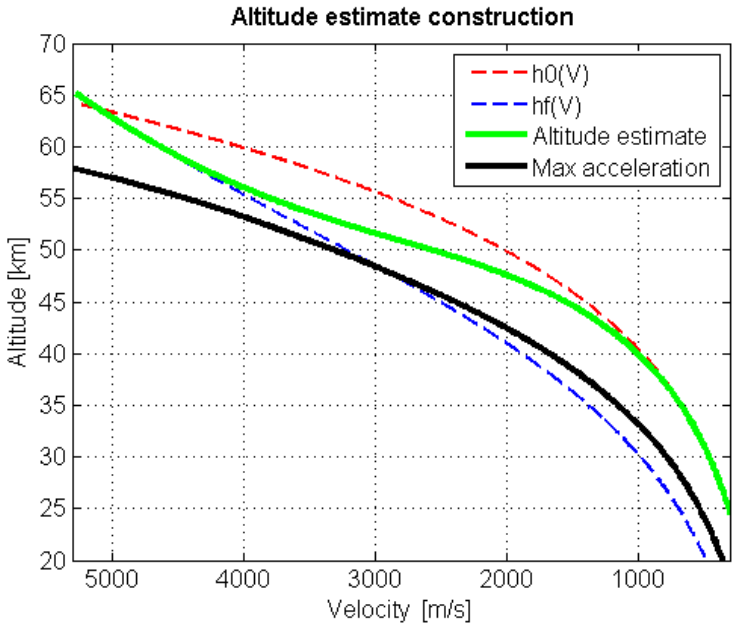

Figure 5.3: Estimation of the altitude profile using the collocation method: the blue profile meets initial conditions, while the red profile meets final conditions, and the green profile meets both.

The weights are selected so that the estimated profile is compliant with the corridor constraints, and ensure that the obtained profile has a continuous derivative and meets exactly initial and final conditions:

1. $w_0(V) + w_f(V) = 1, \quad \forall V \in [V_0, V_f]$;
2. $\frac{\mathrm{d}\, w_0}{\mathrm{d}\, V}$ and $\frac{\mathrm{d}\, w_f}{\mathrm{d}\, V}$ are continuous;
3. $w_0(V_0) = 1$ and $w_f(V_f) = 1$.

The altitude profile $\hat{h}(V)$ is thus computed using

$$\hat{h}(V) = w_0(V)\, h_0(V) + w_f(V)\, h_f(V). \tag{5.23}$$

Once the profile $\hat{h}(V)$ is known, $\frac{d\hat{h}}{dV}$ is computed by direct analytical differentiation

$$\frac{\mathrm{d}\, h}{\mathrm{d}\, V} = \frac{\mathrm{d}\, w_0(V)}{\mathrm{d}\, V} h_0(V) + w_0(V) \frac{\mathrm{d}\, h_0(V)}{\mathrm{d}\, V} + \frac{\mathrm{d}\, w_f(V)}{\mathrm{d}\, V} h_f(V) + w_f(V) \frac{\mathrm{d}\, h_f(V)}{\mathrm{d}\, V}. \tag{5.24}$$

Knowledge of the estimate of $\hat{h}(V)$ further enables approximate determination of air density $\hat{\rho}$ (using (5.19)) and of C_D. Knowledge of both is necessary for estimating drag $\hat{D}$. Finally, $\hat{D}$ and $\frac{\mathrm{d}\,\hat{h}}{\mathrm{d}\, V}$ are used to compute $\hat{\gamma}$ using equation (5.17).

Once $\hat{h}$ and $\hat{\gamma}$ are known, the only profile missing is the FPA derivative profile $\hat{\dot{\gamma}}$. This profile is obtained by numerical differentiation of $\hat{\gamma}$. However, this approach does not ensure that initial and final conditions are met. In order to correct for this, fitting functions are used, to enable meeting initial and final conditions. The approximate expression for $\hat{\dot{\gamma}}$ becomes

$$\frac{\mathrm{d}\hat{\gamma}}{\mathrm{d}V} = \frac{\mathrm{d}\hat{\gamma}}{\mathrm{d}V_{\mathrm{N}}} + \alpha \exp(a_{\mathrm{e},0} V + b_{\mathrm{e},0}) \sin(a_{\mathrm{s},0} V + b_{\mathrm{s},0}) + \beta \exp(a_{\mathrm{e,f}} V + b_{\mathrm{e,f}}) \sin(a_{\mathrm{s,f}} V + b_{\mathrm{s,f}}), \tag{5.25}$$

where $\frac{\mathrm{d}\hat{\gamma}}{\mathrm{d}V_{\mathrm{N}}}$ is the numerical derivative of $\hat{\gamma}$ and the sinusoidal fitting functions have no free parameters. Only coefficients α and β are determined so that initial and final conditions are met by the $\frac{\mathrm{d}\hat{\gamma}}{\mathrm{d}V}$ profile, while the underlying shape of the $\frac{\mathrm{d}\gamma}{\mathrm{d}V_{\mathrm{N}}}$ profile is not modified.

Approximate evaluation of the equations of motion

The estimated variables $\hat{h}$, $\hat{\gamma}$ and $\hat{\dot{\gamma}}$ and the constructed bank angle (5.15) are plugged into (5.16) and the profile for ρ is determined. The reference altitude profile is then determined using the atmospheric database, defined as in section 2.3.2.

In order to determine the reference profile for γ, the altitude profile h is numerically derivated and $\frac{\mathrm{d}h}{\mathrm{d}V_{\mathrm{N}}}$ is determined. Moreover, h is also used to determine the other variables appearing in (5.17): C_D, using the vehicle aerodynamic database, as discussed in section 2.3.2, and gravity g, through $g = \mu/(R+h)^2$. These variables are all plugged in (5.17) and the FPA reference profile is obtained.

In this way the coupled set of (5.3a) and (5.3b) is solved and a longitudinal profile for the state-space vector $[h\ \gamma]^T$ with respect to velocity V is determined.

5.4.3 Downrange estimation using the Least Squares method

Knowledge of the reference profile $[h(V)\ \gamma(V)]^T$ allows direct evaluation of the derivative of downrange with respect to velocity using expression (5.2). In order to integrate analytically the expression with respect to V, $\mathrm{d}s/\mathrm{d}V$ is approximated by a function depending on V with direct analytical primitive. A polynomial function with unknown coefficients, that are determined with linear Least Squares [40], is selected. The polynomial form $\hat{s}$ used to approximate $\dot{s}$ is given by

$$\frac{\mathrm{d}\hat{s}}{\mathrm{d}V} = (\mathrm{a} + \mathrm{b}V) \left[1 + \sum_i c_i \Phi_i(V, \alpha) \right] \tag{5.26}$$

where the coefficients a and b of polynomial $\mathrm{a} + \mathrm{b}V$ are determined so that initial and final conditions on $\dot{s}$ are satisfied. The arbitrary polynomial function $\Phi_i(V, \alpha)$ must be zero at $V = V_0$ and $V = V_{\mathrm{f}}$. This implies that $\hat{\dot{s}}$ precisely meets initial and final conditions. Furthermore, $\hat{\dot{s}}$ is analytically integrable in V.

The Least Squares method allows direct determination of coefficients c_i in $\hat{\dot{s}}$. It is known that for a system with observation vector y, unknown parameter vector x and data matrix F

$$y = Fx, \tag{5.27}$$

the linear Least Squares solution is given by [40]

$$\hat{x} = \left(F^{\mathrm{T}}F\right)^{-1} F^{\mathrm{T}}y. \tag{5.28}$$

It is possible to use this result in the estimation of parameters c_i. Writing

$$\frac{\mathrm{d}s}{\mathrm{d}V} - (\mathrm{a} + \mathrm{b}V) = \sum_i \Phi_i(V, \alpha)(\mathrm{a} + \mathrm{b}V)\, c_i \tag{5.29}$$

and taking

$$y = \frac{\mathrm{d}\hat{s}}{\mathrm{d}V} - (\mathrm{a} + \mathrm{b}V), \quad x = \bar{c} = [c_1, c_2, \cdots, c_n]^T \tag{5.30}$$

and

$$F = \begin{bmatrix} \Phi_1(V_0, \alpha)(\mathrm{a} + \mathrm{b}V_0) & \Phi_2(V_0, \alpha)(\mathrm{a} + \mathrm{b}V_0) & \cdots & \Phi_n(V_0, \alpha)(\mathrm{a} + \mathrm{b}V_0) \\ \vdots & \vdots & \ddots & \vdots \\ \Phi_1(V_f, \alpha)(\mathrm{a} + \mathrm{b}V_f) & \Phi_2(V_\mathrm{f}, \alpha)(\mathrm{a} + \mathrm{b}V_\mathrm{f}) & \cdots & \Phi_n(V_\mathrm{f}, \alpha)(\mathrm{a} + \mathrm{b}V_\mathrm{f}) \end{bmatrix}, \tag{5.31}$$

coefficients $\bar{c}$ are given by evaluation of (5.28).

Once the $\bar{c}$ coefficients are determined, the approximation of the downrange derivative $\dot{s}$ in terms of a polynomial function is known. This polynomial function is written as

$$\frac{\mathrm{d}\hat{s}}{\mathrm{d}V} = \mathrm{a} + \mathrm{b}V + \sum_i f_i(V, \alpha + 1), \tag{5.32}$$

with $f_i(V, \alpha + 1) = \Phi_i(V, \alpha)(\mathrm{a} + \mathrm{b}V)\, c_i$. Integration follows

$$\hat{s}(V) = s_0 + \mathrm{a}V + \frac{\mathrm{b}}{2}V^2 \sum_i F_i(V, \alpha + 2), \tag{5.33}$$

where s_0 is the initial condition for downrange.

The integrated polynomial expression provides the desired downrange profile with respect to velocity V.

5.4.4 Bank angle determination

The bank angle law $\sigma(V, p_\mathrm{n})$, defined as in (5.15) depends on velocity V only, and has three free parameters p_i so that initial condition σ_0, final condition σ_f and the downrange requirement are all met.

Once the $f_i(V)$ functions are selected, two of the three p_n parameters are determined so that intial and final bank angle conditions are satisfied: $p_{n,0}$ is determined so that $\sigma(V_0, p_n) = \sigma_0$ and $p_{n,\mathrm{f}}$ is determined so that $\sigma(V_f, p_n) = \sigma_\mathrm{f}$. Only the intermediate parameter $p_{n,\mathrm{i}}$ (for simplicity, p_i) remains free for determination, which is done using an intermediate value for bank angle $\sigma(V_\mathrm{i}, p_\mathrm{i}) = \sigma_\mathrm{i}$.

In order to find the correct σ_i that ensures meeting the downrange requirement, a predefined number of values in a reasonable interval $S = [\sigma_{\min}\ ,\ \sigma_{\max}]$ are assigned to σ_i. For each σ_i sample, the associated free parameter p_i is found and a bank angle law is constructed. Once this bank angle law is known, a reference profile is generated and total downrange (5.13) is computed. For each bank angle law, which is the same as for each value of σ_i (or equivalently p_i), an associated total downrange is obtained. Ultimately, this allows defining intermediate bank angle as a function of total downrange, $\sigma_\mathrm{i}(s_\mathrm{t})$.

Table 5.1: Nominal initial and final conditions

State	Initial conditions	Final conditions	Units
λ	2.5	-	deg
ϕ	-93.3	-	deg
h	65183	24000	m
V	5270	300	m/s
γ	-0.1832	-12.8	deg
ψ	84.9851	89.3	deg

The desired total downrange $s_{t_{\mathrm{D}}}$, derived from initial and final conditions

$$s_{t_{\mathrm{D}}} = s_0 - s_{\mathrm{f}}, \tag{5.34}$$

is then used to evaluate the function $\sigma_{\mathrm{i}}(s_{\mathrm{t}})$, and obtain the intermediate bank angle $\sigma_{\mathrm{i,D}}$. In this way, a bank angle law that meets the downrange criteria and initial / final conditions is determined. Finally, it is only necessary to generate the reference trajectory profile associated with the final bank angle law.

A full longitudinal reference trajectory $\bar{x}(V)$ and the associated reference command $u(V)$ are thus determined.

5.5 Implementation and tests

5.5.1 Implementation setting

The reference trajectory and bank angle profile generation procedure described in section 5.4 is tested as to evaluate its performance, and particularly its accuracy with respect to downrange. The RPG is run at the triggering of the targeting phase and generates the reference trajectory and the associated bank angle law, that are fed to the lower-level LQR gain-scheduled controller of Enhanced E-Guide (see the end of section 4.3) to enable reference trajectory tracking.

One issue that must be delt with in the testing of the algorithm is the crossrange control. The crossrange control method adopted was a simple heading error corridor selected prior to simulation, similar to the Shuttle solution [17] (detailed in chapter 3). This method issues a bank reversal command to change the sign of the bank angle when maximum heading error is reached, thus keeping the RV within the limits of the heading error.

It is important to note that longitudinal motion and lateral motion are not decoupled (contrarily to what is assumed in the RPG procedure) in the the equations of motion (2.1), used for entry simulation. Therefore, the effects of lateral motion will forcefully result in crossrange deviation from target, which means that the actual distance to target is different from the downrange to target, and this will deteriorate the performance of the RPG algorithm. While this effect is taken into account in the implementation of the RPG procedure, it is possible to further improve the performance of the algorithm by introducing estimates of the lateral profile. As discussed before, that is out of the scope of this work, but should be added in the future.

5.5.2 Nominal simulations

A nominal simulation was conducted to assess the RPG performance. The nominal inital conditions for the targeting phase were taken directly from a nominal full re-entry simulation using Enhanced E-Guide, and are presented in table 5.1.

Note that final latitude and longitude are not strictly imposed. Instead, the final downrange requirement of $s_{\mathrm{f}} = 93$ km is enforced.

Throughout simulation perfect knowledge of atmosphere and of the aerodynamic database, as presented in 2.3.2, is assumed. The reference profiles generated by the algorithm and provided to the controller for tracking are depicted in figures 5.4 to 5.7. In these plots the true profile flown by the vehicle is also depicted with the dashed line.

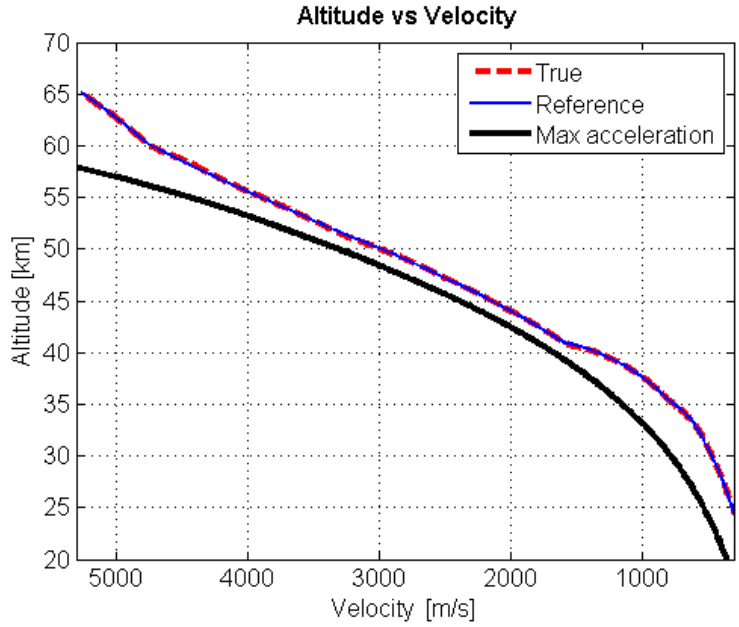

Figure 5.4: Reference and nominal profiles for altitude.

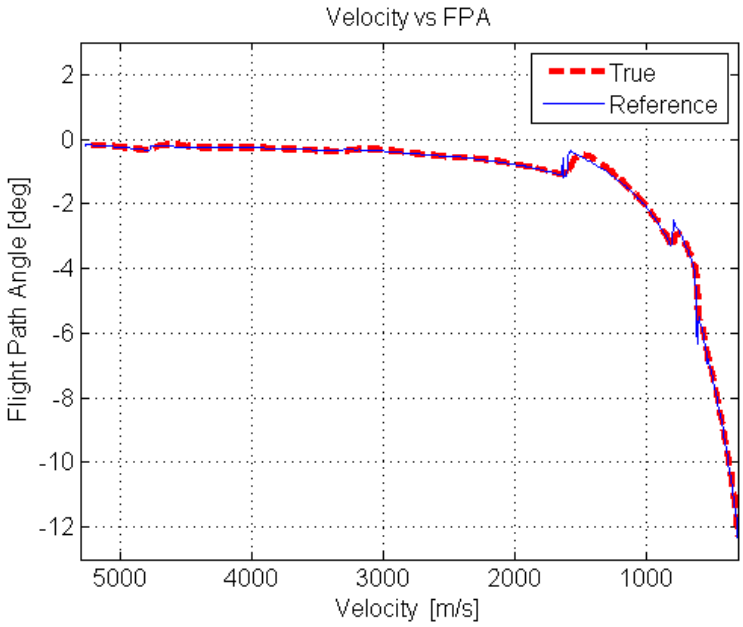

Figure 5.5: Reference and nominal profiles for FPA.

From figures 5.4 to 5.6 it is seen that the reference profiles are all feasible and tracked with an error of about 60 m in the case of the altitude profile, and about 0.1 deg in the case of the FPA profile, all reaching final conditions as desired. The bank angle refence command shown in figure 5.7 is tracked with an average error margin of 2 deg. In figure 5.8 the trajectory of the vehicle is depicted, showing its precise targetting ability in the nominal case.

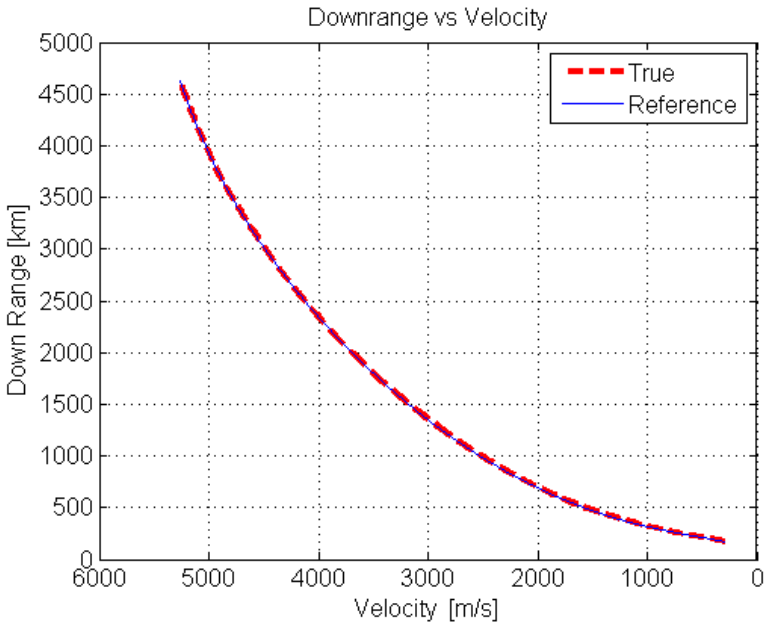

Figure 5.6: Reference and nominal profiles for downrange.

Table 5.2: Configuration used for the Monte-Carlo shots

State	Nominal initial conditions	Standard deviation	Units
λ	2.5	0.05	deg
ϕ	-93.3	2.5	deg
h	65183	30	m
V	5270	5	m/s
γ	-0.1832	0.001	deg
ψ	84.9851	0	deg

5.5.3 Monte-carlo tests

For further validation of the targeting ability of the algorithm, a Monte-Carlo test was performed using the uncertainties in initial conditions as presented in table 5.2.

Since the main objective of the Monte-Carlo tests is to assess the longitudinal targeting ability of the profile generation algorithm, the most perturbed initial condition was longitude. It should be further noted that latitude and heading were slightly perturbed and not perturbed at all, respectively, because the algorithm does not deal with lateral motion. Velocity, as the independent variable, was perturbed only to a 3-sigma error of 15 m/s for off-nominal targeting phase triggering. Perturbations in altitude and FPA were such that the predefined final conditions can be met. It should be noted that due to high sensitivity to FPA, if initial FPA is significantly different (i.e., 0.1 deg) from the nominal reference, then final FPA must also be changed.

Furthermore, uncertainties in the atmosphere and in the vehicle database were also considered. Regarding the atmosphere, an uncertainty centered in the reference density profile with 20% standard deviation was considered, while for the aerodynamic database a perturbation of 10% of the reference values was assumed, as discussed in chapter 2.

The Monte-Carlo test consisted of 1000 shots with the uncertainty set described above, for a 3-sigma (99.7%) success probability with a 95% confidence interval. The results of the tests are depicted in figures 5.9 to 5.11.

The results show that the RPG enables a good targeting precision. In the histogram in 5.11, it is seen that the final downrange dispersion amounts to a 10 km interval around the desired target. The bias of 2 km shown in the histogram could further be corrected once the lateral motion is accounted for, which would additionally

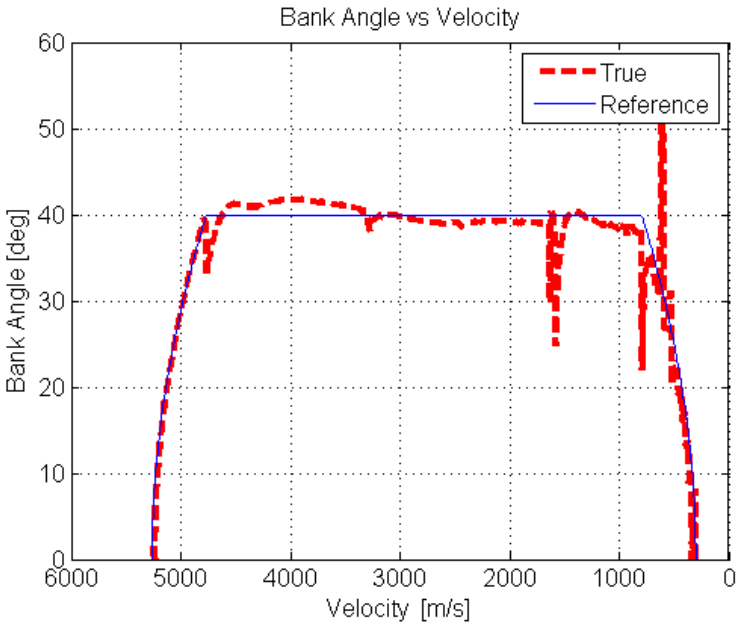

Figure 5.7: Reference and nominal profiles for bank.

reduce the width of the 10 km interval.

5.6 Application: vehicle downrange capability

A measure of the downrange to target is always available, as the RV's navigation system is able to estimate its current position, and the landing site position is known. Apart from knowing this downrange measure, it is important to know whether the RV is able to cover the given downrange or not.

In sections 5.3 and 5.4 guidance laws were derived that had as a goal meeting the downrange requirements. The application of these guidance methods to the prediction of the RV downrange capability comes for free from their derivation. In fact, if the solutions obtained are solved for downrange instead of bank angle, setting the bank angle to zero $\sigma\left(V\right)=0$ deg will provide the maximum downrange capbility of the vehicle, as that is the case where lift is maximum in the upward direction, which implies that the rate of descent is smallest and that downrange is maximised.

The approximate analytic solution of section 5.3 (5.10) is written in terms of downrange as

$$s=s_0+\frac{R_E}{2}\cos\gamma\frac{C_L}{C_D}\cos\sigma\log\left[\frac{V^2+gr\left(\tan\gamma\frac{C_L}{C_D}\cos\sigma+1\right)}{V_0^2+gr\left(\tan\gamma\frac{C_L}{C_D}\cos\sigma+1\right)}\right]. \tag{5.35}$$

Setting constant bank angle solution to zero provides the minimum final downrange to target, when velocity $V=V_f$.

Regarding the RPG algorithm, downrange capability is directly obtained by setting the bank angle law to zero. In this case, the bank angle determination step described in section 5.4.4 is not required, as the bank angle is determined *a priori*.

5.7 Remarks

The derivation and the results presented in this chapter show that the RPG procedure for the targeting phase of Enhanced E-Guide complies with initial and final conditions requirements, as well as the entry corridor

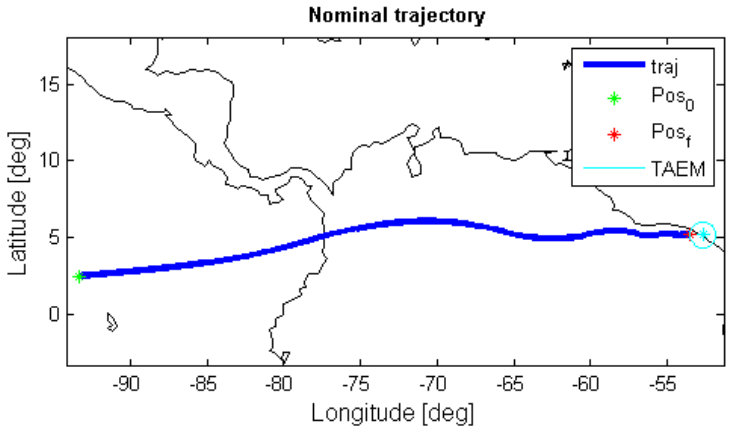

Figure 5.8: Nominal targeting trajectory.

constraints. The algorithm allows for flexible targeting trajectory generation, thus being able to cope with the set of uncertainties considered. Moreover, the instantaneous profile generation deems this algorithm suitable for onboard installation.

While the tests performed used a high lift-over-drag vehicle as baseline, there is no reason for this approach not to work with moderate or low lift-over-drag vehicles, provided that final conditions (namely donwrange requirement) are adjusted.

In the future, the RPG procedure could be further enhanced with the addition of lateral profile generation. This would improve the landing site targeting results, and enable even greater dispersions at the initial conditions. In this respect, solutions like a corridor for maximum heading error as used in [3] and [17] could be implemented. Other solutions, like the one proposed in [34, 35], which reduce the number of bank reversals, would also be suitable for integration with the solution of the targeting problem.

It is important to note that the analytical approach described in 5.3, while not providing completely satisfactory results, was fundamental for a deeper understanding of the guidance problem. Its derivation imparted an insight to the impacts of the approximations performed in the accuracy of the final solution, and provided an important background for the development of the RPG procedure.

Finally, the application of these guidance approaches to downrange prediction could be important for the triggering of the targeting phase. Enhanced E-Guide uses velocity to determine the moment when the targeting phase should be triggered, which does not ensure that there is enough downrange margin to reach target. Prediction of the downrange capability of the RV could be used instead, which would further improve the targeting results.

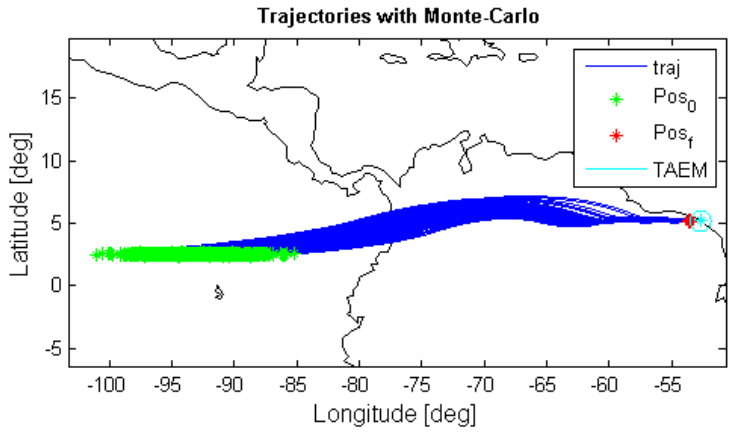

Figure 5.9: Targeting trajectories from Monte-Carlo test.

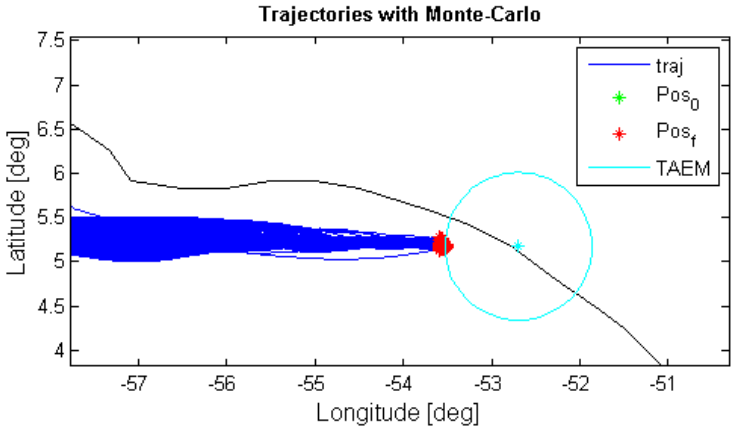

Figure 5.10: Detail of TAEM targeting from Monte-Carlo test.

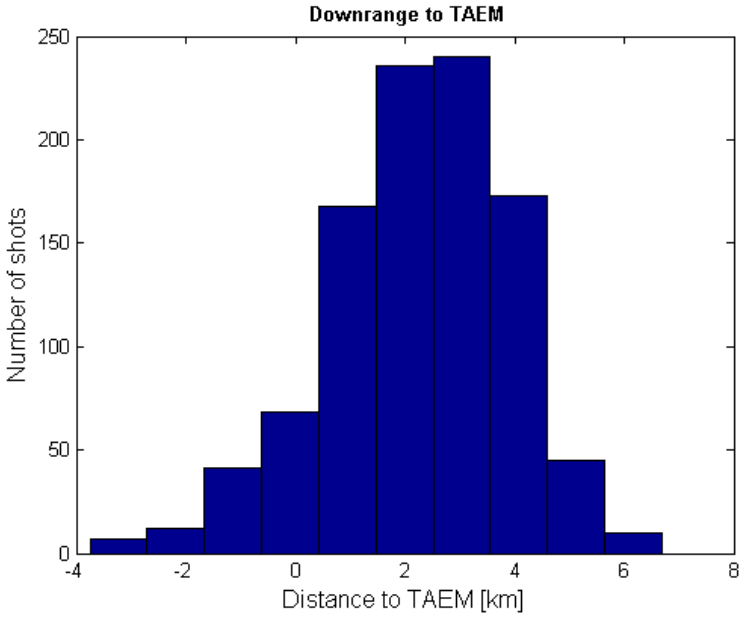

Figure 5.11: Histogram of the downrange to TAEM interface for the Monte-Carlo test results.

Chapter 6

REACTIVE tool

6.1 Introduction

The tool developed, named REACTIVE, is a guidance and control design tool that integrates all the guidance solutions presented in the previous chapters. It had two main drivers for its development: firstly, consolidation and integration of all guidance algorithms and RVs available in one single tool. Secondly, the generalization of the guidance algorithms so that they could be used for the respective L/D class of RVs. Complying with these objectives, REACTIVE is a tool that not only collects the available algorithms but does so in a criterious manner, so as to have one guidance solution for each type of vehicle, and further generalizes these solutions so that they are applicable to the associated L/D class of RVs.

In this regard, all the guidance solutions presented in previous chapters were integrated in REACTIVE. The simulator described in chapter 2 constitutes the core of REACTIVE, to which the Shuttle Entry Guidance, as discussed in chapter 3, the Apollo Entry Guidance and the Enhanced E-Guide algorithms, as presented in chapter 4, and the newly developed procedure that enhances the targeting abilities of Enhanced E-Guide, thoroughly analysed in chapter 5[1], have been added. This integration step consisted in the re-organization of the algorithms so that they could be installed in parallel under the same tool. Therefore, the aerodynamic databases and the vehicle parameters associated to each baseline RV were normalized, and the guidance parameters structures were uniformized. The tool was thus shaped to run all the vehicles and guidance schemes available. Furthermore, the process by which new RVs and guidance schemes are added to the tool was simplified, to allow for possible future expansions on the RV and guidance databases.

The integrated algorithms were also generalized, as detailed in the associated chapters, in order to make their implementation adaptable to RVs with different aerodynamic characteristics from those used as baseline. Generalization consisted in making the Apollo, Shuttle, and Enhanced E-Guide entry algorithms suited for low, moderate, and high lift-over-drag RV classes, respectively, instead of being restricted to the baseline vehicles they were initially designed for. Therefore, more than collecting pre-existing guidance schemes, REACTIVE recycles them so that they can be used for the simulation of new concept vehicles. The results obtained with the generalized algorithms will be discussed in this chapter.

Finally, REACTIVE was also extended to the Mars scenario, with the installation of an atmospheric database and environment parameters. It is thus possible to select, prior to simulation, not only the type of RV and guidance algorithm desired, but also the scenario: Earth or Mars. In the future, new scenarios may be added, as it is trivial to add new scenario databases to REACTIVE.

[1] This procedure is also integrated in REACTIVE but will not be further discussed in this chapter, as it was already viewed in detail in chapter 5.

6.2 REACTIVE tool integration

6.2.1 Hierarchical decomposition

REACTIVE implementation in MATLAB is based on the merging of the simulator (described in chapter 2) with all the guidance schemes algorithms, and the associated RVs' and guidance databases which are used in simulation. The hierarchical/functional decomposition of the core of REACTIVE is depicted in figures 6.1, 6.2, and 6.3.

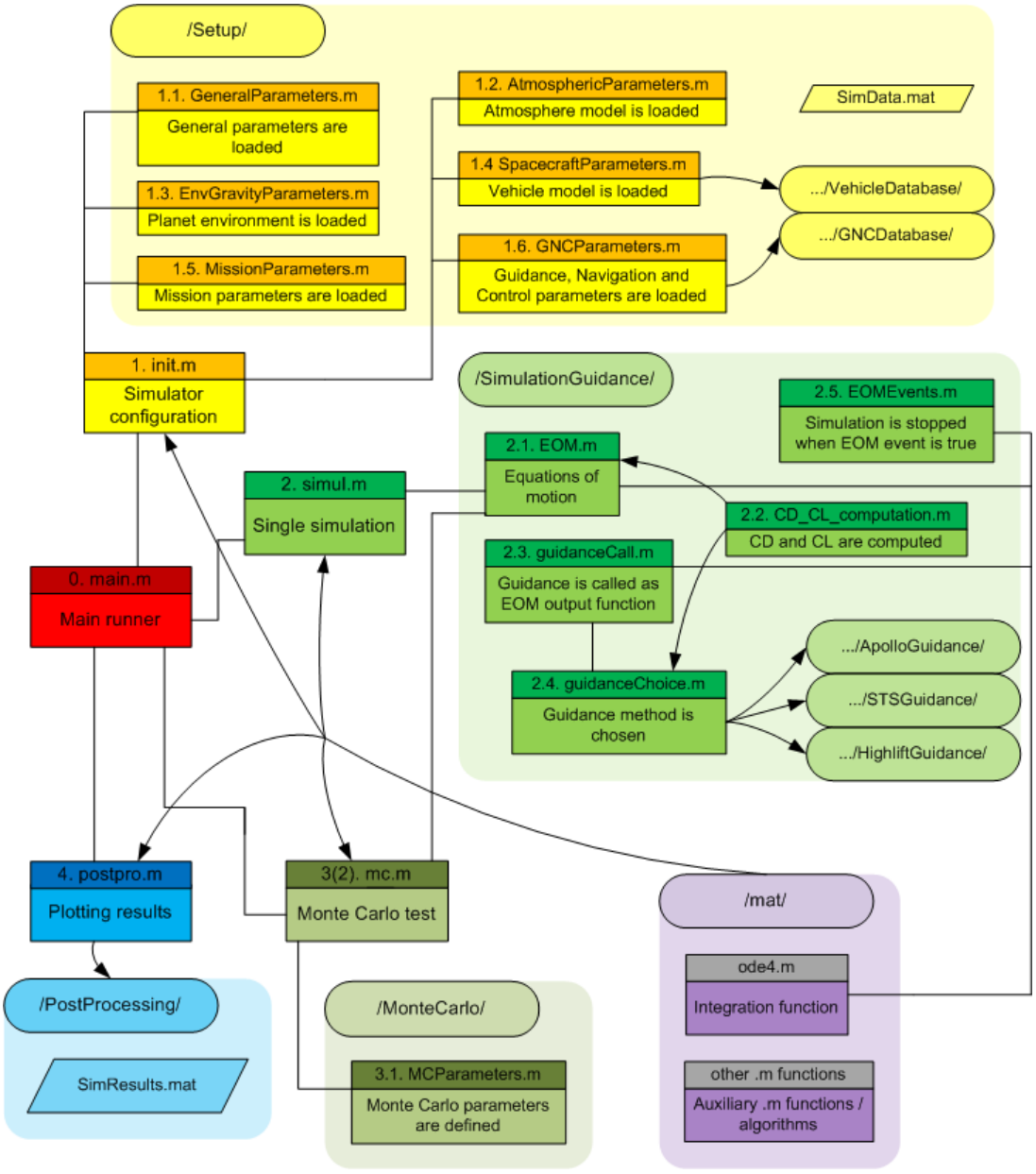

Figure 6.1: Decomposition of REACTIVE tool [14]: the four core functions main.m, init.m, simul.m, mc.m, and postpro.m (as described in chapter 2), and second layer functions.

REACTIVE is structured using the four core functions of the simulator described in chapter 2, init.m, simul.m, mc.m, and postpro.m, with each core function associated to a folder containing the related subfunctions: the init.m is related to the Setup folder, which contains all the databases and parameter definitions; the simul.m is related to the SimulationGuidance folder, which contains all the simulation functions, and the guidance schemes functions; the mc.m is related to the MonteCarlo folder, where the uncertainty parameters

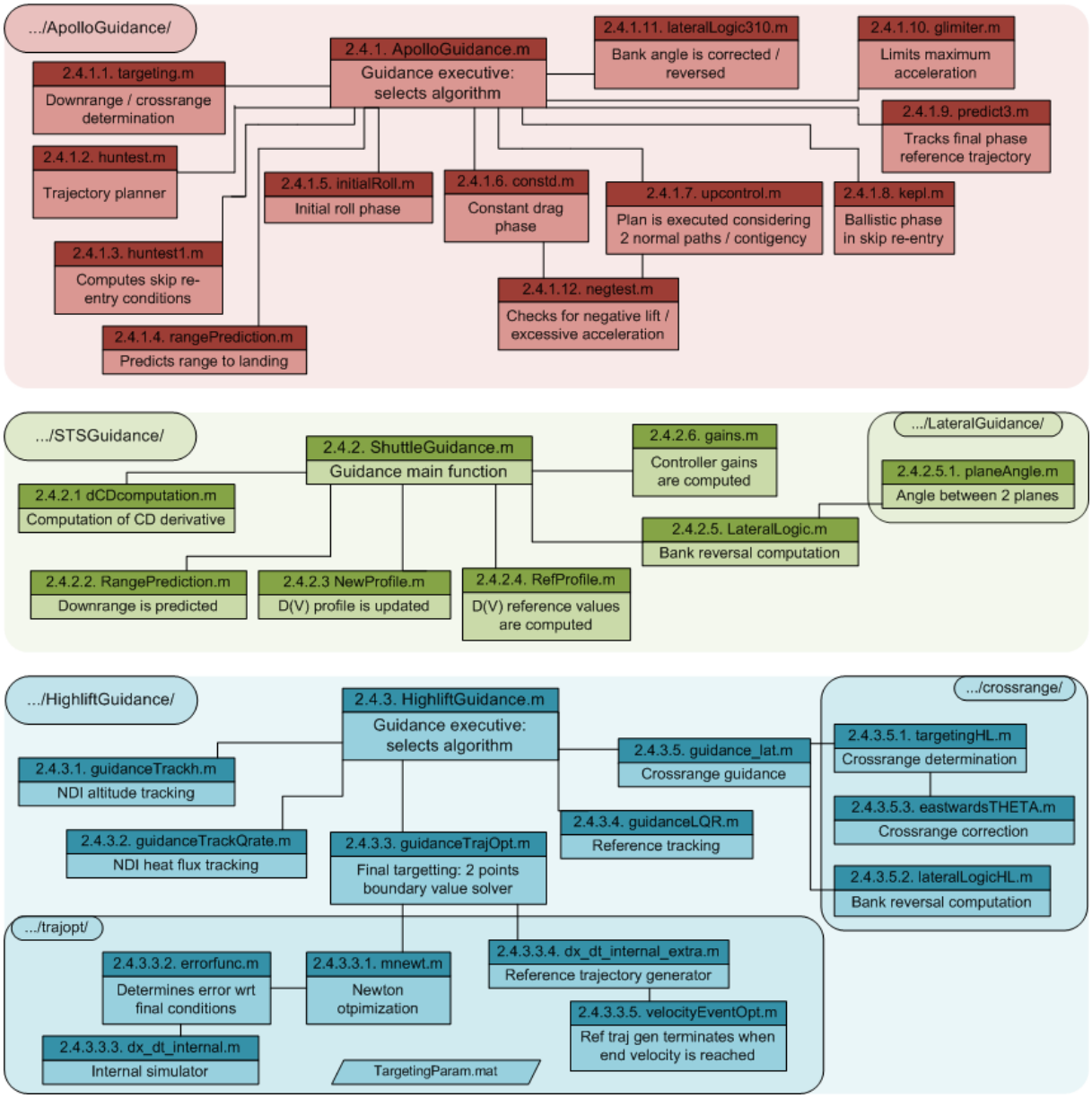

Figure 6.2: Decomposition of REACTIVE tool [14]: third and fourth layers below the SimulationGuidance folder.

are defined; the postpro.m is related to the PostProcessing folder, which contains the functions for processing the outputs of simulation.

This organization makes the addition of new vehicles and guidance schemes simple and flexible, being only required to add an associated parameter database in the initialization function under the Setup folder, and creating a function under the simulation folder that implements the desired guidance algorithm. In the same way, it is possible to add new atmospheric databases and planet environments to the tool. In fact, this has enabled the addition of three more vehicles to REACTIVE, as well as one new guidance scheme, in subsequently developed work.

6.2.2 Entry vehicles & guidance schemes roundup

In table 6.1, the guidance schemes implemented in REACTIVE and their associated vehicle class are depicted.

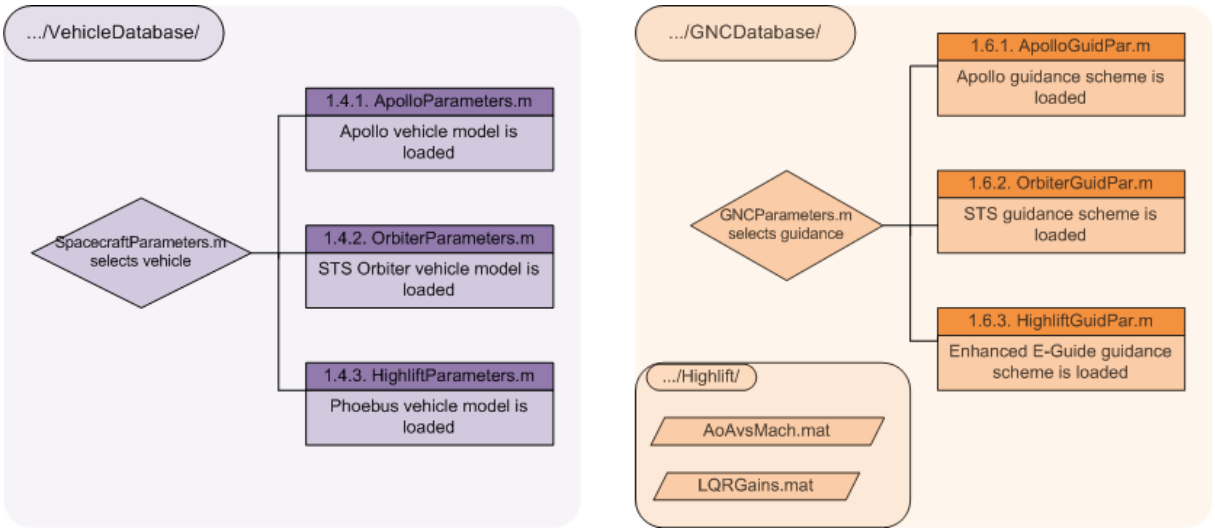

Figure 6.3: Decomposition of REACTIVE tool [14]: third and fourth layers below the Setup folder.

Guidance Sheme	Baseline vehicle	L/D class
Apollo Entry Guidance	Apollo Commnand Module	Low
Shuttle Entry Guidance	Shuttle Orbiter	Moderate
Enhanced E-Guide	PHOEBUS vehicle	High

Table 6.1: Guidance schemes and vehicles

Entry vehicles

The baseline vehicles used were presented in sections 3.2 (Shuttle Orbiter), 4.2 (Apollo CM), and 4.3 (Phoebus). In table 6.2 some relevant data associated to each baseline RV is depicted, for comparison.

Parameters		Apollo CM	Shuttle Orbiter	Phoebus
Mass	kg	5500	69000	5000
Presented area	m^2	12.6	250	61.9
Mass / presented area	kg/m^2	438	276	81
L/D		0.3	1	2
Max. heat flux	kW/m^2	2000	750	2000
Max. acceleration	g	10	2.1	6
Downrange / crossrange	km	3700/320	10000/1300	55000/3800

Table 6.2: Baseline RVs main parameters [8, 12, 18, 23, 27]

The parameters presented in table 6.2, while being relative to each specific RV, should be interpreted as being representative of the associated broader class of vehicles, that is defined by the L/D ratio. The L/D ratio determines the relative equilibrium of the aerodynamic forces, thus impacting decisively the entry profile described by the RV, as was discussed in chapter 1 and further confirmed in the test section of chapter 2.

It should be noted that RV presented area and mass, as well as the constraints of maximum heat flux and aerodynamic acceleration are associated to the mission for which each RV was designed for. While for the RV conception and design mission definition is critical, for the simulation of the entry profiles it suffices to have defined the EIP conditions and the path constraints. Therefore, from the GC point of view, these constraints

are not associated to the RV itself but rather to the mission, and should thus not be distinctive of a RV class.

Regarding the downrange / crossrange capability of each RV, it is possible to distinguish the impact that the characteristic L/D has on this parameter: the greater the L/D, the greater is the downrange / crossrange capability of the RV.

In figures 6.4 the RVs concept drawing is shown. For the remaining of the chapter the RVs depicted in the figures are representative of their associated class, and not of any RV in particular.

(a) Low L/D vehicle (b) Moderate L/D vehicle (c) High L/D vehicle

Figure 6.4: Concept illustrastion of the different RVs in REACTIVE

Guidance schemes

The guidance algorithms added to REACTIVE were thoroughly discussed in chapters 3 and 4. They comprise different techniques of entry guidance, which are summarized in table 6.3. They were further generalized, as described in those chapters, in order to become adaptable to different RV configurations.

Guidance Scheme	Category	Description
Apollo Entry Guidance	-	Phase 1: RV capture by directing lift vector downwards
	Reference profile tracking	Phase 2: tracking of a profile mapped with respect to velocity via gain-scheduled PID control
Shuttle Entry Guidance	Reference profile tracking	Tracking of a drag-velocity profile with gain-scheduled PID control
Enhanced E-Guide	Feedback linearization	Phase 1: Reference altitude and heat flux tracking with NDI technique
	Reference profile tracking	Phase 2: tracking of a reference profile with a gain-scheduled LQR controller

Table 6.3: Guidance schemes global description

6.3 Results

6.3.1 Guidance schemes with associated vehicle class

RVs belonging to each L/D class were tested on the associated guidance schemes, in a Monte-Carlo campaign of 100 shots each. In every testing set, the atmospheric uncertainty setting shown in table 2.3 was considered, and a 3-sigma dispersion of 10% in the RV aerodynamic database was assumed.

The first RV tested was the low L/D, with the initial conditions and uncertainties shown in table 6.4.

EIP condition	Units	Nominal	Standard deviation
Latitude	[deg]	-5.11	1
Longitude	[deg]	134.79	1
Altitude	[km]	120	-
Velocity	[m/s]	8750	10
FPA	[deg]	-3.57	0.02
Heading	[deg]	58.65	0.2

Table 6.4: Setting used for testing the low L/D RV on the Apollo Entry Guidance algorithm.

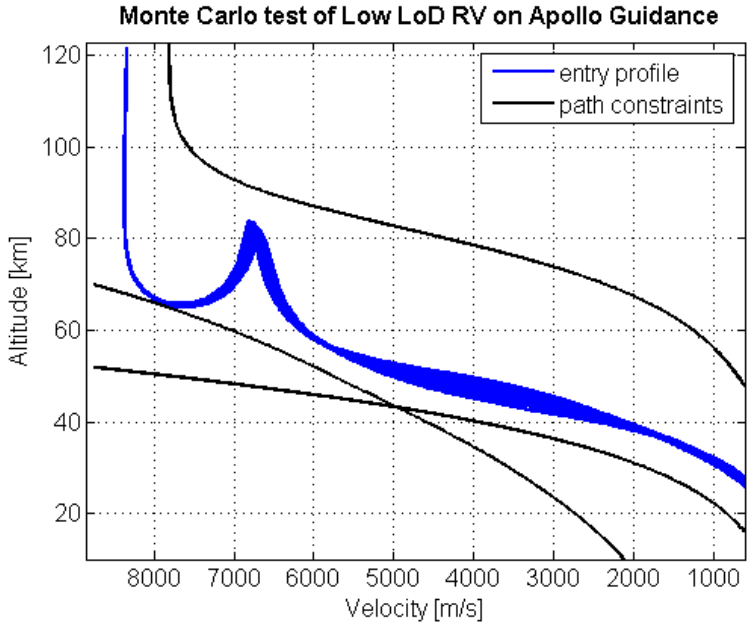

Figure 6.5: Monte-Carlo test of the low L/D RV on the Apollo Entry Guidance: altitude-velocity plot of the entry profile with path constraints.

The results obtained allows to conclude that the RV was compliant with all the path requirements (figure 6.5), and that the most critical phase in the low L/D re-entry is right after atmospheric capture, when the RV experiences significant heat fluxes. Nonetheless, the generalized Apollo Entry Gudiance was able to run on the low L/D RV, and was able to cope with all the uncertainties considered.

The moderate and high L/D RVs were subsequently tested on the Shuttle Entry Guidance and Enhanced E-Guide, respectively, with the Monte-Carlo setting shown in table 6.5.

The results obtained are again compliant with the path constaints considered. The moderate L/D is able to track the reference profile, as depicted in figure 6.6, and the altitude and heat rate references of the NDI phases are also tracked by the high L/D RV, shown in figure 6.7.

Overall, the results obtained show that the integration and consolidation of the algorithms was successful. REACTIVE is thus able to run the implemented guidance schemes on arbitrary vehicles of the associated L/D class.

EIP condition	Units	Moderate L/D Nominal	High L/D Nominal	Standard deviation
Latitude	[deg]	-30.83	20.01	2
Longitude	[deg]	-164.06	-61	2
Altitude	[km]	120	120	-
Velocity	[m/s]	7450	10550	10
FPA	[deg]	-1.21	-4.38	0.05
Heading	[deg]	65.60	90.37	0.4

Table 6.5: Setting used for testing the moderate and high L/D RV on the Shuttle Entry Guidance and Ehanced E-Guide algorithms, respectively.

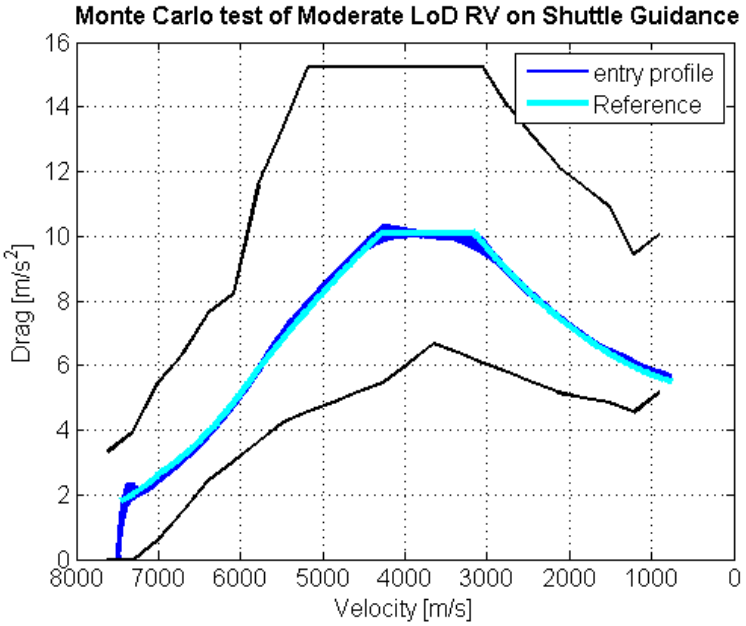

Figure 6.6: Monte-Carlo test of the moderate L/D RV on the Shuttle Entry Guidance: drag-velocity plot of the entry profile, with the tracked reference profile and path constraints.

6.3.2 L/D class study

The guidance algorithms implemented were further tested for different L/D RVs of the associated class, in order to explore the limits of applicability of each algorithm. The results show that the Apollo Entry Guidance is suitable for RVs in the range $0.2 < L/D < 0.6$. For lower values of L/D, the control margin is not enough to track the reference profile in the targeting phase, and is not enough to avoid violation of the constraints right after capture. This is visible in figure 6.8, for the case of $L/D = 0.2$, where right after the vehicle is captured into the planet atmosphere there is barely sufficient lift available to avoid violation of the maximum heat flux constraint. For higher L/D values, the capsule has an undesired oscillatory motion that may result in the violation of the constraints. The example for $L/D = 0.5$ in figure 6.8 is approximately a limit case.

Regarding the Suttle Entry Guidance algorithm, it was concluded that it is suitable for $L/D > 0.8$. Below this value, the RV does not have the L/D margin to track the reference drag-velocity profile. This is further shown in figure 6.9, where for the $L/D \approx 0.8$ considered the RV is not able to track satisfactorily the reference profile in the early and latest parts of re-entry. For higher L/Ds, the RVs seem to run perfectly well in the Shuttle Entry Guidance, as the higher the L/D margin, the easier it is to track the reference.

Finally, the Enhanced E-Guide is the most demanding of the three algorithms in terms of L/D requirements.

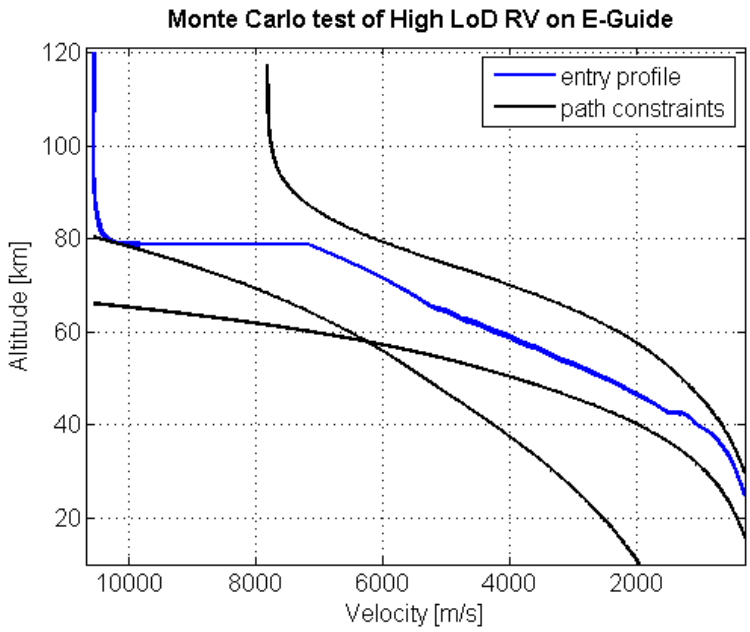

Figure 6.7: Monte-Carlo test of the high L/D RV on the Enhanced E-Guide: altitude-velocity plot of the entry profile with path constraints.

It is only suitable for RVs with $1.8 < L/D < 2.5$, as the L/D margin is critical for the tracking of the reference altitude in the first NDI phase. For L/Ds below this threshold, it was verified that the RV was not able to track the reference altitude and skipped out of the atmosphere. This is further shown in figure 6.10, for a RV $L/D = 1.7$. For higher L/Ds, a problem concerned with the LQR controller starts to show in the last phase. Clearly, as documented in figure 6.10 for the $L/D = 2.5$ case, there is an undesired oscillatory motion below $V = 5$ km/s. This results from the scheduled gains of the controller not being adequate to the new vehicle configuration, as it is different from the one used in their determination.

6.3.3 Mixing guidance schemes and associated vehicle class

In REACTIVE it is also possible to mix the guidance schemes and the RV class. As an example of this, the Shuttle Entry Guidance is tested with the low and high L/D RVs. Following the previous discussion, it is expected that the low L/D RV performs poorly in the tracking of the drag-velocity profile, while the high L/D RV shoud excel at that. The results confirm this supposition, as is shown in figures 6.11 and 6.11.

As predicted, the low L/D vehicle is not able to track the reference profile, as it has not enough L/D margin to do so. However, the approach followed in the Shuttle Entry Guidance method could in theory be applicable to low L/D RVs, provided that the reference profile was re-designed and adapted to this type of RVs. On the other hand, the high L/D RV tracks satisfactorily the drag-velocity reference profile.

6.4 Extension to Mars scenario

Mars atmosphere [20, 36] and environment [24] have been added to REACTIVE's database. The atmospheric air density Mars model is depicted in figure 6.13, while in table 6.6 the main parameters characterizing the Mars environment are shown.

Mars gravitic acceleration is modest when compared to Earth's, and its atmosphere is less dense and relatively unknown regarding its composition. Entry strategies have thus relied on capsule-like RVs with $L/D \approx 0$. While this constrains the applicability of GC solutions to this planet scenario, it would be possible to tailor the Apollo Entry Guidance for Mars entry, provided that some minimum L/D is available [31].

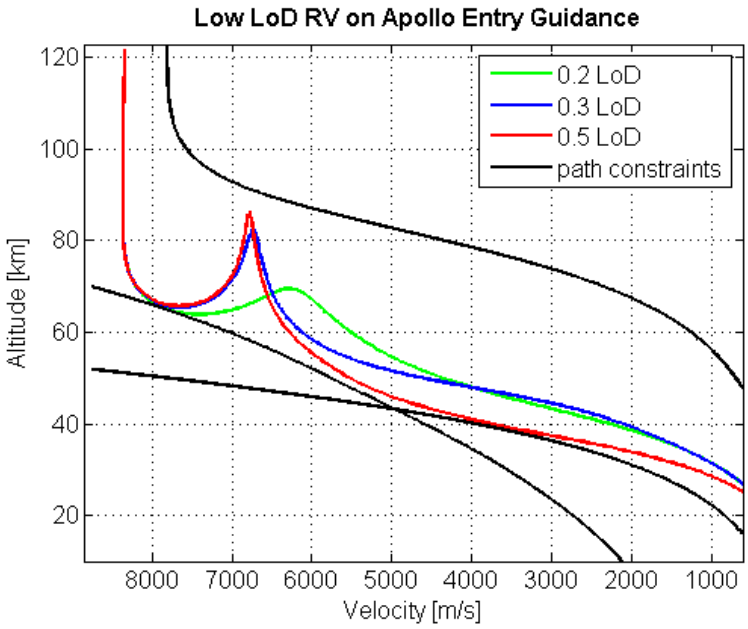

Figure 6.8: Low L/D RVs on Apollo Entry Guidance, in the altitude-velocity plane: entry profiles and path constraints.

Parameters	Symbol	Units	Values
Gravitational parameter	μ	$[\mathrm{m}^3/\mathrm{s}^2]$	4.2828×10^{13}
Rotation rate	ω	[rad/s]	7.1011719×10^{-5}
Equatorial radius	R	[m]	3396.2×10^3

Table 6.6: Mars environment parameters

6.5 Remarks

From the the tests performed it is noted that the integration of all the algorithms in the REACTIVE simulation environment was successful. Notably, this was the most arduous task undertaken in the development of REACTIVE, as all the guidance algorithms were prototyped using different baseline simulators. Therefore, each had specific intricacies related to their implementation that had to be modified or re-implemented, according to the REACTIVE environment.

The results obtained with REACTIVE futher allow to conclude that the higher the L/D, the higher is the control authority available. In other words, with higher L/Ds the bank angle variation interval, from full bank at $\sigma \approx 90$ deg to zero bank at $\sigma \approx 0$ deg, produces a more diverse pool of entry profiles. Ultimately this allows for flexible entry profile tracking and real time adaptation to uncertainties.

It should be stressed that REACTIVE is not a mere collection of algorithms. The guidance schemes implemented can be freely used, and even combined, to evaluate past entry solutions, or to devise and test new entry approaches for different scenarios and RVs. In fact, it is in this respect that REACTIVE offers most of its potential, as it aims to contribute to the better understanding of the already developed guidance and control approaches, and ultimately use them as background for the design of new entry approaches.

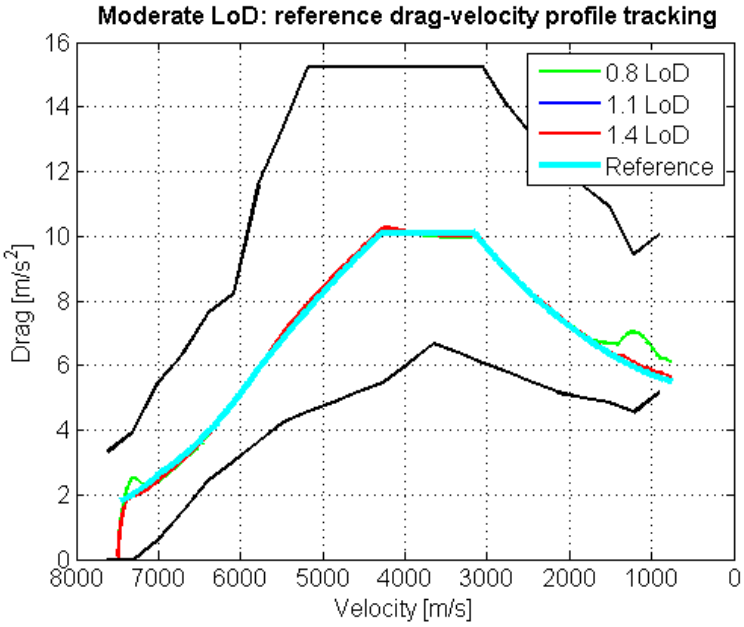

Figure 6.9: Moderate L/D RVs on Shuttle Entry Guidance in the drag-velocity plane: entry profiles, drag-velocity reference and path constraints.

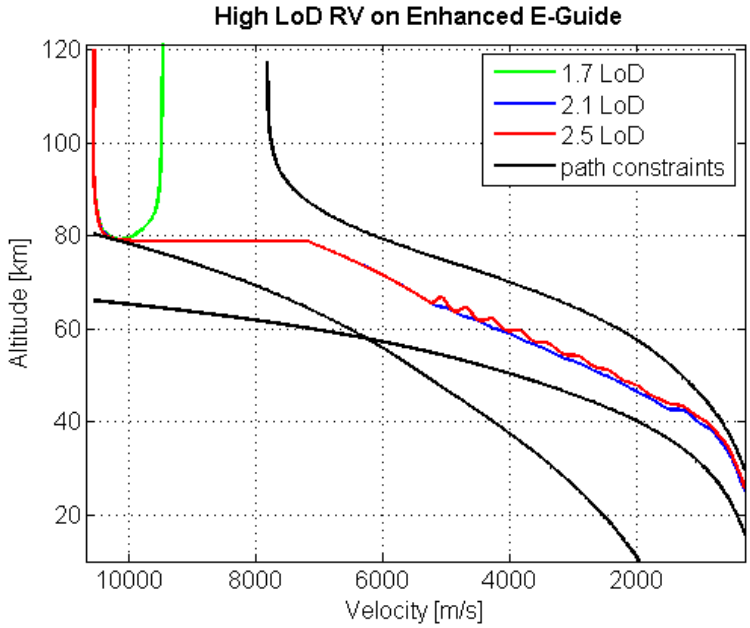

Figure 6.10: High L/D RVs on Enhanced E-Guide in the altitude-velocity plane: entry profiles and path constraints.

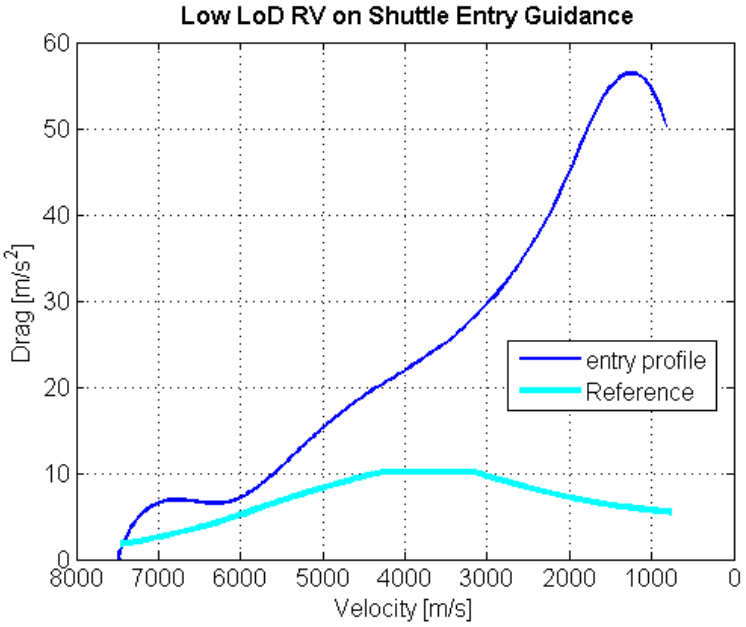

Figure 6.11: Low L/D RV on the Shuttle Entry Guidance algorithm in the drag-velocity plane: entry profile and drag-velocity reference profile.

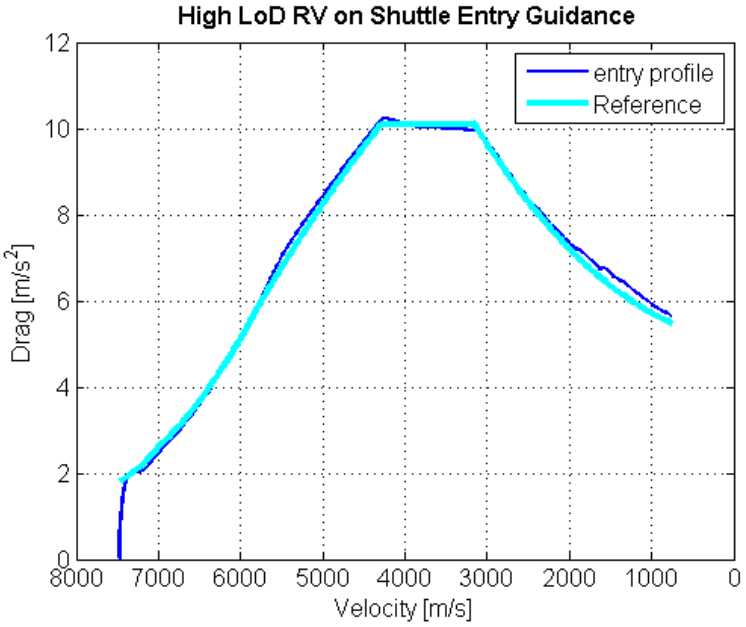

Figure 6.12: High L/D RV on the Shuttle Entry Guidance algorithm in the drag-velocity plane: entry profile and drag-velocity reference profile.

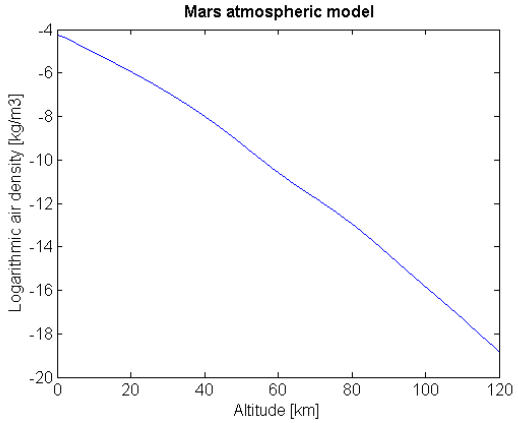

(a) Nominal air density-altitude model;

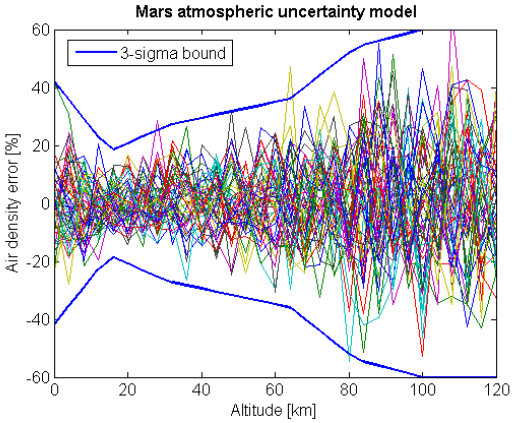

(b) 3-sigma bounds for uncertainty and randomly generated atmospheric perturbations (in percentage) in air density with respect to altitude;

Figure 6.13: Mars atmospheric model: air density with respect to altitude.

Chapter 7

Final remarks

7.1 Conclusions

In this work three entry guidance schemes, the Apollo Entry Guidance, the Shuttle Entry Guidance, and Enhanced E-Guide, were revisited. The Apollo Entry Guidance, developed by NASA in the sixties for the Apollo Command Module, a capsule-like RV with low L/D, and Enhanced E-Guide, an innovative entry guidance algorithm developed by GMV for the Phoebus high L/D RV concept, were already prototyped and made available. The Shuttle Entry Guidance, developed by NASA a decade later for the moderate L/D Shuttle Orbiter, was prototyped [17] from the beginning and tested.

For the integration of these guidance approaches in a single simulation environment, a 3-DoF simulation setting was implemented, and the three algorithms were further consolidated and generalized. This enabled each of the guidance schemes to run on RVs belonging to the associated L/D class, instead of being restricted to the specific RVs used as baseline.

Furthermore, a semi-analytical guidance approach that solves the TBVP problem of the TAEM targeting phase for an high L/D RV was developed. This procedure generates a reference profile fully compliant with the boundary conditions and constraints of the problem, as well as a bank angle law that ensures meeting the downrange requirement. These can be fed to a lower level controller for reference tracking. The results obtained under Monte-Carlo testing show that the procedure is able to cope with the uncertainties considered, due to flexible profile generation. The procedure is also deemed suitable for on-board installation, as its mostly analytical implementation allows for instantaneous entry profile generation and is not computationally demanding. It is noted that despite the tests conducted used a high L/D RV as baseline, there is no reason for this approach not to work with moderate or low L/D RVs, provided that final conditions (namely donwrange requirement) are adjusted accordingly.

Finally, REACTIVE, an entry simulation tool that allows for the design and testing of guidance and control solutions in a 3-DoF setting, was also developed. It results from the integration and consolidation of all the implemented algorithms. The tool thus comprises generalized algorithms suitable for low, moderate and high L/D RVs, which enable testing entry solutions for all RV L/D classes. Following the interest that NASA and ESA have on missions to planet Mars, the tool has also been extended to the Mars scenario, and the way it is implemented simplifies the process of adding new environments and atmospheres, new RV databases, and new guidance schemes.

On a more general note, it is observed that the guidance solutions commonly used in successful entry missions tend to be dependent on a reference profile tracking, which is also the case for most of the algorithms implemented in REACTIVE. In fact, the real-tested manned RVs, which include the Apollo CM, the Soyuz, and the Shuttle Orbiter, do not have significant L/D margin (or enough control authority) to use more sophisticated entry algorithms. Taking into account the sensitivity of the manned missions, it becomes clear

that the entry guidance algorithms must be reliable, predictable, and require low computational loads. Hence, reference profile tracking with gain-scheduled PID control, which is seemingly the most universally tested approach, is the preferred solution.

However, this is certainly not the future of re-entry. The advent of high L/D vehicles permits envisioning enormous potential for the development of innovative solutions. Examples of this are the NDI approach in the Enhanced E-Guide algorithm, and promising approaches as the Model Predictive Control technique for re-entry [39], or dynamic controller synthesis using Robust Control Theory [30]. Other hot topics, as neural networks [5, 46], spline construction or reinforcement learning [7], may also be viable solutions for RVs with significant L/D in the future, but they still have to be proven in other less demanding contexts.

7.2 Future work

7.2.1 Crossrange control in the profile generation procedure

In the future, the profile generation procedure should be upgraded in terms of crossrange control. When testing, the impact of the crossrange effect in the performance of the algorithm was modeled as a constant heading error discounted from the total downrange. However, the results obtained with the profile generation procedure would surely improve if a more accurate approximation of the real effects of lateral motion was taken into consideration.

In this regard, some techniques are available [13, 35]. Furthermore, the availability of the complete longitudinal profile should simplify the computation of a precise estimate of the heading error, and its inclusion in the downrange equation.

7.2.2 Evolution of REACTIVE

REACTIVE aims at becoming a complete design tool for entry guidance and control solutions in the future. In this respect, there are three fundamental upgrades:

- Implementation of 6-DoF dynamics;
- Addition of robust control setting to deal in a systematic way with uncertainties;
- Improvement of the user interface and possible integration with visualization tools.

The implementation of the 6-DoF dynamics is the most important upgrade in expanding REACTIVE's capabilities. Namely, while the current 3-DoF allows for outer loop GC design and re-entry profile analysis, the 3-DoF setting where only the RV attitude is considered is suitable for the development of inner closed-loop control solutions, and the full 6-DoF simulation setting would enable the testing and validation of the complete GNC solution. Therefore, all three configurations should be included in the future development of REACTIVE, which further suggests that this upgrade should be incremental, so as not to lose the detailed analysis capability that each of the 3-DoF/6-DoF settings provides.

The robust control setting addition would allow for the systematic modeling and analysis of entry uncertainties, and for the assessment of the guidance and control systems performance. The uncertainty modeling is to use the Linear Fractional Transformation (LFR) and Linear Fractional Representation techniques [32], where it is then possible to employ small-gain theorem from Robust Control Theory to synthetise appropriate control functions. However, the non-linearities of the re-entry problem could pose significant difficulties in the system linearization and uncertainty extraction that is required for the robust control approach.

Finally, the improved user interface would be a welcome addition, as it would simplify the process of interacting with the tool and thus broaden the number of people that would be able to use it: potentially, it could be used by any aerospace engineer.

Bibliography

[1] National Aeronautics and Space Administration. Landing the space shuttle orbiter. *NASA facts*, 2007.

[2] Aerospaceweb. Atmosphere and spacecraft re-entry. http://aerospaceweb.org. [Online; accessed 29-June-2011].

[3] I. Bogner. Description of Apollo Entry Guidance. Technical memorandum, NASA, 1966.

[4] J. Branco. *Technical note on Reference Frames*. GMV, 2010. Internal document.

[5] M. H. Breitner. Robust optimal onboard reentry guidance of a space shuttle: Dynamic game approach and guidance synthesis via neural networks. *Journal of Optimization Theory and Applications*, 107(3):481–503, 2000.

[6] C. L. Chen and Y. C. Liu. Solution of two-point boundary-value problems using the differential transformation method. *Journal of Optimization Theory and Applications*, 99(1):23–35, 1998.

[7] Q. P. Chu. Advanced flight control lecture notes. Control and Simulation Faculty of Aerospace Engineering, 2009.

[8] E. Di Sotto and J. Branco. *High Lift-over-Drag Earth Re-entry - Guidance Techniques for Earth Re-entry for Human Missions*. GMV, 2.0 edition, 2009.

[9] E. Di Sotto, J. Branco, R. Savino, M. De Stefano Fumo, R. Monti, M. Taushe, R. Janovsky M. Scheper, J. Apeldoorn, and R. C. Molina. PHOEBUS: GNC design and performance assessment for super orbital re-entry. In *American Institute of Aeronautics and Astronautics conference*, 2009.

[10] Greg A. Dukeman. Profile-Following Entry Guidance using Linear Quadratic Regulator Theory. *American Institute of Aeronautics and Astronautics Guidance, Navigation, and Control Conference and Exhibit*, pages 5–8, 2002.

[11] J. Campos Ferreira. *Introducao a analise Matematica*. Fundacao Calouste Gulbenkian, 7 edition, 1985.

[12] M. De Stefano Fumo, R. Savino, M. Taushe, U. Ewald, R. Monti, J. Branco, and E. Di Sotto. *High Lift-over-Drag Earth Re-entry - Entry Guidance Performance Verification*. DIAS and OHB and GMV, 1.0 edition, 2009.

[13] Michael D. Griffin and James R. French. *Space Vehicle Design*, chapter 6 Athmospheric Entry, pages 231 – 271. Education Series. American Institute of Aeronautics and Astronautics, 2 edition, 1991.

[14] Luis Guerreiro. *Architecture Design Document - REACTIVE*. GMV, Lisboa, 2010. Internal document.

[15] V. M. Guibout and D. J. Scheeres. Solving two-point boundary value problems using the hamilton-jacobi theory. In *2nd WSEAS Int. Conference on Applied and Theoretical Mechanics*, Venice, Italy, 2006.

[16] J. H. Columbia's sacrifice. http://www.columbiassacrifice.com/&0_shttlovrvw.htm, 2008. [Online; accessed 21-June-2011].

[17] J. C. Harpold and C. A. Graves. Shuttle Entry Guidance. Technical memorandum, NASA, 1979.

[18] Ernest R. Hillje. Entry flight aerodynamics from apollo mission as-202. Technical Note D-4185, NASA, Manned Spacecraft Center, Houston, Texas, 1967.

[19] A. Krishnan, U. Rajeev, and R. Harikumar. Trajectory control of a winged entry vehicle to a reference drag-energy profile. In *10th National Conference on Technological Trends*, 2009.

[20] Stephen R. Lewis, Mathew Collins, Peter L. Read, François Forget, Frédéric Hourdin, Richard Fournier, Christophe Hourdin, Olivier Talagrand, and Jean-Paul Huot. A climate database for mars. *Journal of Geophysical Research-Planets*, 104(E10):24177–24194, 1999.

[21] Songxin Liang and David J. Jeffrey. An analytical approach for solving nonlinear boundary value problems in finite domains. To be published, 2010.

[22] K. D. Maese and J. P. Kremer. Shuttle entry guidance revisited using nonlinear geometric methods. *Journal of Guidance, Control and Dynamics*, 17(6):1350–1356, 1994.

[23] NASA. http://www.nasa.gov. [Online; accessed 22-June-2011].

[24] NASA. Mars fact sheet. http://nssdc.gsfc.nasa.gov/planetary/factsheet/marsfact.html. [Online; accessed 1-July-2011].

[25] NASA. *Space Shuttle Technical Conference*, Texas, 1983. NASA Conference Publication 2342, Part 1.

[26] Heitor Pina. *Metodos Numericos*. McGraw-Hill of Portugal, 1995.

[27] Space Division Public relations department. Apollo spacecraft news reference. Technical report, North American Rockwell Corp., 1972.

[28] Rodrigo Haya Ramos, Davide Bonetti, and Gabriele De Zaiacomo. High lift-to-drag re-entry concepts for space transportation missions. In *American Institute of Aeronautics and Astronautics conference*, 2010.

[29] Frank J. Regan and Satya M. Anandakrishnan. *Dynamics of Atmospheric Re-Entry*. Education Series. American Institute of Aeronautics and Astronautics, 1966.

[30] Obaid Ur Rehman, Baris Fidan, and Ian Petersan. Minimax lqr control design for a hypersonic flight vehicle. In American Institute of Aeronautics and Astronautics, editors, *16th AIAA/DLR/DGLR International Space Planes and Hypersonic Systems and Technologies*, Canberra, ACT 2610, Australia, 2009.

[31] Jeffrey S. Robinson and Kathryn E. Wurster. Trajectory and aeroheating environment development and sensitivity analysis for capsule-shaped vehicles. *American Institute of Aeronautics and Astronautics*, 2005.

[32] Carsten Scherer. Robust control lecture notes. Delft Center for Systems and Control, TU Delft, Mars 2009.

[33] University of California San Diego Scripps Institution of Oceanography. Satellite geodesy. http://topex.ucsd.edu. [Online; accessed 22-June-2011].

[34] Zuojun Shen and Ping Lu. Onboard generation of three-dimensional constrained entry trajectories. *Journal of Guidance, Control and Dynamics*, 26(1), 2003.

[35] Zuojun Shen and Ping Lu. Dynamic lateral entry guidance logic. *Journal of Guidance, Control, and Dynamics*, 27(6), 2004.

[36] SRE-PAP. Mrep mars environmental document. Sp, ESA, Keplerlaan 1, 2201 AZ Noordwijk, The Netherlands, 2010.

[37] J. Stoer and R. Bulirsh. *Introduction to Numerical Analysis*, chapter 7.3. New York Springer-Verlag, 1980.

[38] Michael E. Tauber. A review of high-speed, convective, heat-transfer computation methods. Technical Paper 2914, NASA, Ames Research Center, Moffett Field, California, 1989.

[39] W. R. van Soest, Q. P. Chu, and J. A. Mulder. Combined feedback linearization and constrained model predictive control for entry flight. *Journal of Guidance, Control, and Dynamics*, 2005.

[40] M. Verhaegen and V. Verdult. *Filtering and System Identification - A Least Squares Approach*, pages 28–32. Cambridge University Press, 2007.

[41] K. F. Wakker. *Astrodynamics - I*, chapter 6 Elliptical orbits. Fundamentals of Astrodynamics. Technische Universiteit Delft, 2007.

[42] Rodney C. Wingrove. A study of guidance to reference trajectories for lifting re-entry at supercircular velocity. *NASA Technical report*, 1963.

[43] Rodney C. Wingrove. Survey of atmosphere re-entry guidance and control methods. *American Institute of Aeronautics and Astronautics*, 1(9), 1963.

[44] S.-F. Wu, R. R. Costa, Q.-P. Chu, J. A. Mulder, and G. Ortega. Nonlinear dynamic modeling and simulation of the re-entry crew return vehicle. In *4th ESA International Conference on Spacecraft Guidance, Navigation and Control Systems*, ESTEC, Noordwijk, The Netherlands, 1999.

[45] Jan M. Zazula. On graphite transformations at high temperature and pressure induced by absorption of the lhc beam. Project note 78/97, CERN, 1997.

[46] Li Kefeng Ren Zhang, Zhang Qingzhen, and Liu Chengrui. Neural network and adaptive inversion for re-entry vehicle control. In *26th Chinese Control Conference*, Zhangjiajie, Hunan, China, 2007.

[47] Curtis Zimmerman, Greg Dukeman, and John Hanson. Automated method to compute orbital reentry trajectories with heating constraints. *Journal of Guidance, Control, and Dynamics*, 26(4), 2003.

[48] Daniel Zwillinger. *Handbook of Differential Equations*. Academic Press, London, 3 edition, 1997.